



The University of
Nottingham

UNITED KINGDOM • CHINA • MALAYSIA

Tie, Ding Yee (2013) Design and synthesis of indole-thiazole based inhibitors of UDP-galactopyranose mutase. MSc(Res) thesis, University of Nottingham.

Access from the University of Nottingham repository:

http://eprints.nottingham.ac.uk/13796/1/TDY_MSc_thesis_FINAL_VERSION.pdf

Copyright and reuse:

The Nottingham ePrints service makes this work by researchers of the University of Nottingham available open access under the following conditions.

This article is made available under the University of Nottingham End User licence and may be reused according to the conditions of the licence. For more details see:
http://eprints.nottingham.ac.uk/end_user_agreement.pdf

For more information, please contact eprints@nottingham.ac.uk



The University of
Nottingham

UNITED KINGDOM · CHINA · MALAYSIA



**Design and Synthesis of
Indole-Thiazole Based
Inhibitors of UDP-
Galactopyranose Mutase.**

Ding Yee Tie, BSc.

Supervisor: Prof. Neil R. Thomas

December 2013

Abstract

Tuberculosis, which is caused by the pathogenic bacterium *Mycobacteria tuberculosis* (MTB), is an infectious disease that remains a significant worldwide health threat. Galactofuranose (Gal f) residues play an imperative role in the growth of MTB as it is an essential component in the cell wall of this bacterium. UDP-Galactopyranose mutase (UGM) is a flavoenzyme that involved in Gal f biosynthesis. It catalyzes the reversible conversion of UDP-galactopyranose (UDP-Galp) to UDP-galactofuranose (UDP-Gal f).

The absence of both UGM and Gal f residues in humans make UGM a target for new TB therapeutic drugs. This has also brought us to an interest in UGM.

Fourteen potential inhibitors of UGM were identified by alternating the R groups of the structure found computationally (Figure 1), and successfully synthesised in this project. Besides, HPLC assay was carried out to determine the purity of these inhibitors. Subsequently, docking experiments were performed to dock these compounds into the X-ray structure of *Deinococcus radiodurans* UGM. Further insight of the docking result is evaluated.

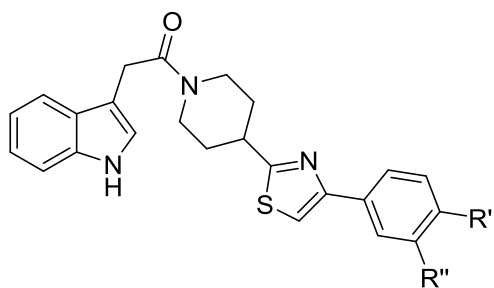


Figure 1 General structure of the potential inhibitors of UGM identified. R' and R'' are different substituents.

Acknowledgements

I would like to express my gratitude to my supervisor, Professor Neil R. Thomas for his supervision and his suggestions throughout this project. Besides, I would like to thank him for giving me the opportunity to do this project.

At the same time, I would like to thank my co-supervisor, Terry May, for his patience in guiding me throughout my project, helpful discussions, and proof-reading my thesis.

Furthermore, I would like to thank the NRT group, especially James Krupa, Inderpal Sehmi, and Tatiana Jaramillo Forcada, who have helped me throughout the project and helped me with the laboratory work. Thank you for the good working atmosphere.

In addition, I would like to thank Aneesa Ahmed for showing me how to use the computational software, and her advice regarding to the computational experiments.

I am grateful to Dr. Linda Varadi, Yee Leong Lee and Chin Beng Tan for the help in my project and proofreading of my thesis.

I wish to thank the University of Nottingham for providing facilities for this research. I would also like to thank the analytical technical staff in the School of Chemistry and the Center for Biomolecular Sciences.

Finally, I would like to thank my parents and friends for their moral support throughout this project.

Abbreviations

Ac	Acetyl
AFB	Acid-fast Gram-positive bacterium
BCG	Bacillus Calmette-Guerin
Boc	<i>N-tert</i> -Butoxycarbonyl
CD4 ⁺	Cluster of differentiation 4
CD8 ⁺	Cluster of differentiation 8
d	Doublet
dd	Doublet of doublets
DCM	Dichloromethane
DIPEA	<i>N,N</i> -Diisopropylethylamine
DMF	Dimethylformamide
DMSO	Dimethyl sulphoxide
dq	Doublet of quartets
drUGM	<i>Deinococcus radiodurans</i> UGM
drUGM _{ox}	Oxidised drUGM
drUGM _{red}	reduced drUGM
ecUGM	<i>Escherichia coli</i> UGM
EEA1	Early endosomal autoantigen 1
ESI	Electro spray ionisation
ESI-MS	Electro spray ionisation mass spectroscopy
Et	Ethyl
FAD	Flavin adenine dinucleotide (oxidized form)
FADH ₂ /FAD _{red}	Flavin adenine dinucleotide (reduced form)
FADH [•]	FADH semiquinone

h	Hour
IR	Infrared spectroscopy
HBTU	<i>O</i> -Benzotriazole- <i>N,N,N',N'</i> -tetramethyl-uronium-hexafluoro-phosphate
HMDO	Hexamethyldisiloxane
HPLC	High performance liquid chromatography
IC ₅₀	Half maximal inhibitory concentration
IR	Infrared spectroscopy
K _d	Dissociation constant
kpUGM	<i>Klebsiella pneumoniae</i> UGM
LFERs	Linear free energy relationships
LR	Lawesson's reagent
m	Multiplet
M	Molar
MDR	Multi-drug resistant
Me	Methyl
Mol	Mole
Mp	Melting point
MS	Mass spectroscopy
MTB	<i>Mycobacterium tuberculosis</i>
mtUGM	<i>Mycobacteria tuberculosis</i> UGM
NTM	Nontuberculous mycobacteria
NMR	Nuclear magnetic resonance
PIX	Positional isotope exchange
RNIs	Reactive nitrogen intermediates
RT	Room temperature

s	Singlet (NMR)
SET	Single electron transfer
S _N 1	Nucleophilic substitution monomolecular
S _N 2	Nucleophilic substitution bimolecular
TB	Tuberculosis
^t Bu	Tertiary Butyl
td	Triplet of doublets
<i>Tert</i>	Tertiary
TFA	Trifluoroacetic acid
TLC	Thin layer chromatography
tt	Triplet of triplets
UDP	Uridine 5'-diphosphate
UDP-Galp	UDP-galactopyranose
UDP-Galf	UDP-galactofuranose
UGM	Uridine 5'-diphosphate galactopyranose mutase
WHO	World Health Organisation
XDR	Extensively drug-resistant

Table of Contents

1 Introduction	11
1.1 Tuberculosis	11
1.1.1 Symptoms.....	12
1.1.2 Causes	13
1.1.3 Transmission (mechanism).....	14
1.1.4 Diagnosis.....	15
1.1.5 Prevention, treatment and resistance.....	15
1.2 <i>Mycobacterium tuberculosis</i>	18
1.2.1 General Characteristics.....	18
1.2.2 Cell wall structure	20
1.2.3 Pathophysiology.....	21
1.2.4 Strain variation	21
1.3 Uridine 5'-diphosphate galactopyranose mutase (UGM)	23
1.3.1 Crystal structure and binding site of UGM.....	24
1.3.2 Mechanism of UGM.....	31
1.3.3 UGM inhibitors reported in literatures.....	41
1.4 Aims	44
2 Results & Discussions	46
2.1 Chemical synthesis	47
2.2 HPLC analysis of the analogues.....	61
2.3 <i>In silico</i> evaluation.....	64

3 Conclusion and Future Work	80
4 Experimental	82
4.1 General	82
4.2 Procedures and Data	84
4.2.1 Chemical synthesis	84
4.2.1.1 Synthesis of <i>tert</i> -Butyl 4-carbamoyl piperidine-1-carboxylate (19) ⁶⁸	84
4.2.1.2 Synthesis of <i>tert</i> -butyl 4-carbamothioyl piperidine-1-carboxylate (20) ⁶²	85
4.2.1.3 Synthesis of 12-(1 <i>H</i> -indol-3-ylacetyl)piperidine-15-carbothioamide (21) ^{70, 71}	86
4.2.1.4 General procedure of Hantzsch thiazole synthesis of indole analogues. ⁷²	87
4.2.1.4.1 Synthesis of 11-{15-[21-(25,26-Dichloro-phenyl)-thiazol-18-yl]1-piperidin-12-yl}-10-(1 <i>H</i> -indol-3-yl)-ethanone (22).....	88
4.2.1.4.2 Synthesis of 10-(1 <i>H</i> -indol-3-yl)-11-(15-(21-phenylthiazol-18-yl)piperidin-12-yl)ethanone (23).....	89
4.2.1.4.3 Synthesis of 10-(1 <i>H</i> -indol-3-yl)-11-(15-(21-(26-nitrophenyl)thiazol-18-yl)piperidin-12-yl)ethanone (24)	90
4.2.1.4.4 Synthesis of 10-(1 <i>H</i> -indol-3-yl)-11-(15-(21-(<i>p</i> -tolyl)thiazol-18-yl)piperidin-12-yl)ethanone (25).....	91
4.2.1.4.5 Synthesis of 11-(15-(21-(26-bromophenyl)thiazol-18-yl)piperidin-12-yl)-10-(1 <i>H</i> -indol-3-yl)ethanone (26).....	93

4.2.1.4.6	Synthesis of 10-(1 <i>H</i> -indol-3-yl)-11-(15-(21-(26-methoxyphenyl)thiazol-18-yl)piperidin-12-yl)ethan-11-one (27).....	94
4.2.1.4.7	Synthesis of 11-(15-(21-(26-fluorophenyl)thiazol-18-yl)piperidin-12-yl)-10-(1 <i>H</i> -indol-3-yl)ethanone (28).....	95
4.2.1.4.8	Synthesis of 11-(15-(21-(25-chlorophenyl)thiazol-18-yl)piperidin-12-yl)-10-(1 <i>H</i> -indol-3-yl)ethanone (29).....	97
4.2.1.4.9	Synthesis of 26-(21-(15-(10-(1 <i>H</i> -indol-3-yl)acetyl)piperidin-12-yl)thiazol-18-yl)benzotrile (30).....	98
4.2.1.4.10	Synthesis of 10-(1 <i>H</i> -indol-3-yl)-11-(15-(21-(26-(trifluoromethoxy)phenyl)thiazol-18-yl)piperidin-12-yl)ethanone (31).....	99
4.2.1.4.11	Synthesis of 11-(15-(21-([23,29'-biphenyl]-26-yl)thiazol-18-yl)piperidin-12-yl)-10-(1 <i>H</i> -indol-3-yl)ethanone (32).....	101
4.2.1.4.12	Synthesis of 11-(15-(21-(25-fluorophenyl)thiazol-18-yl)piperidin-12-yl)-10-(1 <i>H</i> -indol-3-yl)ethanone (33).....	102
4.2.1.4.13	Synthesis of 11-(15-(21-(26-chlorophenyl)thiazol-18-yl)piperidin-12-yl)-10-(1 <i>H</i> -indol-3-yl)ethanone (34).....	104
4.2.1.4.14	Synthesis of 10-(1 <i>H</i> -indol-3-yl)-11-(15-(21-(26-(trifluoromethyl)phenyl)thiazol-18-yl)piperidin-12-yl)ethanone (35).....	105
4.2.2	HPLC purity analysis of the inhibitors	106
4.2.3	<i>In silico</i> studies	107

5 References..... 108

1 Introduction

1.1 Tuberculosis

Tuberculosis (TB) is an infection caused by *Mycobacterium tuberculosis*, which primarily affects the lungs.² It is spread by inhaling tiny droplets released by infected person when they cough or sneeze. TB is the most extensive cause of death in the World today, especially in less economically developed countries. The World Health Organisation (WHO) reported that there were almost 9 million new cases of TB in 2011 and 1.4 million of TB deaths (Figure 2).³

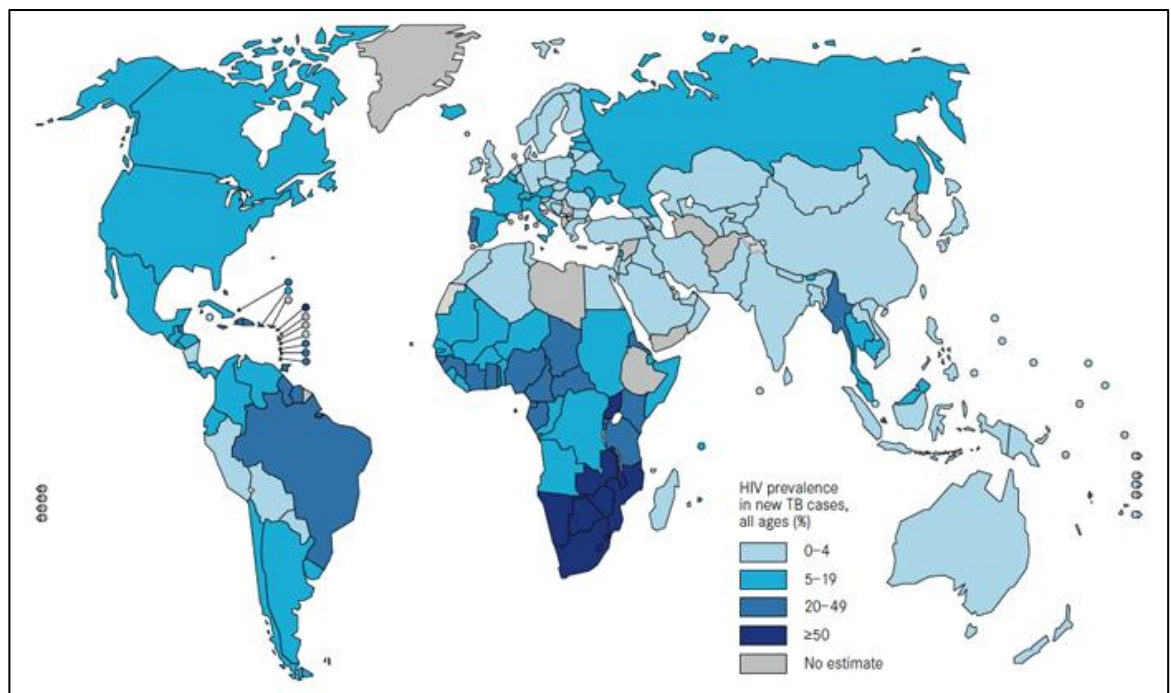


Figure 2 Estimated TB incidence rate in 2011.^{3, 4}

1.1.1 Symptoms

TB generally takes months or even years from the time of exposure until the symptoms develop. These differ depending on which part of the body is affected. In certain cases, the body is infected but no symptom develops. This is known as latent TB. On the other hand, if the bacteria cause symptoms, it is called active TB. There are two types of TB infection, which are pulmonary tuberculosis and extrapulmonary tuberculosis.⁵

Pulmonary TB is the infection on lungs. The symptoms include lack of appetite, weight loss, persistent cough (with phlegm that may be bloody) of more than three weeks, breathlessness, high body temperature of 38 °C, night sweats, tiredness, and inexplicable pain for weeks.⁶ In the case of extrapulmonary tuberculosis, this occurs outside the lungs. It is common in people who have weaker immune systems, predominantly people with a HIV infection. People with latent TB are more likely to develop extrapulmonary TB. The symptoms depend on the part of the body which is affected. TB of the lymph node has the symptoms of persistent painless inflammation of the lymph nodes. The swollen nodes can release fluid over a period of time;⁷ Skeletal TB will cause painful bones, loss of movement in the affected bone or joint and the affected bone may fracture easily; Gastrointestinal TB will cause abdominal pain, diarrhoea, and rectal bleeding; Central nervous system TB will cause headache, stiff neck, blurred vision, and unstable mental state.⁸

1.1.2 Causes

The main cause of TB is a small aerobic non-motile bacillus, *Mycobacterium tuberculosis* (MTB). It is spread in a similar way as the common cold or flu. However, it is not as contagious as the infection will only occur when one spends prolonged periods in close contact with an infected person. Moreover, not everyone with TB is infectious. In general, people with extrapulmonary TB do not spread the infection.⁵

Other TB-causing MTB complexes include *Mycobacterium bovis*, *Mycobacterium africanum*, *Mycobacterium microti* and *Mycobacterium canetti*. *Mycobacterium bovis* used to be a common cause of TB until the introduction of pasteurised milk, which has largely reduced this as a public health problem in developed countries.⁹ *Mycobacterium africanum* is not widespread except in certain parts of Africa.¹⁰ *Mycobacterium microti* is mostly found in immunodeficient people.¹¹ A few cases that involve *Mycobacterium canetti* have only been seen in African emigrants.¹²

Furthermore, the other known pathogenic mycobacteria include *Mycobacterium leprae* and *Mycobacterium marinum*. *Mycobacterium kansasii* and *Mycobacterium avium* are part of the nontuberculous mycobacteria (NTM) group. NTM cause neither TB nor leprosy. However, they cause pulmonary diseases similar to TB, such as skin disease or lymphadenitis.^{5, 13}

1.1.3 Transmission (mechanism)

The transmission of TB starts when people with active pulmonary TB sneeze, cough, speak or spit.⁴ These actions release infectious droplets that are 0.5 to 5.0 µm in diameter. A sneeze can produce up to 40,000 droplets and each of these may transmit the disease as the infectious dose of bacteria is very low (<10 bacteria may cause an infection).^{14, 15}

Infection rate increases when one has close, long, or frequent contact with people infected with TB. Only people with active TB will transmit the disease. There are several factors that affect the probability of transmission. For instance, the duration of exposure, the number of infectious droplets expelled by the carrier, the level of immunity in the uninfected person, the effectiveness of ventilation, the virulence of the MTB strain, and others.¹⁶ Transmission of TB can also occur when one ingests TB infected meat. For instance, *Mycobacterium bovis* causes TB in cattle.⁵

The chain of transmission can be circumvented through isolation of patients with active disease and treatment with effective anti-tuberculosis regimens.¹⁷

1.1.4 Diagnosis

A complete medical evaluation for TB must include medical history, a physical examination, a chest X-ray and microbiological examination. It may also include a tuberculin skin test, other scans and X-ray, surgical biopsy.¹⁸

The common method to diagnose TB worldwide is sputum smear microscopy, which was developed more than 100 years ago. Bacteria are observed in sputum samples examined under a microscope. Recently, the use of rapid molecular tests for the diagnosis of TB and drug resistant TB is increasing. Besides, TB is diagnosed using a culturing method in those countries with more developed laboratory capacity.^{4,19}

It is difficult to diagnose active tuberculosis based only on signs and symptoms as some patients are immunosuppressed and may have these symptoms for other reasons.¹⁸

1.1.5 Prevention, treatment and resistance

Bacillus Calmette-Guerin (BCG) was the first vaccine for TB that was developed in France between 1905 and 1921.²⁰ This vaccine is widely used as part of the TB control programme in many countries, especially for infants. For countries where TB is uncommon, BCG is only administered to people at high risk. BCG has a protective efficacy of greater than 80% towards preventing serious forms of TB in children.²¹ As for preventing pulmonary TB in adolescents and adults, its protective efficacy ranges from 0 to 80%.⁵

For people diagnosed with TB, an appropriate treatment should be given. Generally, a conventional short-course therapy will be given. The most effective combination is isoniazide, rifampicin, ethambutol, and pyrazinamide for two months, followed by isoniazide and rifampicin for 4 months.¹ This therapy is also effective for patients with HIV infection.⁴ A single antibiotic is usually used for latent TB treatment, while a combination of several antibiotics are used for active TB.⁵

The first line TB drugs are used initially to treat TB, and second line TB drugs are used when resistance to first line therapy, multi-drug resistant tuberculosis (MDR-TB) or extensively drug-resistant (XDR) tuberculosis occur. The first line TB drugs and second line TB drugs are listed in Figure 3, together with the structures (Figure 4).

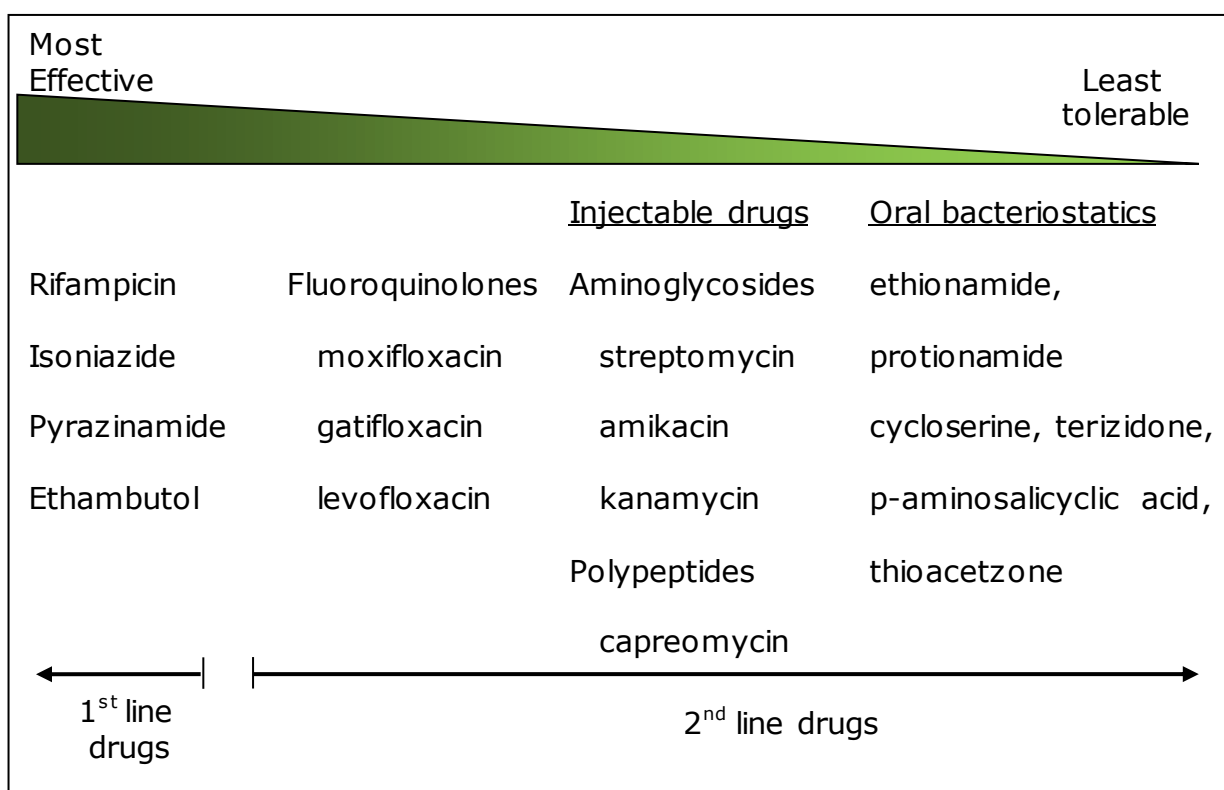


Figure 3 Current prescribed antituberculars. The first-line drugs and various classes of second-line drugs in descending order of tolerability and potency.¹

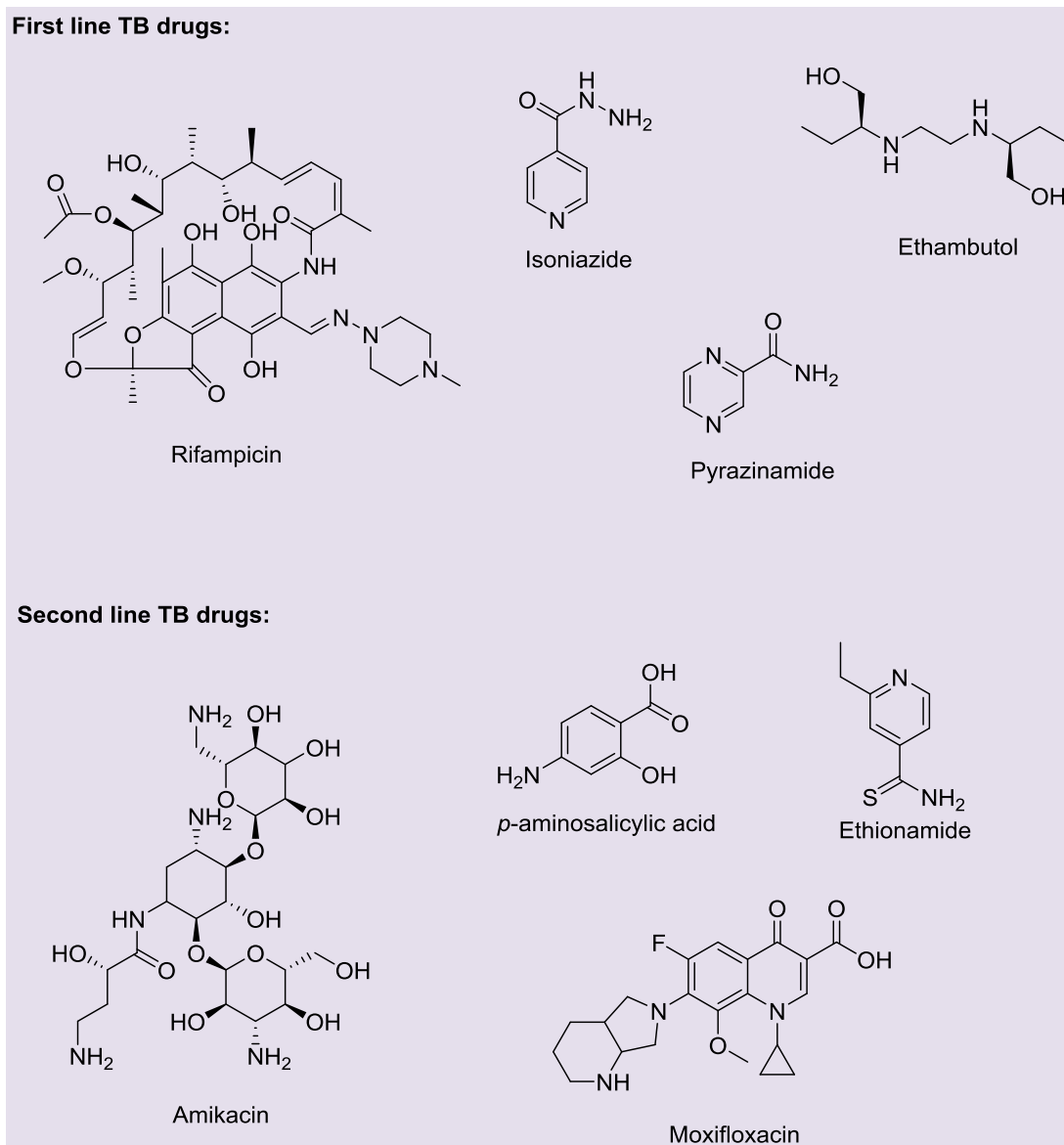


Figure 4 Structures of the first line and second line TB drugs.

Drug resistant TB is spread in a similar way as regular TB. Primary resistance occurs when a person is infected with a resistant strain of TB. Secondary resistance develops during TB therapy when the patient is given an inadequate treatment.²² MDR-TB is defined as resistance to the two most effective first-line TB drugs, which are rifampicin and isoniazid.¹⁹ XDR-TB is resistant to at least rifampicin and isoniazid, plus to any quinolone and at least one injectable second-line agent (see Figure 3).⁴

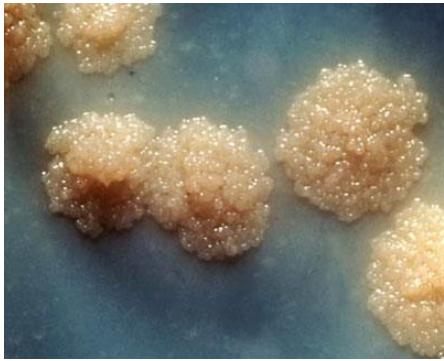
1.2 *Mycobacterium tuberculosis*

1.2.1 General Characteristics

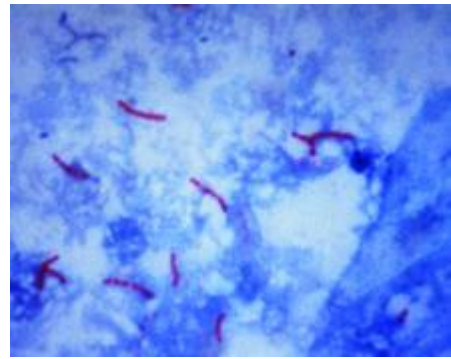
Mycobacterium tuberculosis (**Error! Reference source not found.** (a)) as first discovered by the German physician and scientist, Robert Koch on March 24, 1882.⁵ It is the causative agent of tuberculosis and infects primarily mammalian respiratory system (e.g. lungs). MTB is an aerobic, nonmotile bacillus that is classified as a Gram positive bacterium due to the presence of cell wall and lacks of phospholipid outer membrane.²³ It either stains very weakly Gram-positive or is impervious to any bacteriological stain due to high lipid and mycolic acid content in its cell wall.²³

Since MTB does not seem to fit the Gram-positive category from the empirical point of view (i.e. they generally do not retain the crystal violet stain well), it is classified as an acid-fast Gram-positive bacterium (AFB) as it retains certain stains after being treated with acidic solution.⁷ The acid-fast staining technique, called Ziehl-Neelsen staining, dyes AFBs a bright red that stands out clearly against blue background (**Error! eference source not found.**(b)). An auramine-rhodamine stain and fluorescent microscopy are other ways to visualize AFBs.⁵ MTB requires high levels of oxygen to grow.²³

MTB divides with an exceptionally slow rate compared with other bacteria (*E. coli* divides every 20-30 minutes), which is every 16 to 20 hours.⁵ The unusual cell wall of MTB enables it to endure mild disinfectants and survive in a dry state for weeks.²⁴



(a)



(b)

Figure 5 (a) Colonies of *Mycobacterium tuberculosis* growth on a culture plate.⁵ (b) Microscope image of red-stained TB bacteria.⁵

1.2.2 Cell wall structure

The bacteria are classified in the genus *Mycobacterium* based on the fact of their acid-fastness, a high (60-70 mol %) guanine plus cytosine (G+C) content in their deoxyribonucleic acid (DNA), and the presence of mycolic acid (Figure 6) containing 70-90 carbons. There are other species of acid-fast bacteria (i.e. *Norcardia*, *Tsukamurella*, *Rhodococcus*, *Gordonia*), but they stain less intensely due to their shorter mycolic acids chains.²⁴

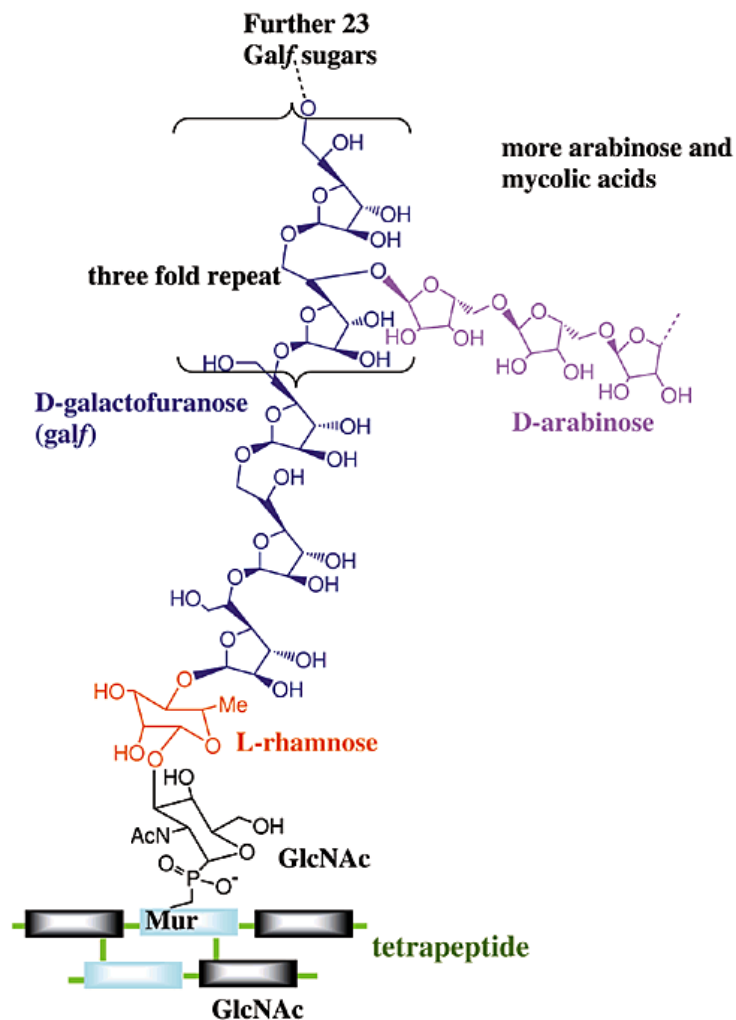


Figure 6 Cell wall of MTB showing key role of UDP-Galf and molecular structure of mycolic acids.²⁵

The cell wall of MTB is hydrophobic, waxy and rich in mycolic acids, which makes it a key virulence factor. The inner layer is composed of peptidoglycan which is covalently linked to an arabinogalactan layer. The outer membrane contains mycolic acids, (mannose-capped) lipomannan, and mannoglycoproteins.

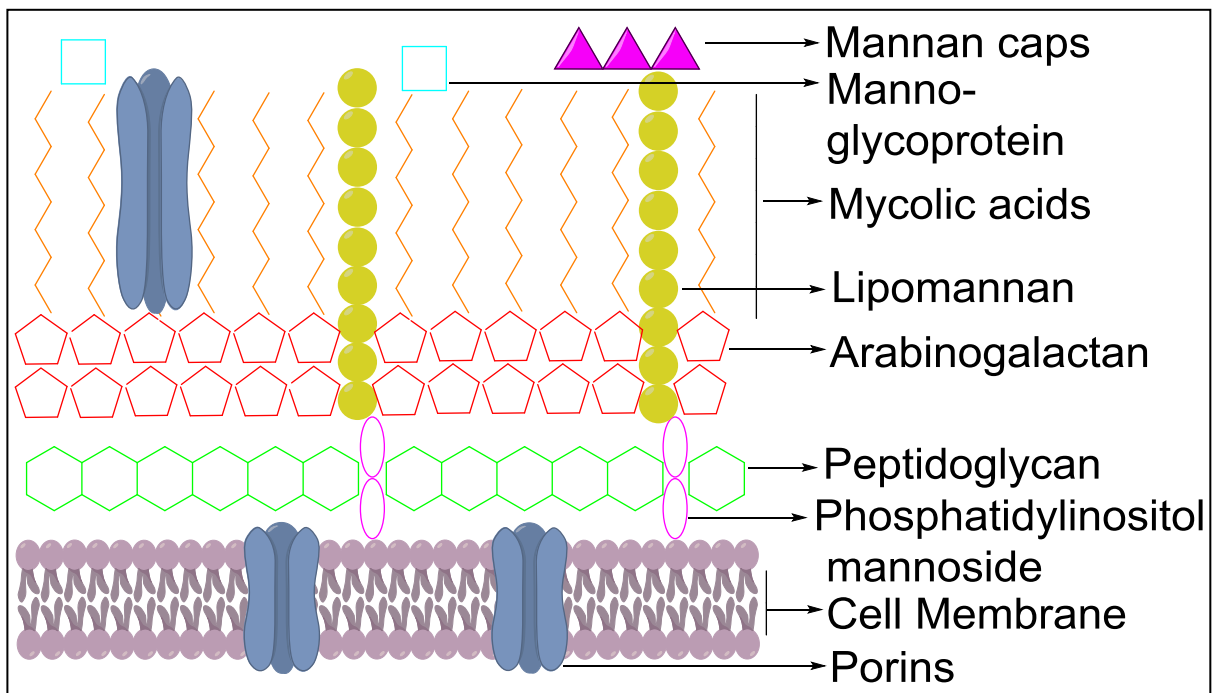


Figure 7 A schematic representations of the major components of the **Mycobacteria cell wall and their distributions.**

1.2.3 Strain variation

MTB is a pathogenic bacteria species in the genus *Mycobacterium*, within the order *Actinomycetales* that comprises a number of well characterised species. The most common species are MTB and *Mycobacterium leprae* (Leprosy). The genetic variation of MTB results in significant phenotypic differences between clinical isolates. Different strains of MTB are connected with different geographic regions. Nevertheless, phenotypic studies show that the development of new diagnostics and vaccines has

no relation to the strain variation. Yet, micro-evolutionary variation does influence the relative fitness and transmission dynamics of antibiotic-resistant strains.^{5, 26}

1.2.4 Pathophysiology

Normally, when a host is infected with MTB, the immune response will increase by eliciting cluster of differentiation 4 (CD4⁺) and cluster of differentiation 8 (CD8⁺) T cells as well as antibodies specific for mycobacterial antigens. It is believed that the bacterial pathogen persists in the host even though the immune response is sufficient to stop the progression to active disease.^{27,28}

The bacterium can survive within macrophage, which are responsible for eliminating microbes. Two major antimicrobial mechanisms of macrophages are phagolysosome fusion and the production of toxic reactive nitrogen intermediates (RNIs). RNIs (e.g. nitric oxide, nitrite, and nitrate) are toxic molecules produce by the immune system which helps in the destruction of pathogens.²⁹ Infected macrophages can be detected by CD4⁺ T cells.⁵

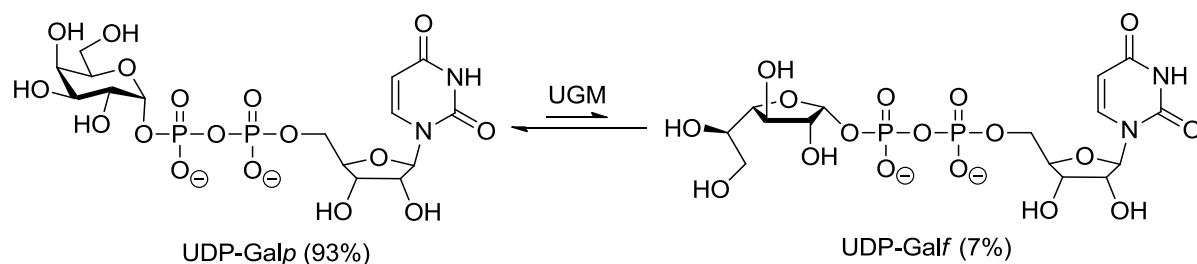
Mechanisms have been developed by MTB in order to avoid detection by the host and allow them to persist within macrophages. They can survive by modulating antigen presentation to prevent the detection of infected macrophages by T cells. Moreover, they can also survive by evading macrophage killing mechanisms that is mediated by nitric oxide and related RNIs.²⁷

MTB is spread through air when people with active MTB infection sneeze, cough or spit. A single sneeze can release up to 40,000 droplets.¹⁴ A droplet nuclei (0.5 to 5.0 μm in diameter) contains no more than 3 bacilli. It can remain air-borne for long period of time. After droplet nuclei are inhaled, they enter the lungs and MTB is taken up by alveolar macrophages. However, the bacterium is unable to be digested. The MTB cell wall prevents the fusion of the phagosome with a lysosome. MTB tends to block the bridging molecule, early endosomal autoantigen 1 (EEA1). However, the blockade does not prevent fusion of vesicles filled with nutrients. Subsequently, the bacteria multiply continuously within the macrophage. The *UreC* gene that is carried by bacteria will prevent the acidification of the phagosome.³⁰ Besides, to evade macrophage-killing mechanisms, the bacteria will develop various mechanisms to escape from the toxicity of the RNIs.^{5, 27}

1.3 Uridine 5'-diphosphate galactopyranose mutase (UGM)

UGM, a flavoprotein with the flavin adenine dinucleotide (FAD) coenzyme bound noncovalently, plays an essential role in galactofuranose biosynthesis in microorganisms. It is vital for viability in mycobacteria. UGM (Rv3809c) is *glf*-encoded enzyme³¹ that catalyzes the reversible interconversion of UDP-galactopyranose (UDP-Galp) into UDP-galactofuranose (UDP-Galf) (Scheme 1).²⁵ UDP-Galf is the activated precursor of *D*-Galactofuranose (Galf) residues, which are the crucial component of the arabinogalactan complex found in certain pathogenic bacteria such as *Klebsiella pneumoniae* and *Escherichia coli*. UGM is

shown to be essential for the growth and survival of *M. tuberculosis* and other pathogenic bacteria.^{3, 32}



Scheme 1 The overall reaction catalysed by UGM. The equilibrium favours formation of the six-membered pyranose form over the five membered furanose form.³³

1.3.1 Crystal structure and binding site of UGM

The mutase is a mixed α/β class of protein (the secondary structure is composed of α -helices and β -strands along the backbone, where β -strands are mostly parallel) that exists as a dimer.³⁴ Each monomer binds one molecule of FAD. The first crystal structure of UGM (Figure 8) from *E. coli* (ecUGM) was reported by Sanders *et al.* at a resolution of 2.4 Å (PDB code: 1I8T).²⁵ The flavin nucleotide was found to be located in a cleft lined with conserved residues (H56, Y311, R340, Y346, and D348). According to the site-directed mutagenesis studies performed, the cleft contains the substrate binding site together with the sugar ring of the UDP-galactose neighbouring to the exposed isoalloxazine ring of FAD. Sanders *et al.* concluded that this enzyme was only active when the flavin was reduced.²⁵

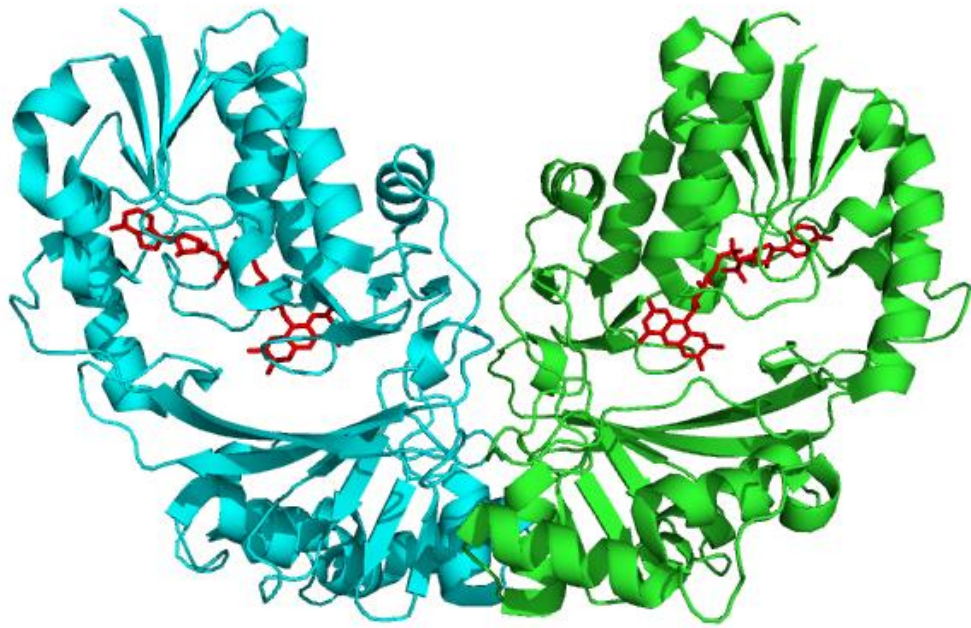
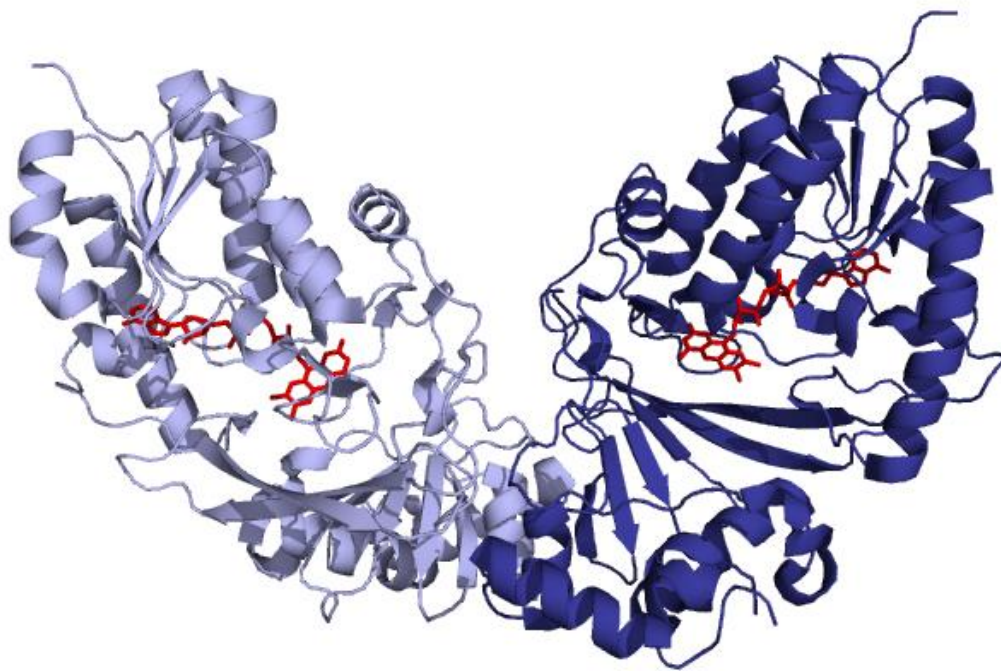
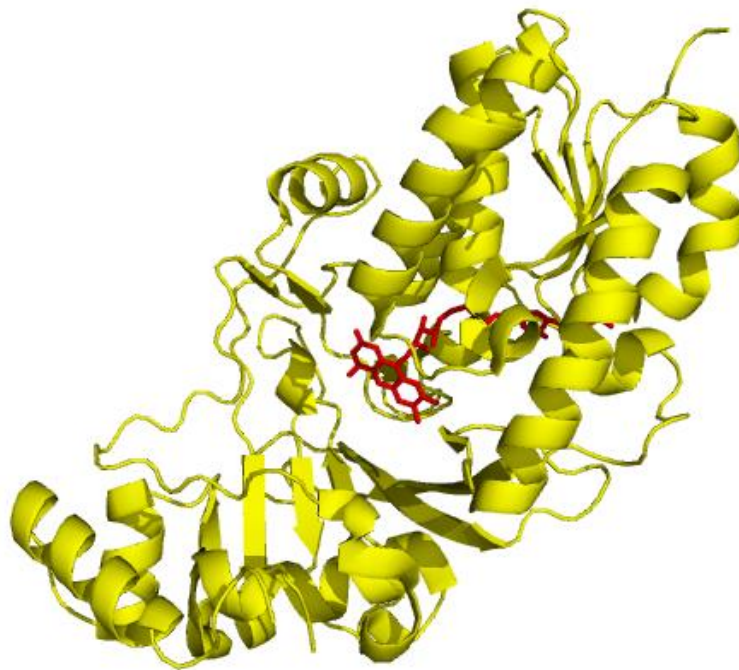


Figure 8 Ribbon diagram of *E. coli* UGM dimer. Monomer A is coloured blue; and monomer B is coloured green; FAD is shown in red.

More recently, the crystal structures of *M. tuberculosis* UGM (mtUGM) and *K. pneumoniae* UGM (kpUGM) was reported by Beis *et al.* at resolutions of 2.25 Å and 2.35 Å, respectively.³⁵ The site-directed mutagenesis study of kpUGM residues revealed that mutation of the conserve arginine (Arg174/ R174) of a mobile loop located away from the active site was found to affect the substrate binding and catalytic activity. The sequence identity of ecUGM with mtUGM and kpUGM are 42% and 37%, respectively (Figure 14). Based on Figure 9, the folds of the proteins from mtUGM and kpUGM are similar to ecUGM.



(a)



(b)

Figure 9 (a) The dimer structure of the mtUGM. Monomer A coloured in light blue; Monomer B coloured in deep blue; and FAD coloured in red. (b) The monomer structure of kpUGM is coloured in yellow; and FAD in red.

Partha *et al.* reported the crystal structure of UGM from *Deinococcus radiodurans* (drUGM) in complex with UDP-Galp (PDB code: 3HDQ).³⁶ The crystal structure of drUGM:UDP-Galp complexes with FAD_{red} were resolved to 2.50 Å resolution. An unusual folded conformation of UDP-Galp is located in the active site (Figure 10). The anomeric carbon of the galactose (UDP-Galp) is at a favourable distance (2.8 Å) from N5 of FAD, which is identified to be situated next to the putative substrate binding site.

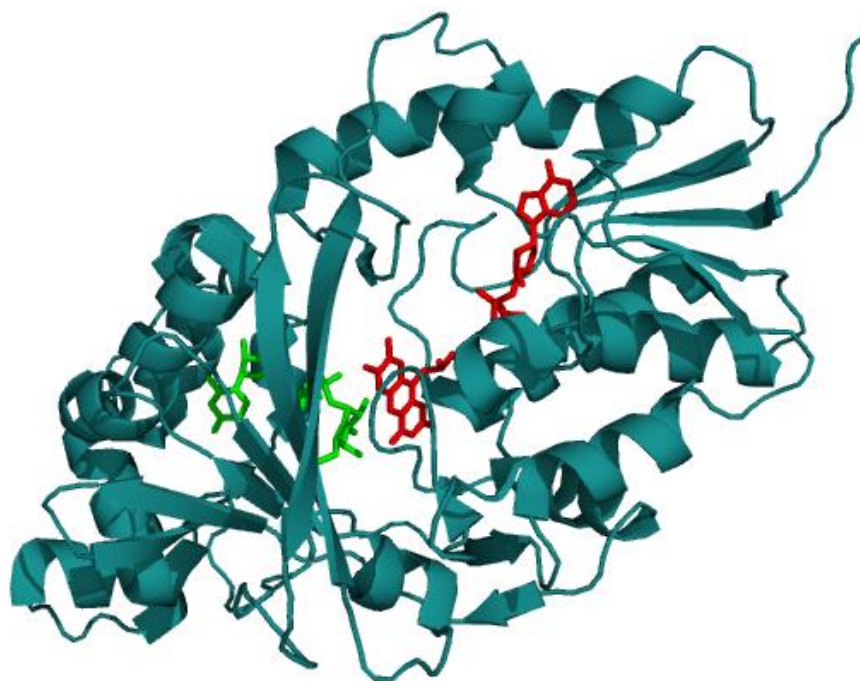


Figure 10 Ribbon diagram of a monomer of drUGM_{red} in complex with UDP-Galp. The FAD and UDP-Galp are shown as sticks with the colour of red and green, respectively.

Partha *et al.* mentioned that reduced drUGM (drUGM_{red}) has a different FAD conformation compared to oxidised drUGM (drUGM_{ox}). The isoalloxazine ring of FAD in drUGM_{red} has butterfly-like bent conformation (Figure 11 (a)) with the N5 of FAD nearer to the sugar moiety of substrate binding site (Figure 11 (b)).

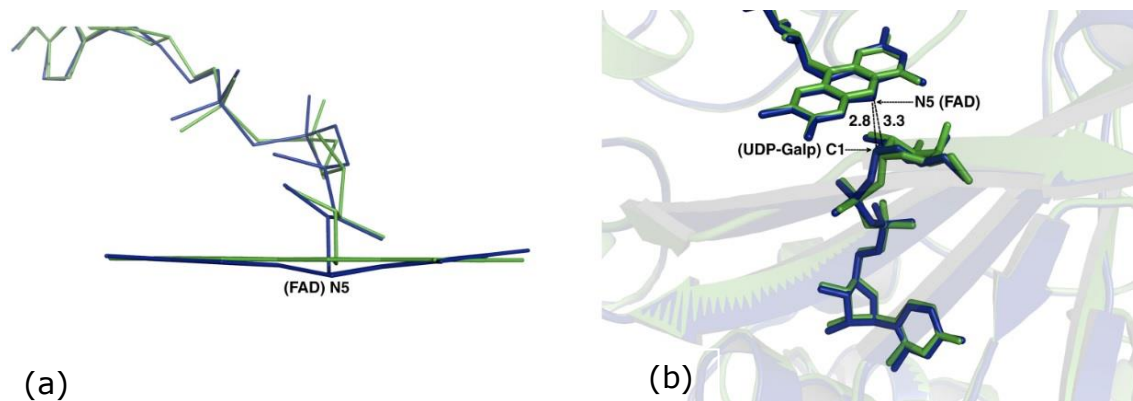


Figure 11 (a) Conformation comparison between FAD of drUGM_{red} (blue) and drUGM_{ox} (green). (b) Overlay of FAD of drUGM_{red} (blue) and drUGM_{ox} (green). Note that N5 of fad in drUGM_{red} is closer to the C1 of UDP-Galp compare to drUGM_{ox}.³⁶

Additionally, the electron density of the sugar in drUGM_{red} is clearer (Figure 12), which is assumed to stabilize the sugar conformation. Moreover, drUGM_{red} has a greater affinity for substrate than oxidized drUGM, which explains the possible bond formation between FAD and substrate in the mechanism of UGM (Section 1.3.2).³⁶

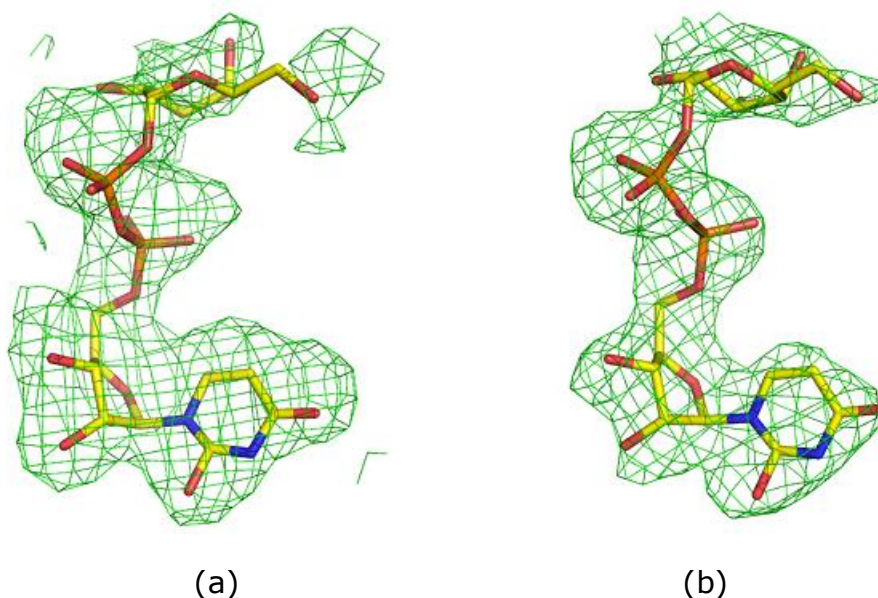


Figure 12 Comparison of the electron density of the sugar between drUGM_{ox} (a) and drUGM_{red} (b). The density of the sugar moiety in drUGM_{red} is more clearly defined compared to drUGM_{ox}.³⁶

Interestingly, when UDP-Galp binds in the active site of drUGM it adopts an unusual fold, which is different compared to the fully extended or fully folded substrate conformations observed in the structures of other of UDP-Galp utilising enzymes (Figure 13).^{36,37}

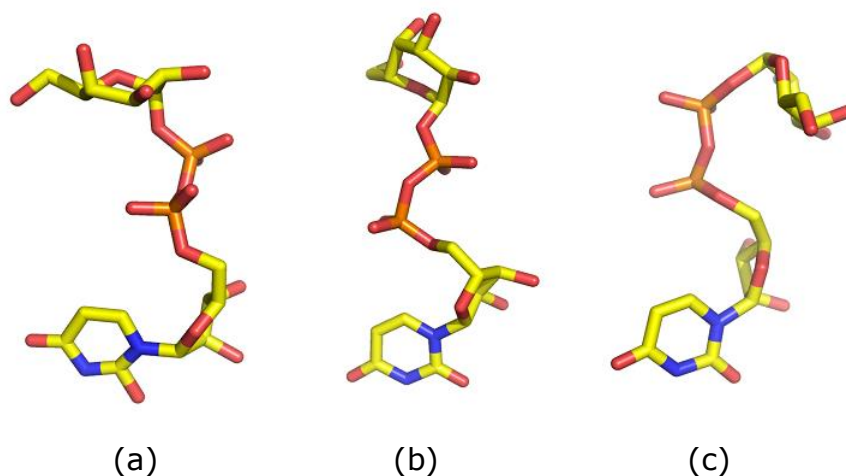


Figure 13 The conformations of UDP-Galp in drUGM_{ox} (a), UDP-galactosyltransferases (b), and UDP-galactose-4-epimerase (c).

With the structural information reported in previous research, a multi-sequence alignment using T_COFFEE³⁸ was carried out to identify conserved amino acid residues between different organisms (Figure 14). The sequence numbers for conserved key active site residues of UGM from *K. pneumoniae*, *E. coli*, *M. tuberculosis*, *D. radiodurans*, and *A. fumigatus* are given in Table 1. As shown in Table 1, most of the residues involved in substrate binding are highly conserved among these UGMs.

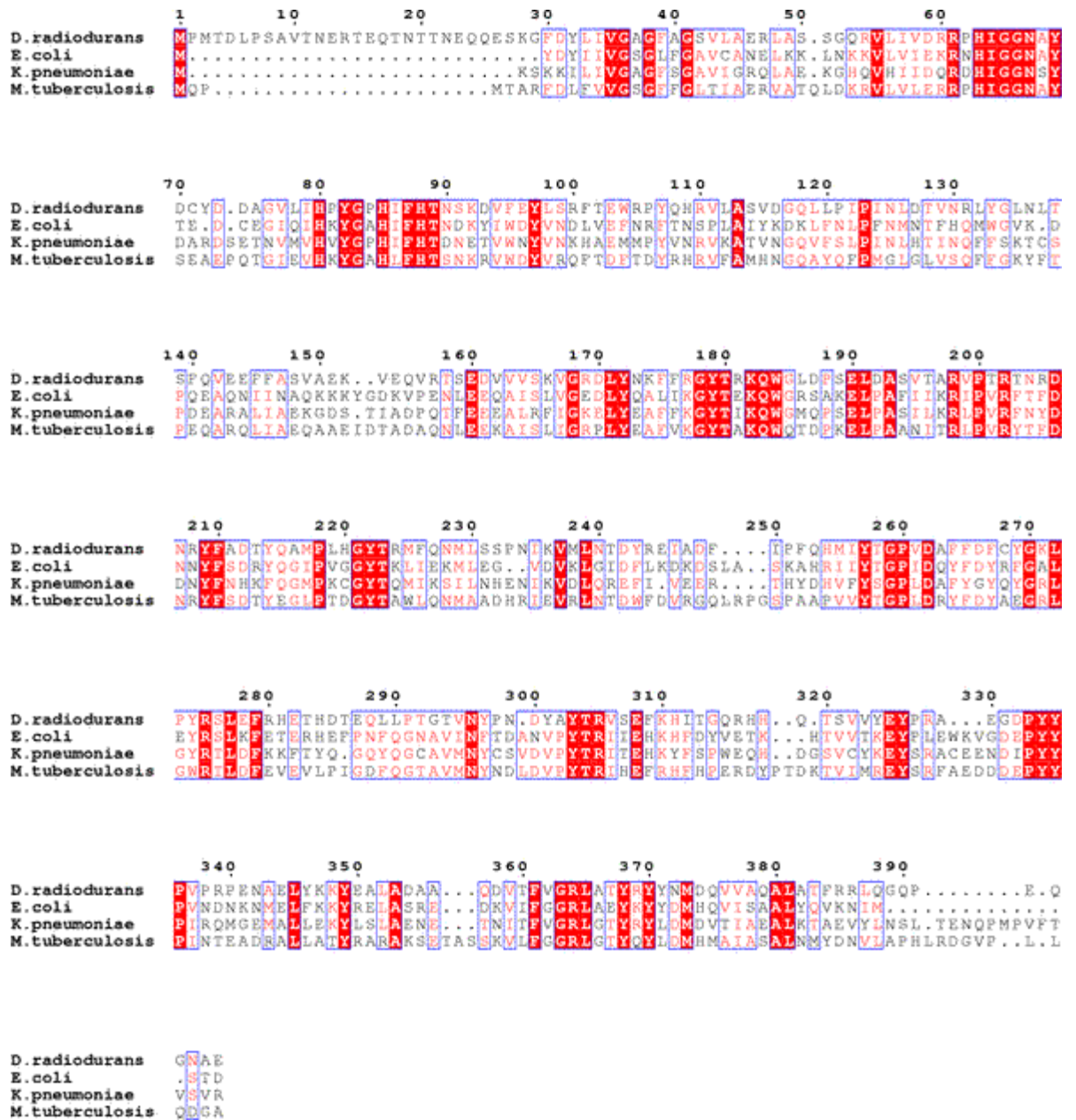


Figure 14 Sequence alignment of UGMs from *D. Radiodurans*, *E. coli*, *K. pneumoniae*, and *M. Tuberculosis*.^{25, 36, 39} The sequence identity/similarity is based on the alignment of four sequences. The alignment was generated using T_COFFEE³⁸ and the graphic is produced by ESPrInt⁴⁰. The red boxes denote the identical residues between the UGMs. Red characters denote the similarity in a group.

Table 1 Sequence numbers for conserved active site residues in different species of UGM.^{36, 41, 42}

<i>D.</i> <i>radiodurans</i>	<i>M.</i> <i>tuberculosis</i>	<i>E. coli</i>	<i>K.</i> <i>pneumoniae</i>	<i>A.</i> <i>fumigatus</i>
H88	H65	H56	H60	H63
H109	H89	N80	N84	R91
F175	F157	L147	F151	F158
F176	V158	I148	F152	M159
Y179	Y161	Y151	Y155	Y162
T180	T162	T152	T156	N163
W184	W166	W156	W160	W167
R198	R180	K169	R174	R182
Y209	Y191	R170	Y185	P206
F210	F192	Y181	F186	N207
N296	N282	N268	N270	Y317
R305	R292	R278	R280	R327
E325	E315	E298	E301	E373
Y335	Y328	Y311	Y314	Y419
R364	R360	R340	R343	R447
Y370	Y366	Y346	Y349	Y453
N372	D368	D348	D351	N457

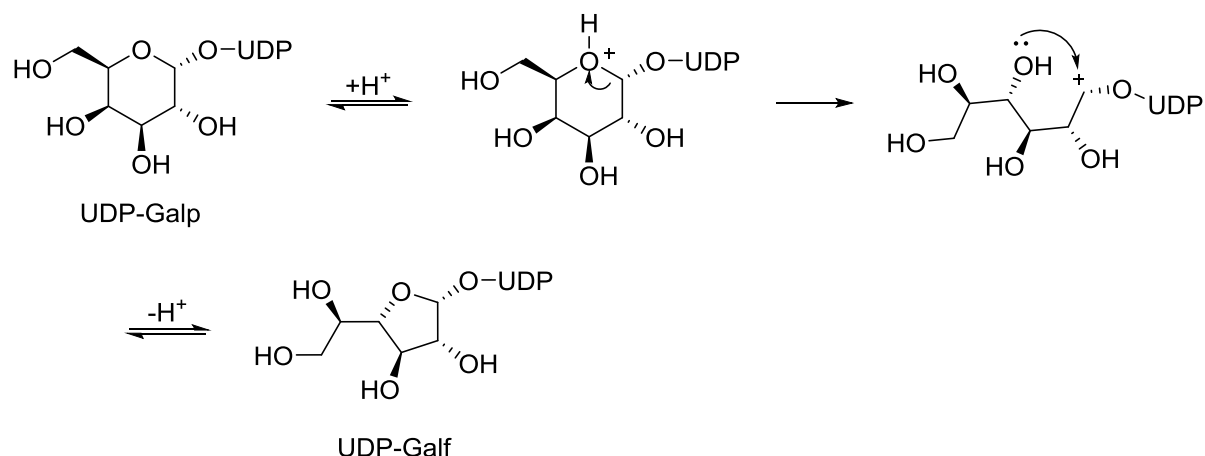
1.3.2 Mechanism of UGM

Several mechanistic studies on UGM have appeared in the literature including X-ray crystallographic, kinetic isotope analyses, spectroscopic and mutagenesis studies.^{25, 33, 36, 39, 43-45} Some published literature suggest that the reduced enzyme is active and the oxidized enzyme is not.^{33, 44, 46} For example, Sanders *et al.* showed that the reduction by dithionite activates the enzyme whilst oxidation by $K_3(FeCN_6)$ inactivates it.²⁵ Studies also suggested that noncovalently associated FAD plays an essential part in catalysis. UGM is catalytically active only when its FAD cofactor is in the reduced form.³³ The reduced FAD (FAD_{red}) was found to have different roles, from facilitating transient electron transfer (single electron transfer) to serving a structural role within the protein

scaffold.^{44, 47, 48} The X-ray crystallographic analysis of UGM structure shows that the enzyme-bound flavin is localized in the putative active site.²⁵ It has been observed that the N5 on FAD is important for UGM catalytic activity.⁴⁹

Previous studies have reported important understandings of the chemical mechanism of the UGM-catalyzed reaction. Although several mechanisms for UGM have been proposed, a clear insight of the catalytic mechanism is still elusive. Besides, the role of FAD cofactor is still puzzling as it can exist in different oxidation and ionic states.⁵⁰ The redox chemistry of this coenzyme is normally carried out through transformations involving either N5 or C4a of the isoalloxazine ring system.⁵¹

Trejo *et al.* proposed the first mechanism of the direct transformation of UDP-Galp into UDP-Galf (Scheme 2) in 1971. They suggested that a ring contraction occurred while the linkage between the sugar and the pyrophosphate remained intact. The mechanism (shown in Scheme 2) shows a preferential protonation of the ring oxygen of the pyranose nucleotide rather than glycosidic oxygen. This is due to the presence of sugar pyrophosphate structure. The pyrophosphate group was expected to decrease significantly the basicity of the glycoside oxygen. Therefore, preferential protonation of ring oxygen atom is more likely to happen.⁵²



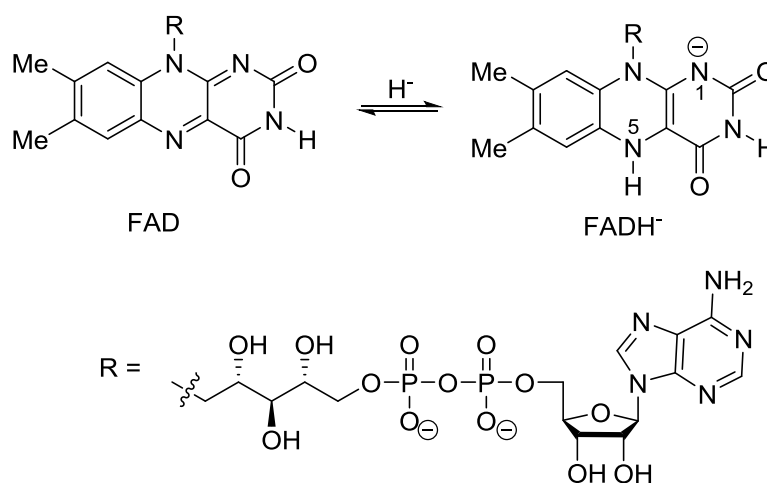
Scheme 2 Direct transformation of UDP-Galp into UDP-Galf as proposed by Trejo *et al.*⁵²

In 1999, Blanchard *et al.* proposed a hypothetical mechanism (Scheme 3) based on the results obtained from the ¹³C NMR and positional isotope exchange (PIX) experiments. They reported that the first step involves the direct nucleophilic attack of the axial 4'-hydroxyl group on C1, results in the breaking of the glycosidic bond, displacing UDP and generating a bicycle acetal. The bond between the ring oxygen and C1 is broken (two possible pathways, a and b are proposed) in the second step. The last step involves the attack of UDP at the anomeric C1 to give UDP-Galf.⁴⁴

Blanchard *et al.* demonstrated that the phosphate group bound to the anomeric position is torsionally unrestricted and statistically scrambled a labelled oxygen atom with the same rate as the reaction itself. This observation led to the conclusion that during turnover the glycosidic bond must be broken as part of the mechanism.⁴⁷

In 2000, Zhang *et al.* demonstrated that the catalytic efficiency of UGM increased by more than 2 orders of magnitude when UGM is in the reduced form. The same result was also observed when FAD was selectively reduced by photoreduction in the presence of 5-deazariboflavin under anaerobic conditions.⁴³

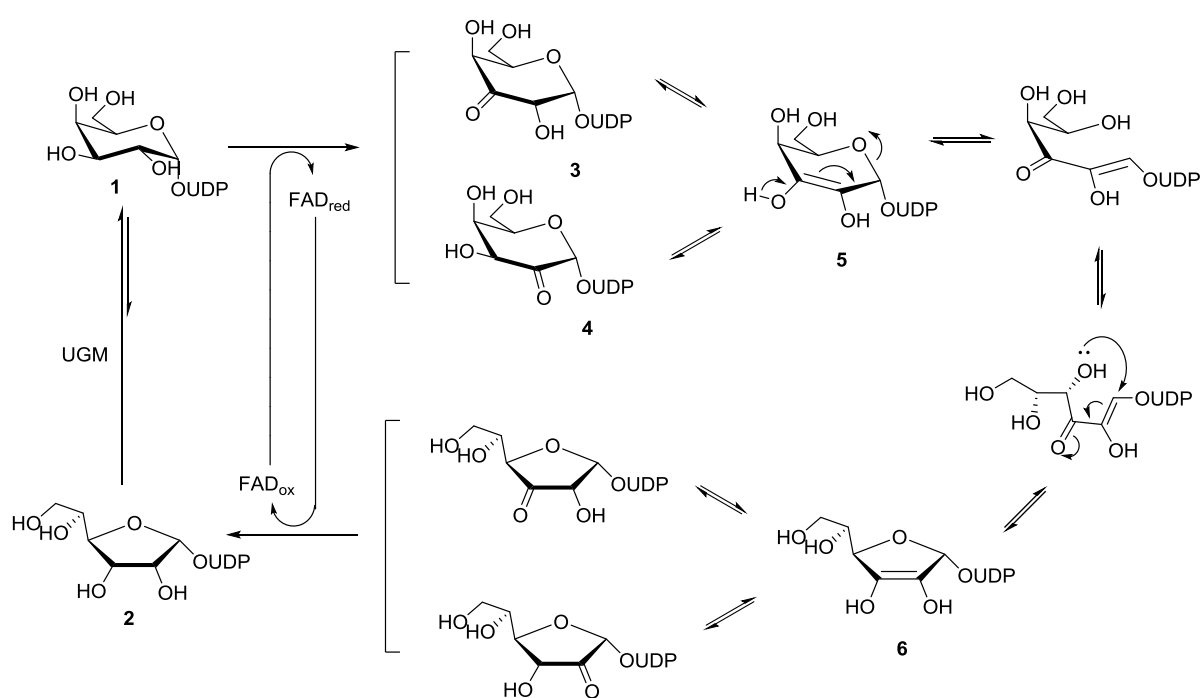
Early studies suggested that reduction of FAD involves transformation of the coenzyme from a highly conjugated planar frame to a “bent butterfly” structure, which may provoke a conformational change within the enzyme that may become more favourable to catalysis. Furthermore, the reduced flavin imparts a more negative character to N1 (Scheme 4), which may be used to stabilize the transiently formed oxocarbenium ion intermediate (Scheme 3) to facilitate catalysis.^{43,46,53}



Scheme 4 FADH⁻ bears a higher electron density at N1.⁴³

Following on from this, a hypothesized redox mechanism was proposed (Scheme 5).^{54, 55} The mechanism was initiated by the oxidation of 2-OH and 3-OH on the galactose moiety (**3/ 4**). The redox capability of FAD was utilized, allowing the oxidation of 2-OH and 3-OH to produce the enediols (**5/ 6**) as possible intermediates. However, this mechanism was

firmly ruled out based on the experiments carried out by Zhang *et al.* in 2001.⁴⁶ Two fluorinated analogues (**7**/**8**, Figure 15) were tested against *Escherichia coli* mutase. The results obtained show that these two compounds act as substrates for the reduced UGM (although **7** was a poor substrate). Since the fluorine substituent is redox inert, a mechanism initiated by the oxidation of 2-OH and 3-OH on the galactose moiety is impossible.⁴⁶



Scheme 5 A hypothesized mechanism for UGM in which the redox capability of FAD is exploited.^{54, 55}

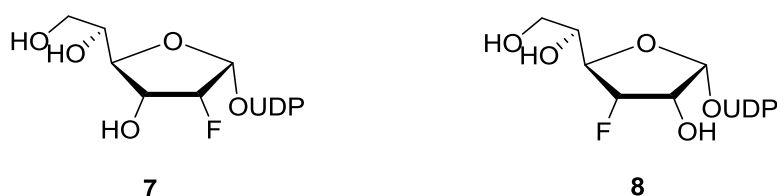
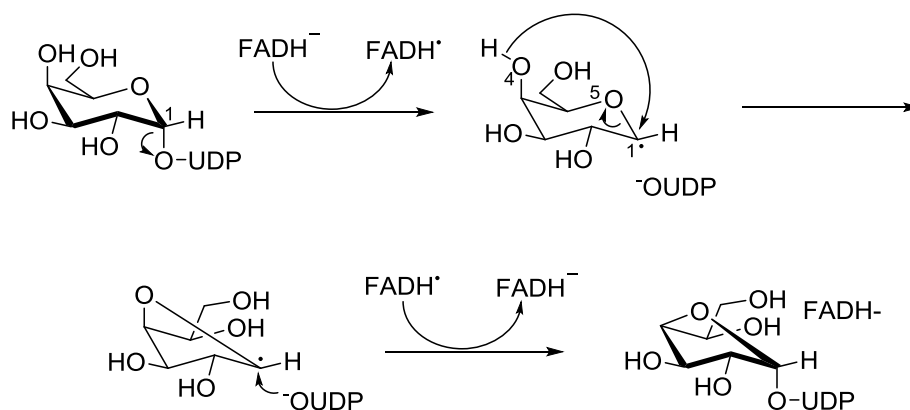


Figure 15 UDP-2F-Galf and UDP-3F-Galf.⁴³

In 2003, Fullerton *et al.* reported that the enzyme is only active when the FAD cofactor is in reduced state, and suggesting that a cryptic-redox reaction may form part of the mechanism. Thermodynamic analysis of the FAD demonstrated that neutral semiquinone (FADH•) is stabilized in the presence of substrate. Also, fully reduced flavin is the anionic FADH⁻, not the neutral FADH₂. This is because the anionic FADH⁻ is an ideal crypto-redox cofactor as it would allow rapid single electron transfer without being slowed by a coupled proton transfer. The thermodynamic analysis data obtained has shown that the semiquinone form of FAD is thermodynamically accessible under conditions of turnover.⁴⁷

A radical-based mechanism (Scheme 6) was suggested by Fullerton *et al.* The mechanism involves a single-electron transfer (SET) to the oxocarbenium to generate an anomeric radical. During the UDP-Galp/UDP-Galf interconversion, the formation of a highly reactive anomeric radical would facilitate ring contraction by inducing nucleophilic attack by O4 at the C1 position, with the cleavage of the anomeric C1-O5 bond. The electron would then transferred from the anomeric position back to the FAD semiquinone.⁴⁷



Scheme 6 Radical mechanism proposed by Fullerton *et al.* in 2003. The anomeric radical is the key intermediate generated by single electron transfer from FADH^- to the oxocarbenium ion.⁴⁷

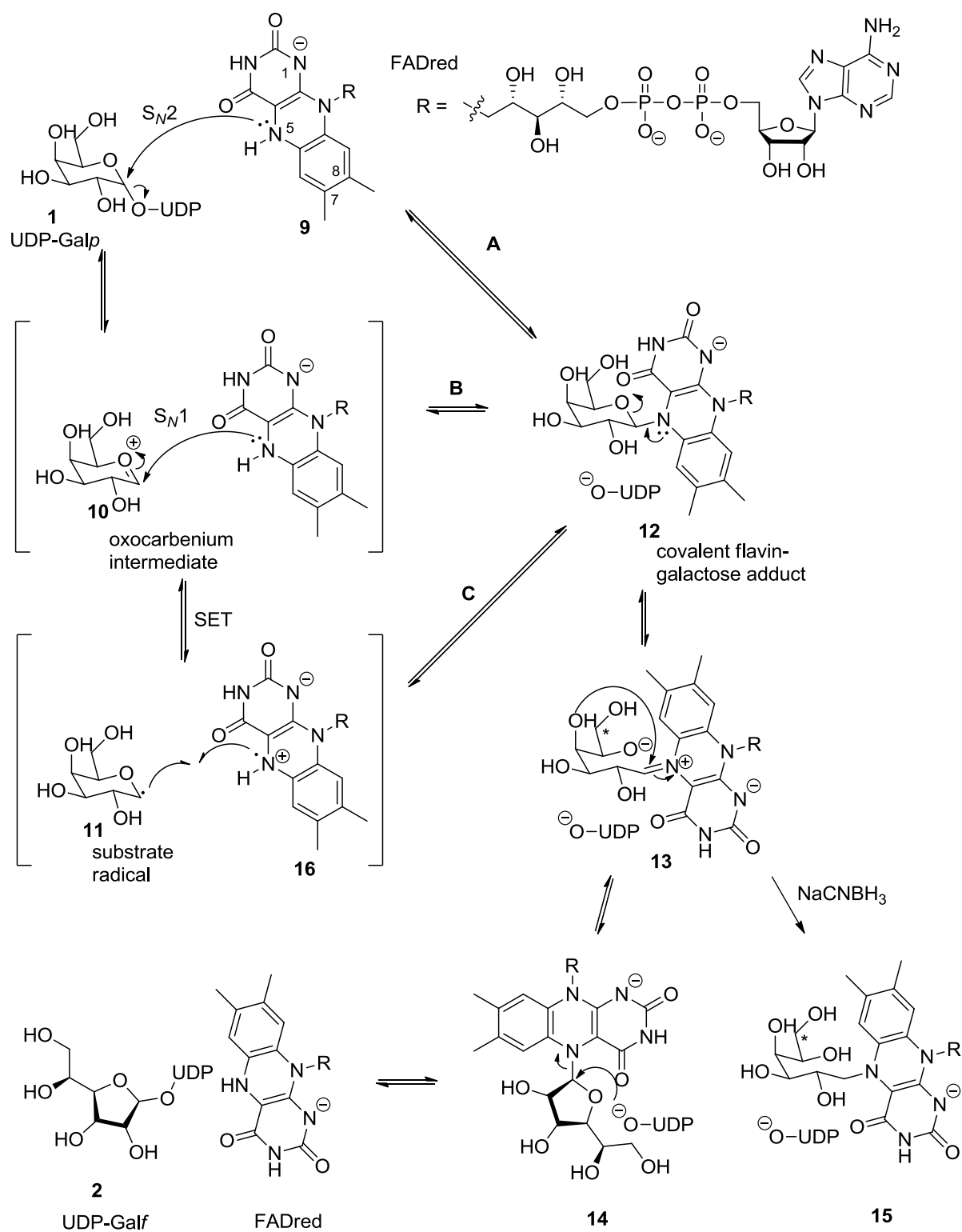
Recently, a proposal for the catalytic mechanism of UGM was reported by Soltero-Higgin *et al.* (Scheme 7, path A).³³ They concluded that only reduced UGM is catalytically active, and the N5 position is only nucleophilic when the FAD is in the reduced state. Thus, the FAD_{red} is being utilized in the catalytic mechanism.

Soltero-Higgin *et al.* also established that the lone pair of electrons at the N5 position of FADH^- is involved in the generation of flavin-derived iminium ion **13** (Scheme 7). This putative intermediate **13** was trapped by treating UGM with radiolabelled UDP-Galp (C6 is radiolabelled, Scheme 7) and sodium cyanoborohydride (NaCNBH_3), and a radiolabelled flavin-galactose adduct **15** was monitored. This adduct was confirmed to be an N5-galactose flavin (**15**) from the ultraviolet-visible spectroscopy and mass spectrometry obtained. The observation of **15** proved that the interconversion of the pyranose and furanose form occur via flavin-derived iminium species **13**.

According to the mechanism proposed (Scheme 7), these intermediates (**12** and **14**) are formed through the nucleophilic attack by N5 of FAD_{red} on the anomeric carbon of **1** (or **2**) with the concerted cleavage of the glycosidic (C1-UDP) bond, which is a typical S_N2-type substitution. Alternatively, **12** and **14** can also be generated through S_N1-type substitution, where elimination of UDP to generate an oxocarbenium intermediate **10** precedes the nucleophilic attack by N5 of FAD_{red}. Nevertheless, the precise protonation state of N1 on each intermediate is still imprecise.^{33,56}

Sun *et al.* summarized three mechanistic hypotheses (Scheme 7) of UGM that were published in previous literatures.⁵⁷ Path A and path B are the mechanisms suggested by Soltero-Higgin *et al.*³³ Alternatively, formation of **12** and **13** may take place through SET from FAD_{red} that is facilitated by the electron-deficient nature of **10** (path C). A radical pair (**11** and **16**) is formed.

The investigation carried out by Sun *et al.* using PIX and linear free energy relationships (LFERs) illustrates that S_N2-type displacement (path A) of UDP from the substrate by N5 of FAD_{red} is preferable.⁵⁷ The findings also prove the nucleophilic participation of FAD_{red} during the UGM catalysis. Thus, they suggested that future development of UGM inhibitors could utilize analogues that specifically target the nucleophilic addition.⁵⁷

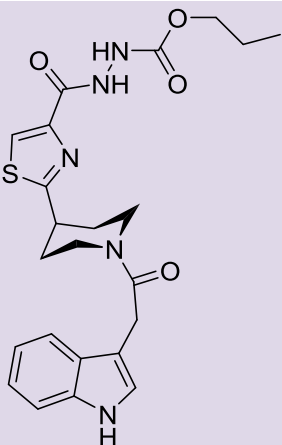
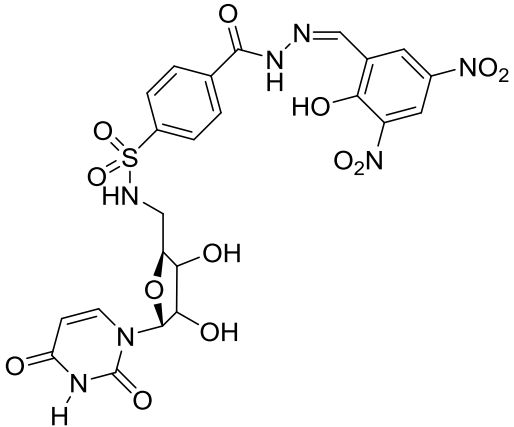


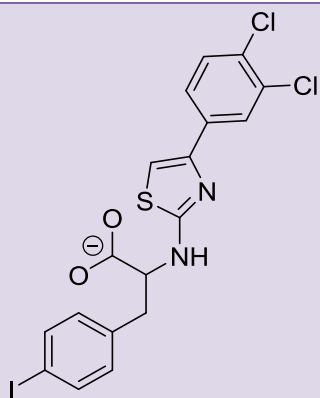
Scheme 7 Proposed mechanism for the interconversion of UDP-Galp and UDP-Galf. A radiolabelled substrate (asterisk, radiolabelled position) can serve as a mechanistic probe. Species 13 was expected to be reduced by NaCNBH_3 to produce N5 galactose flavin.⁵⁷

1.3.3 UGM inhibitors reported in literatures

Several compounds have been designed, synthesised and tested as potential inhibitors against different UGM from different bacteria. A few of these inhibitors have displayed very good inhibitions toward UGM. They include the substituted 2-aminothiazoles, thiazolidinones and pyrazole.^{58,}
⁵⁹ Some of the UDP-sugar substrate based,⁶⁰ nucleotide based,^{42, 61} and non-substrate based^{33, 62} analogues have been develop as UGM inhibitors too. However, only some of these analogues have shown good inhibitory activity against UGM. Following are a few example of the inhibitors found in previous studies together with their inhibitory activities (Table 2).

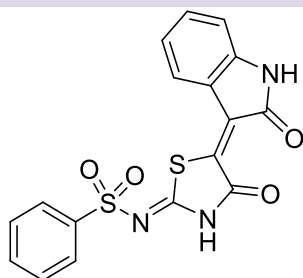
Table 2 Examples of compounds with their inhibitory activity.

Inhibitors	Testing	References
	<p>This indole analogue has been tested against UGM from different species by a HPLC assay. The conversion of UDP-Galp to UDP-Galp, in the presence and absence of inhibitor was monitored. The percentage inhibition at 1 mM of the inhibitor tested against kpUGM was 86%, while the half maximal inhibitory concentration (IC₅₀) tested against kpUGM and mtUGM were 1.0 μM.</p>	<p>Partha <i>et al.</i>⁴²</p>
	<p>This uridine-based compound was examined using a microtiter plate assay against ecUGM. IC₅₀ = 6.0 μM. However, this compound is inactive against mtUGM.</p>	<p>Scherman <i>et al.</i>⁶¹</p>



This 2-aminothiazole analogue has been tested against mtUGM using high-throughput fluorescence polarization (FP) assay.

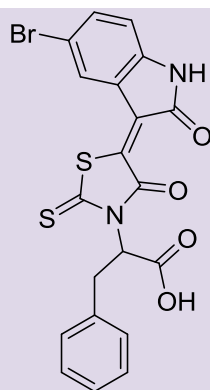
$K_d = 7.4 \mu\text{M}$; % inhibition at 50 μM of inhibitor = 82%.



FP assay and HPLC assay were used to examine this inhibitor against kpUGM.

$K_d = 4.0 \pm 0.7 \mu\text{M}$; *al.*⁵⁶

$IC_{50} = 17 \mu\text{M}$.



FP assay was employed to test this thiazolidinone analogue against kpUGM and

mtUGM. $K_d = 4.3 \pm 0.7 \mu\text{M}$ and $6.1 \pm 0.5 \mu\text{M}$, respectively.

1.4 Aims

As discussed earlier, *D*-Galactofuranose (*Gal_f*) residues are vital component of the arabinogalactan complex found in the cell walls of pathogenic microbes such as MTB, and are crucial for their viability. UGM is a unique flavoenzyme that involved in the biosynthesis of *Gal_f*. It catalyses the reversible conversion of UDP-*Gal_p* and UDP-*Gal_f*. The latter is the activated precursor of *Gal_f* residues.

UGM is targeted for developing novel antibacterial agents due to the importance of UGM in mycobacterial growth. Moreover, the absence of UGM and *Gal_f* residues in humans also make UGM a potential drug target for developing new TB therapeutic drugs that are potentially more effective and less toxic to human cells.^{59, 63}

Efforts have been made in designing a number of nucleotide-based, sugar-based and non-substrate based compounds to inhibit UGM. However, only a few of these have shown inhibitory activity towards UGM. Most of these compounds are reversible competitive inhibitors with low binding affinities. Both sugar-based and nucleotide compounds exhibit poor pharmacokinetics due to their polarity.^{42, 56, 61, 62} Thus, there is clearly a need to design more drug-like inhibitors of novel therapeutic targets such as UGM.

Previously, the Thomas group identified a few novel inhibitors of UGM by structure-based Virtual Screening, which was performed by Dr Ali Sadeghi-Khomami.^{42, 64} It was reported that inhibitors with indole analogue **17** (Figure 16) exhibited more than 80% inhibitory activity

towards UGM at 1mM and IC_{50} value of 1.0 μ M, when tested against kpUGM.⁴²

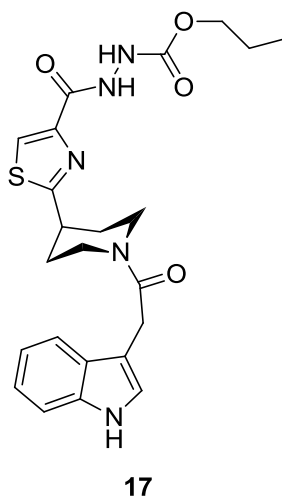


Figure 16 Inhibitor reported by K. Partha et al.⁴²

The aim of my project was to synthesize a series of potential inhibitors, and then *in silico* evaluation of these inhibitors would be performed against UGMs from different species using GOLD, and if time permitted biological evaluation. The crystal structure of drUGM (PDB code: 3HDQ) was to be used for the initial docking experiments. Once this has been achieved, docking of the inhibitors against other species of UGMs, such as kpUGM, mtUGM and ecUGM could then be performed to further evaluate binding mode(s) of the inhibitions.

To determine the potency of these inhibitors, enzyme inhibition assays will be carried out by conducting HPLC assay⁴² and FP assay⁶² in order to determine the percentage inhibition, IC_{50} , and K_d values of these inhibitors. HPLC analyses of these inhibitors will be performed to determine their purity prior to the enzyme inhibition assays.

2 Results & Discussions

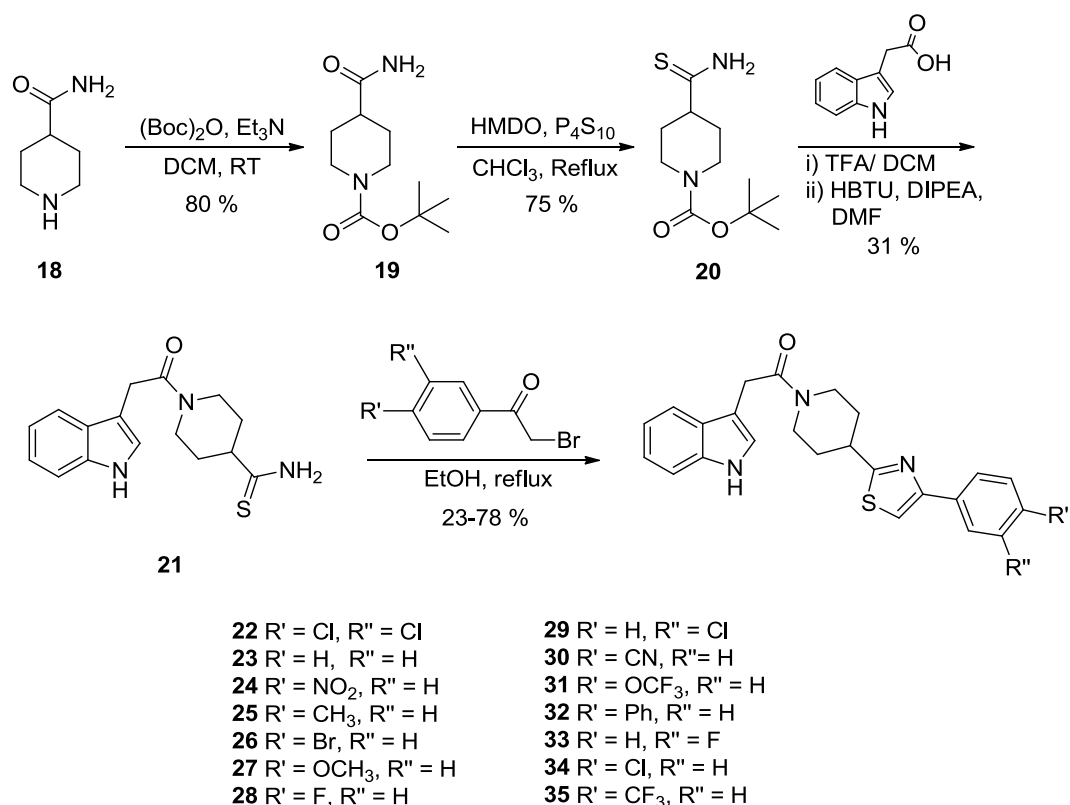
Structure-based virtual screening of the ChEMBL⁶⁵ database was performed by Alex Wichlacz.⁶⁶ Hit compounds identified by this screening process are shown to exhibit promising inhibitory activity towards UGM. One of the compounds with the best hit, which is **22** has been synthesized. The R groups were then alternated with various functional groups to produce a series of different analogues (**23-35**), in order to optimize the binding affinity to the active site of UGM.

In this project, fourteen indole-thiazole based analogues (**23-35**) have been synthesised, each in four steps: protection step; thionation step; deprotection, and amide coupling step; Hantzsch Thiazole synthesis. The reactions were monitored by thin layer chromatography (TLC) and mass spectrometry (MS) to ensure that the starting materials were fully consumed. These analogues were successfully purified using recrystallisation and flash column chromatography. Characterisation of these analogues was performed by utilising MS, NMR, and infrared spectroscopy (IR). The synthesis of some additional inhibitor was attempted, however due to time limitations, these syntheses were not completed.

HPLC analyses have been carried out to determine the purity of the analogues synthesised. At the same time, *in silico* studies of these analogues have been performed to predict their binding positions, binding affinities, and interactions against UGM.

2.1 Chemical synthesis

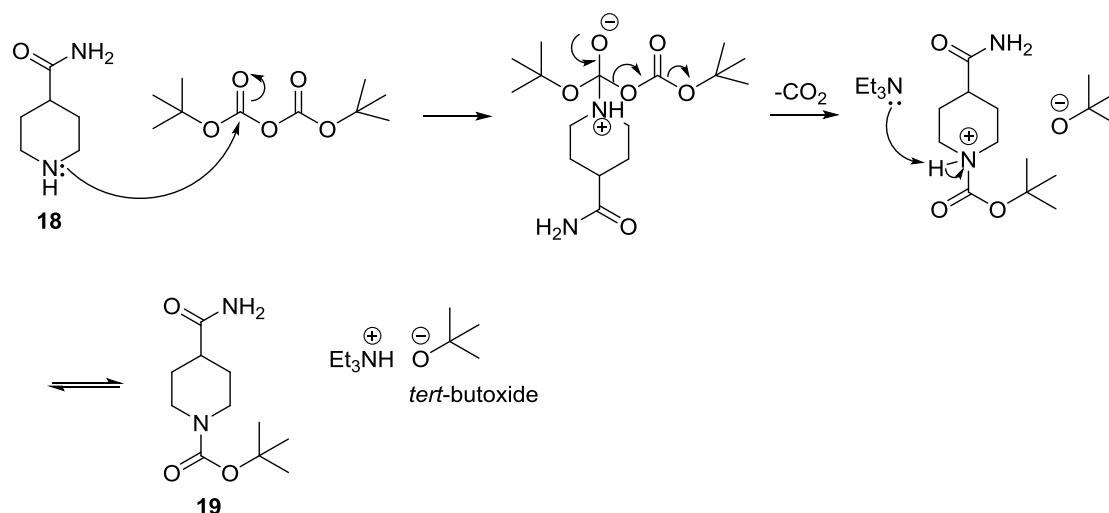
The series of analogues (**22-35**) were synthesised following the route shown in Scheme 8. The route was established previously in the Thomas group for the synthesis of indole analogue **17** (Figure 16).



Scheme 8 Synthesis route of the analogues.

The synthesis was started with the protection of isonipecotamide (**18**) using the *di-tert*-butoxycarbonyl (BOC) group. The reaction mixture was initially a white suspension, and it turned into a colourless solution after 4 hours of stirring with *di-tert*-butyl dicarbonate at ambient temperature. The physical change in the reaction mixture shows that the reaction was proceeding as **18** was found to be insoluble in organic solvents especially dichloromethane and chloroform. With the protecting BOC group added, this compound dissolved in organic solvents. Extraction of the reaction

solution with 1M HCl and brine was enough to produce a pure **19** as a white solid with a good yield of 80%. The product was confirmed by the presence of *tert*-butyl group singlet peak at 1.46 ppm in the ^1H NMR spectrum (section 4.2.1.1). The reaction mechanism of the BOC protecting step is shown in Scheme 9.



Scheme 9 BOC protecting reaction mechanism.

This amine protection reaction has been achieved with the use of catalyst, 4-dimethylaminopyridine (DMAP). However, the yield obtained by using DMAP (61%) was lower comparing to the reaction using triethylamine (80%). Hence, the amine protection reaction using triethylamine was preferable.

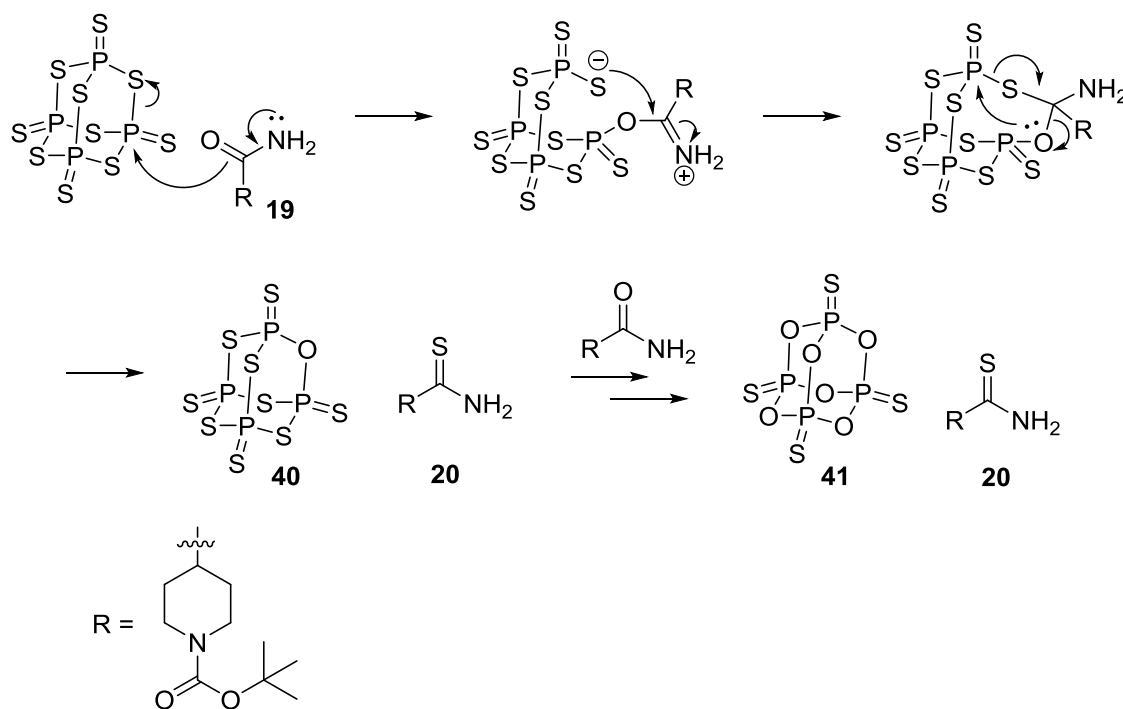
The protection step was followed by the thionation of **19** in the presence of diphosphorus pentasulfide (P_4S_{10}) to form **20**. The combination of P_4S_{10} and hexamethyldisiloxane (HMDO) could efficiently convert amide **19** to carbothioamide **20**. This thionation step has been previously achieved using Lawesson reagents (LR) in the Thomas group. However, a very low yield of product was obtained compared to thionation using

P_4S_{10} /HMDO. Additionally, the phosphorus-derived by-products (**42** and **43**, Scheme 11) could be easily removed by simple aqueous workup, rather than by flash column chromatography, as required in LR reaction. Thus, thionation using P_4S_{10} /HMDO was preferable.

Curphey reported that DCM, chloroform or benzene are the best solvents for thionations using P_4S_{10} / HMDO as they gave better yields.⁶⁷ Thus, in this thionation step, **19** was stirred under reflux in chloroform together with HMDO and P_4S_{10} for 3 hours. HMDO acts to increase the solubility of P_4S_{10} in reaction solvents. Following this, the solution was cooled to 0 °C before 5.3 M potassium carbonate solution, water and acetone were added. The reason for adding water was to hydrolyse the expected by-products, which are trimethylsilylated phosphates and thiophosphates (**42** and **43**, Scheme 11) to the corresponding acids. The resulting acids were water-soluble, and could be readily removed by water extraction. However, the reaction solvent used is immiscible with water. Hence, acetone was added to act as co-solvent in order to create a monophasic solution. As for 5.3 M potassium carbonate solution, it was used to buffer the reaction mixture, so that the strongly acidic conditions caused by hydrolysis of by-products could be avoided.

The last step was the hydrolytic workup of the reaction solution to remove the reaction by-products and yield **20** as a clean oily yellow solid. The 1H NMR of **20** looked similar to **19**. However, the formation **20** could be confirmed by IR and MS. The IR spectrum showed a strong absorption in the thioketones region (1169 cm^{-1}). The reaction mechanism of the

thionation is shown in Scheme 10. Besides, the presence of the Boc methyl groups would also be a diagnostic indicator of **20**.

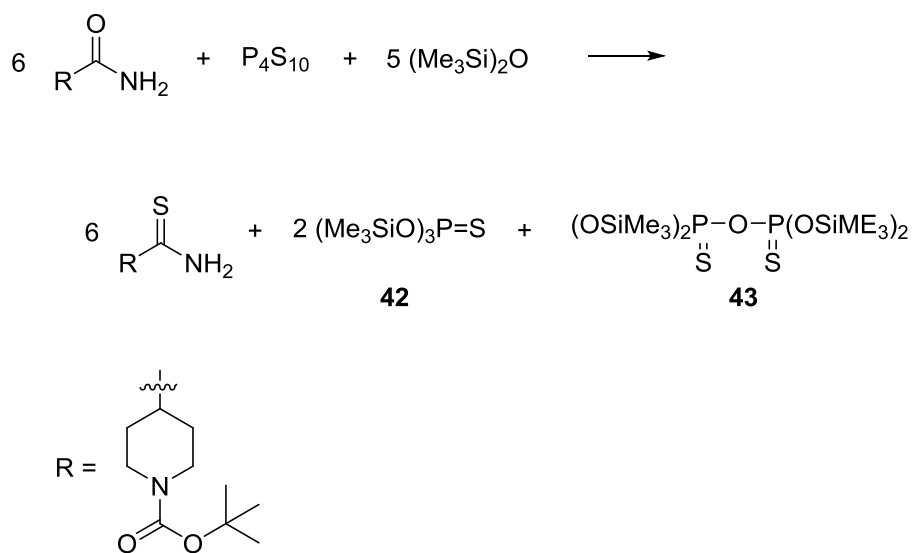


Scheme 10 Thionation reaction mechanism.

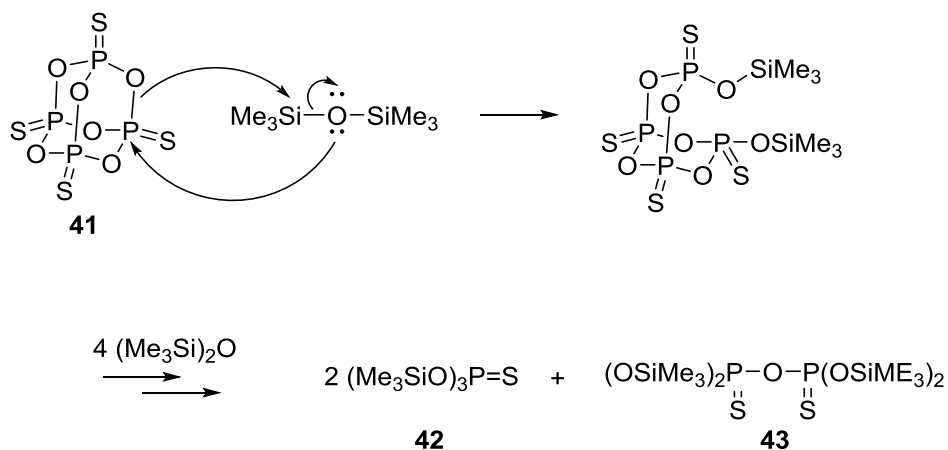
As shown in Scheme 10, the P_4S_{10} initially reacts with **19** to generate the thiocarbonyl intermediates, which yield **20** and species **41**. Subsequently, **41** was reacted with HMDO to give soluble by-products, **42** and **43** (Scheme 11).

Curphey summarised the overall stoichiometry of the thionation reaction, which is shown in Scheme 11. This stoichiometry could be explained in two stages. The first stage involved the atoms exchange of the six bridging sulphur atoms with oxygen, leaving one atom of sulphur per phosphorus, giving structure **41**. At the same time, 6 molecules of carbonyl **19** were converted into thiocarbonyl **20**. At the second stage, five of the six P-O-P units in **41** reacted with five equivalent of HMDO in

the manner shown in Scheme 12. At the end of the reaction, one equivalent of diphosphate **43** was produced and the other two phosphorus atoms appeared as monophosphate **42**.⁶⁷



Scheme 11 The overall stoichiometry of the thionation reaction.⁶⁷

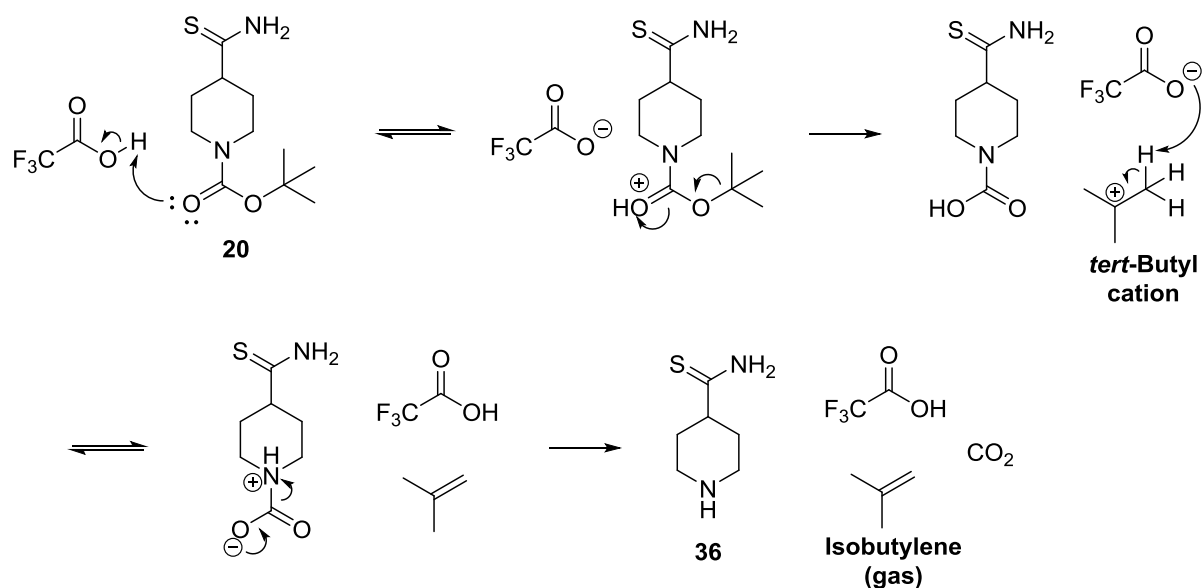


Scheme 12 Reaction of HMDO.

The removal of the BOC group using trifluoroacetic acid (TFA) in DCM was achieved after the thionation step, following by the amide coupling to 3-indoleacetic acid in the presence of HBTU and *N,N*-diisopropylethylamine (DIPEA) in DMF. The deprotection step was

monitored by MS to assure the completion of the reaction was achieved. The reaction solvent was co-evaporated with chloroform in order to azeotropically remove TFA. The resulting brown residue was dried over phosphorus pentoxide under vacuum to remove water, to prevent a side reaction in amide coupling step.

The reaction mechanism of the BOC deprotection is shown in Scheme 13. During the reaction, the *tert*-butyl cation was formed. Deprotonation of the cation form isobutylene, which is a gas. TFA was regenerated at the end of the reaction and CO₂ gas was liberated. The crude product formed (**36**) was carried forward straight to the amide coupling step without the need for purification.



Scheme 13 BOC deprotection reaction mechanism.

Coupling agents play an important role in amide bond syntheses. One of the common amide coupling agents is HBTU. HBTU was first reported in its *O*-isomer form (**37**, Figure 17). Nevertheless, Carpino *et al.* disclosed

the structure of the active HBTU as the *N*-isomer (**38**, Figure 17) rather than *O*-isomer by X-ray crystallography.⁶⁸

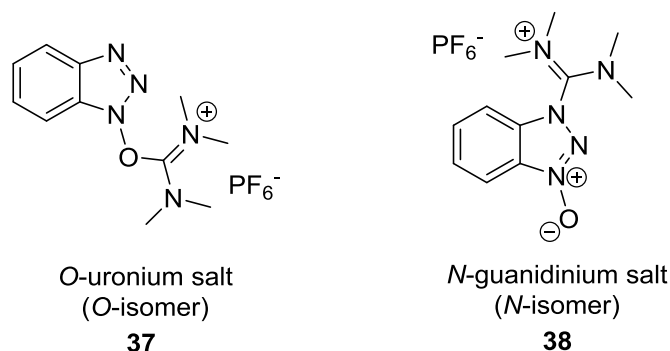


Figure 17 Uronium and guanidinium isomers.

In the amide coupling step, deprotected secondary amine **36** (Scheme 13) was stirred in DMF with HBTU, DIPEA, and 3-indoleacetic acid to yield **21**. DMF was used as the reaction solvent as HBTU possessed good solubility in this solvent. Tertiary amine, DIPEA was chosen as the base in this amide coupling reaction due to its non-nucleophilic property. Also, DIPEA would not cause any degradation on HBTU.

DIPEA acted to deprotonate 3-indoleacetic acid. After that, the coupling reagent, HBTU reacted with deprotonated acid to form active ester, which then reacted with secondary amine to form product **21**. The by-products formed were then removed by extraction and flash column chromatography to yield product **21**. HOBT and DIPEA salts were removed by aqueous sodium hydrogen carbonate wash. The reaction mechanism is shown in Scheme 14.

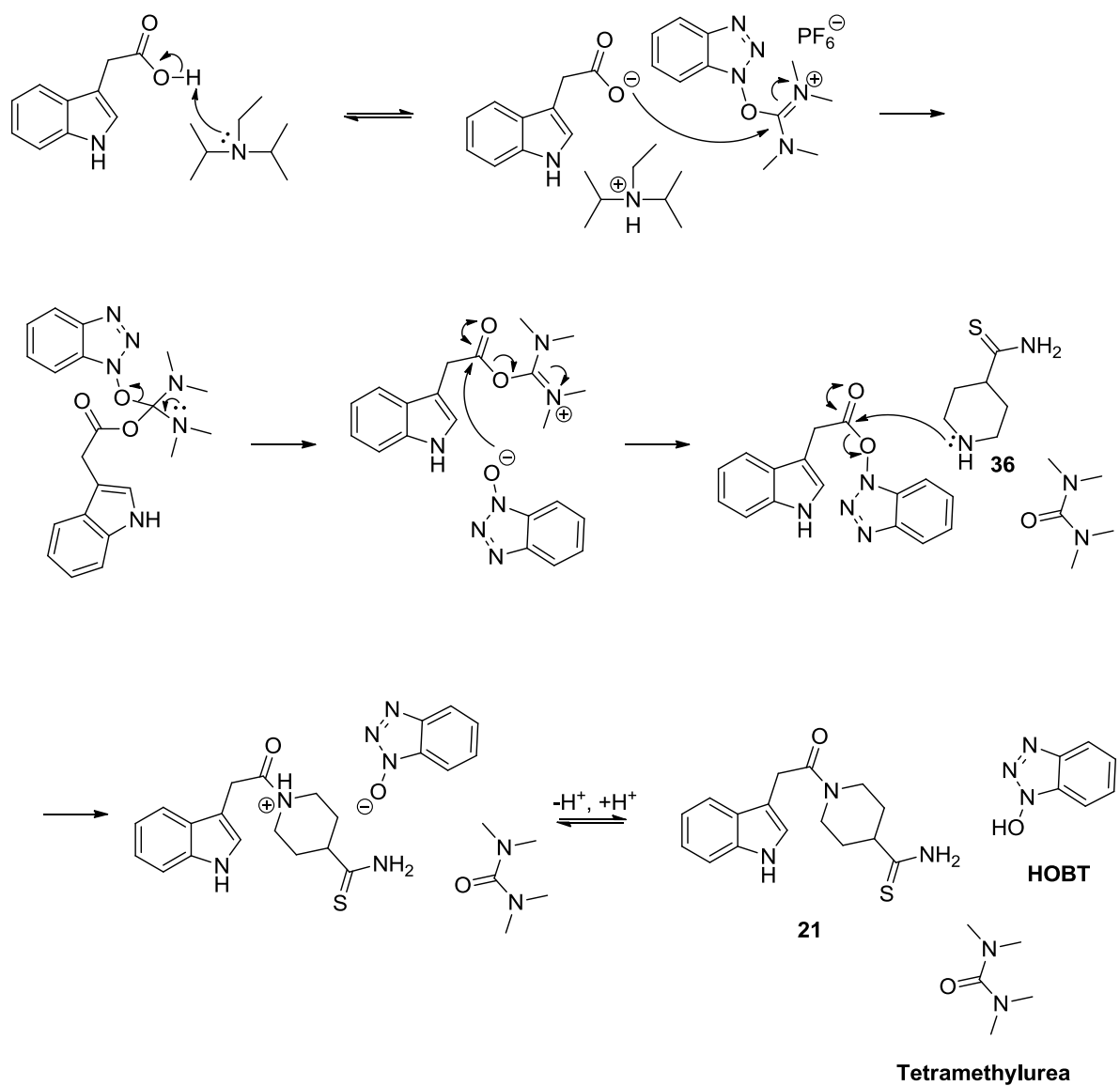
The yield obtained in this reaction was 31%, which is fairly low. This is because the coupling involves a secondary amine (piperidine) and hence was more difficult, due to steric hindrance.

This amide coupling reaction has been initially conducted on a small scale (3.0 g) experiment. It was observed that the scaled up experiment (6.0 g) gave a higher yield (31%) comparing to the small scale experiment (3%).

There has been a difficulty in purifying the crude product when the reaction was being scaled up. Co-elution of the product with the impurities was observed when silica chromatography was carried out. The solvent system used (ethyl acetate: acetone; 99:1) was previously established in the Thomas group. However, the crude product has been successfully purified by the use of the alternative solvent system (ethyl acetate).

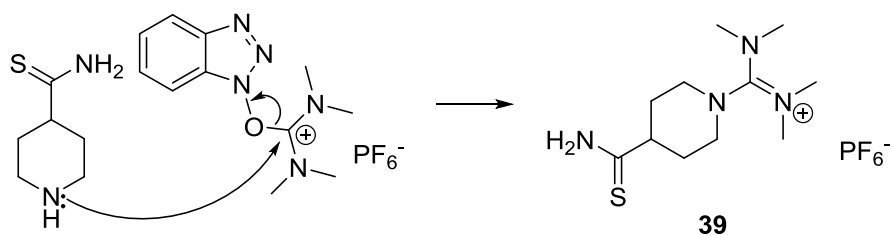
A small amount of the partially purified product has been used in the Hantzsch thiazole synthesis (Scheme 16). However, based on the MS obtained, an unknown impurity appeared to be the major peak compared to the desired product peak, which showed that the substituted 2-bromoacetophenone reacted more readily with the impurity than product **21**. Therefore, purified product **21** has to be used in the next step.

The reaction duration of this amide coupling step is important. An additional TLC spot ($R_f = 0.50$), which is an unknown impurity was observed when one of the reaction batches was left stirring under ambient temperature for 68 h rather than 23 h.



Scheme 14 Amide coupling reaction mechanism using HBTU.

During the amide coupling step, a side reaction might take place when amine (**36**) reacted with HBTU to produce guanidinium by-product (**39**, Scheme 15). This might be one of the reasons why the yield of the product in this reaction step is low.



Scheme 15 Formation of guanidine side product.

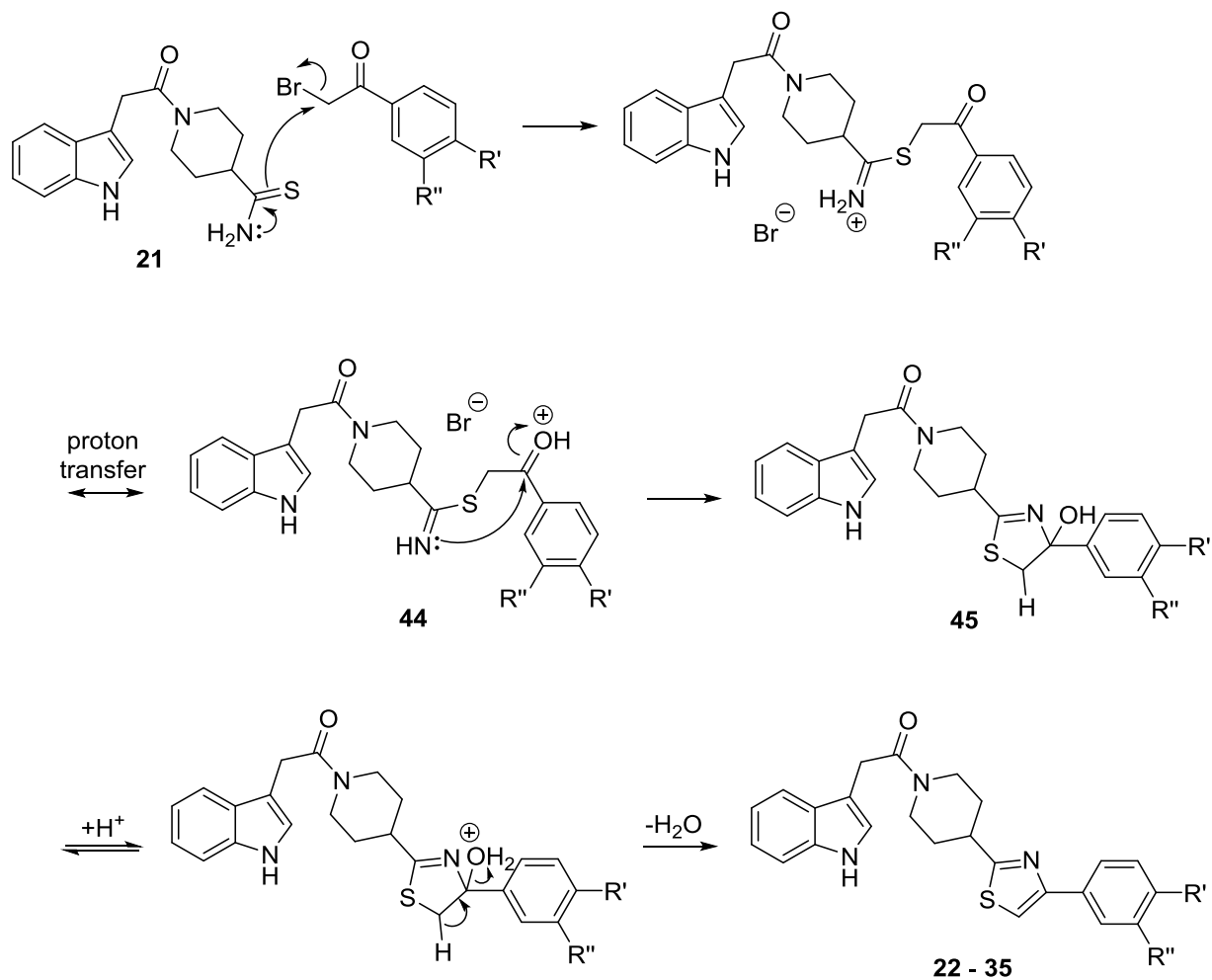
A series of indole analogues (**22-35**) were prepared *via* Hantzsch thiazole synthesis. This synthesis involved condensation of α -haloketones with thioamide. This was achieved by dissolving **21** and substituted 2-bromo-acetophenone in ethanol and stirred under reflux for 3-4 hours.

Many attempts have been approached in purifying the crude product. A first attempt was to purify the crude product *via* gradient flash column chromatography on silica using DCM:MeOH (0-5% v/v) as eluent without any workup being performed. However, most of the products collected were impure, except for analogue **22**. In some cases, fractions collected (**24**, **25**, and **27**), were recrystallised from hot methanol.

After that, extraction was attempted before the flash chromatography using the same solvent system (DCM: MeOH), but no improvement was observed. Therefore, different solvent systems for the silica purification were explored, and the optimal solvent system, DCM: EtOAc (1: 1) was used to purify the rest of the analogues.

The yields obtained for these analogues were between 23-78%. The low yield of some analogues was because the analogue has been purified twice (silica chromatography and recrystallisation) in a step.

In Hantzsch thiazole synthesis mechanism (Scheme 16), the first step is the nucleophilic displacement of bromide by thioamide to produce intermediate **44**. The ketone is then attacked by the nitrogen nucleophile to form a cyclic hydroxyl intermediate **45**. The removal of water in the last step furnishes the final products (**22-35**).

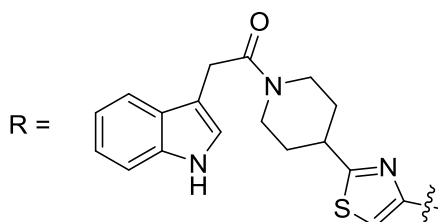


Scheme 16 Hantzsch thiazole synthesis mechanism.

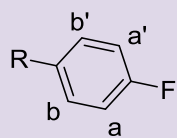
Formations of analogues (**22-35**) were confirmed and these were fully characterised using MS and NMR techniques. The noticeable difference between all these analogues in ¹H NMR spectra is the chemical shift of the aromatic protons in the region of 6.5-8.5 ppm. This is due to the effect of the functional groups (R' and R'') on the aromatic ring. The

protons are deshielded (higher frequency) or shielded (lower frequency) depending on the nature of the functional groups adjacent to them. The protons adjacent (a/a', Table 3) to the electron-withdrawing groups will be deshielded, while the protons adjacent to the electron donating groups will be shielded. The chemical shifts of the aromatic protons are shown in Table 3.

Table 3 NMR shifts of the aromatic protons influenced by different functional groups adjacent to them.



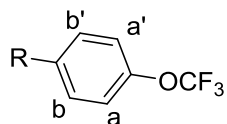
Compounds	δ_H (ppm)
24	$a/a' = 8.21$ (Figure 18 (a)) $b/b' = 7.98$
35	$a/a' = 7.98$ $b/b' = 7.65$
30	$a/a' = 7.96$ $b/b' = 7.69$
32	$a/a' = 7.93$ $b/b' = 7.46$



28

$$a/a' = 7.90$$

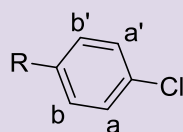
$$b/b' = 7.21$$



31

$$a/a' = 7.88$$

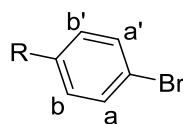
$$b/b' = 7.24$$



34

$$a/a' = 7.78$$

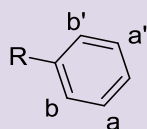
$$b/b' = 7.37$$



26

$$a/a' = 7.73$$

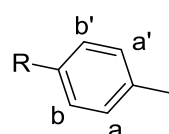
$$b/b' = 7.53$$



23

$$a/a' = 7.41$$

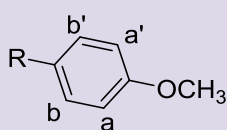
$$b/b' = 7.87$$



25

$$a/a' = 7.20$$

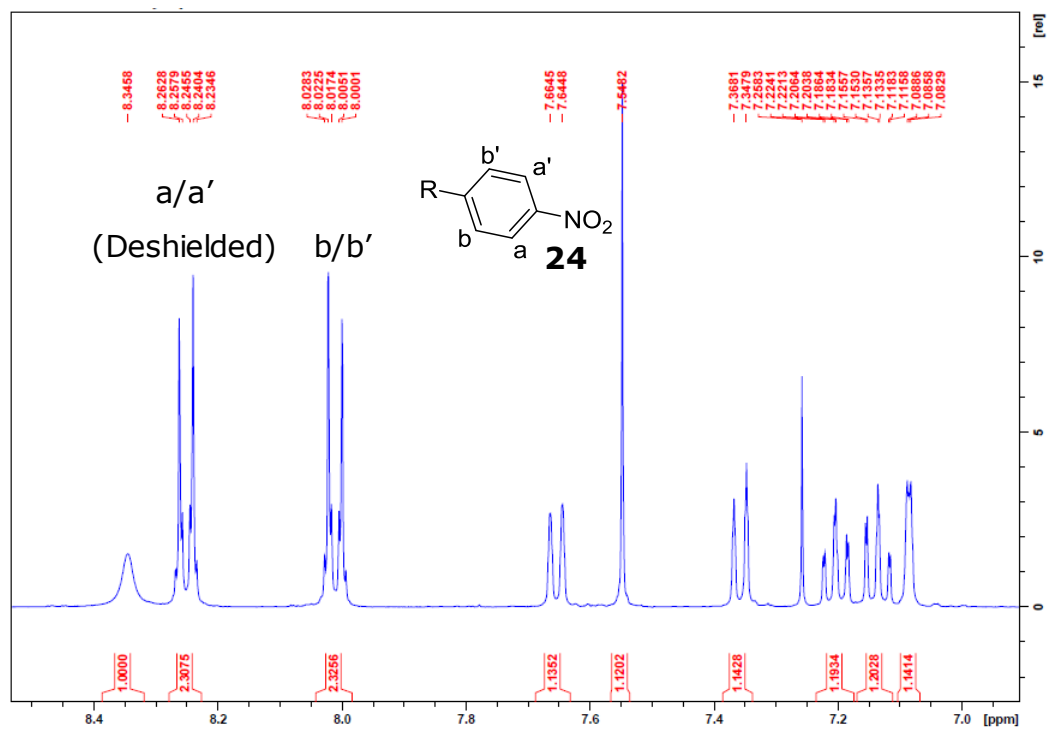
$$b/b' = 7.75$$



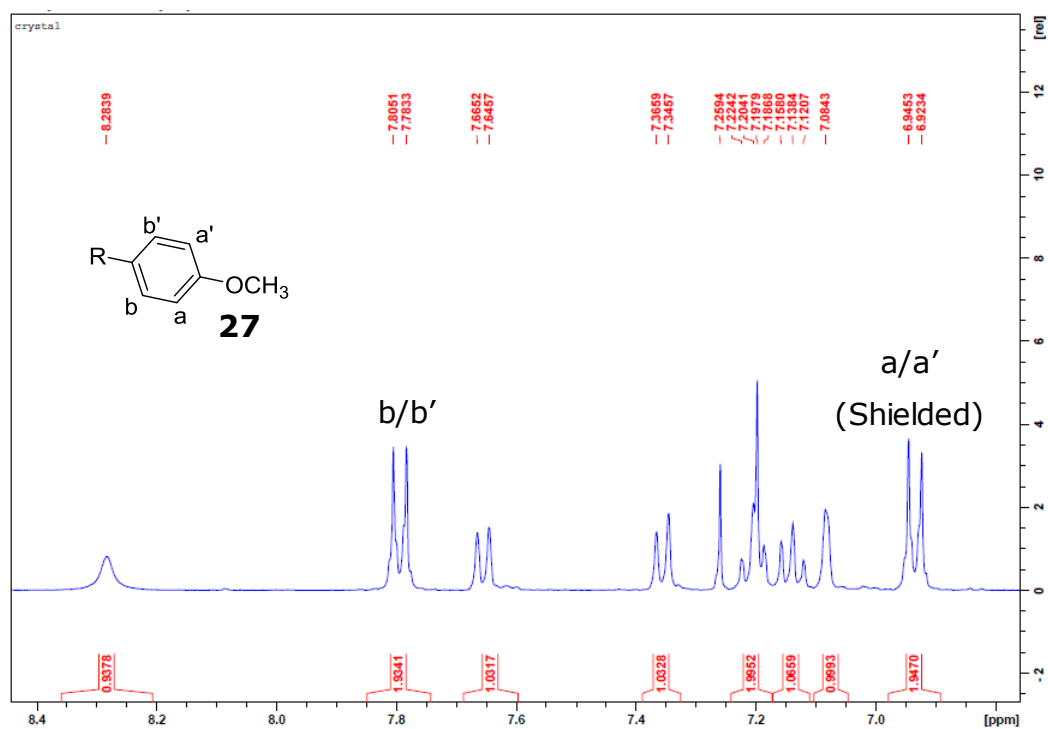
27

$$a/a' = 6.93 \text{ (Figure 18 (b))}$$

$$b/b' = 7.79$$



(a)



(b)

Figure 18 ^1H NMR spectra of (a) **24** and (b) **27** in CDCl_3 at 400 MHz, to show the effect of the substituted functional group to the chemical shifts (ppm).

Another analogue that we attempted to synthesise was **36** (Figure 19). The MS obtained showed the presence of the product. However, the purification of the crude product was difficult. Poor separation of the product and the impurities was observed when different solvent systems were explored. Solvent systems, DCM:MeOH (94:6) and EtOAc:DCM (1:1) gave a good separation, but the fractions collected after silica chromatography was conducted were impure. Due to time limitations, a pure product was not isolated.

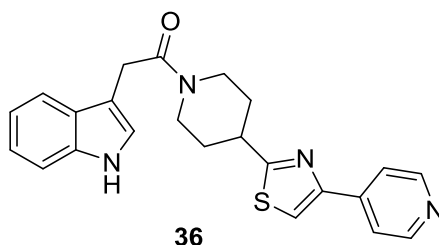
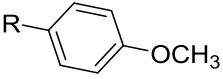
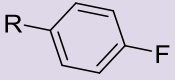
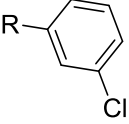
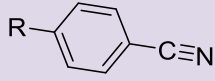
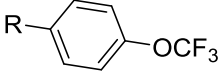
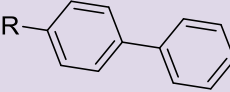
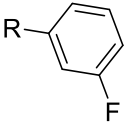
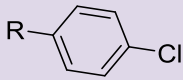
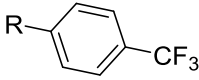


Figure 19 Analogue that was failed to be purified.

2.2 HPLC analysis of the analogues

The purity of the analogues synthesised (**22-35**) were determined by using analytical reversed phase high performance liquid chromatography (RP-HPLC) on a C18 analytical column (Eclipse, XDS-C18, 5 μ m, 4.6 x 150 mm) at ambient temperature (Figure 20). Details of the analysis method can be found in section 4.2.2.

Each of the analogues was dissolved in H₂O: acetonitrile (1:1 v/v). The time frame set per analysis was 20 minutes and the average retention time for the 14 analogues was between 14-17 minutes. The eluted peak was collected so that the content could then be confirmed by MS.

27		95
28		83
29		78
30		81
31		80
32		81
33		85
34		92
35		79

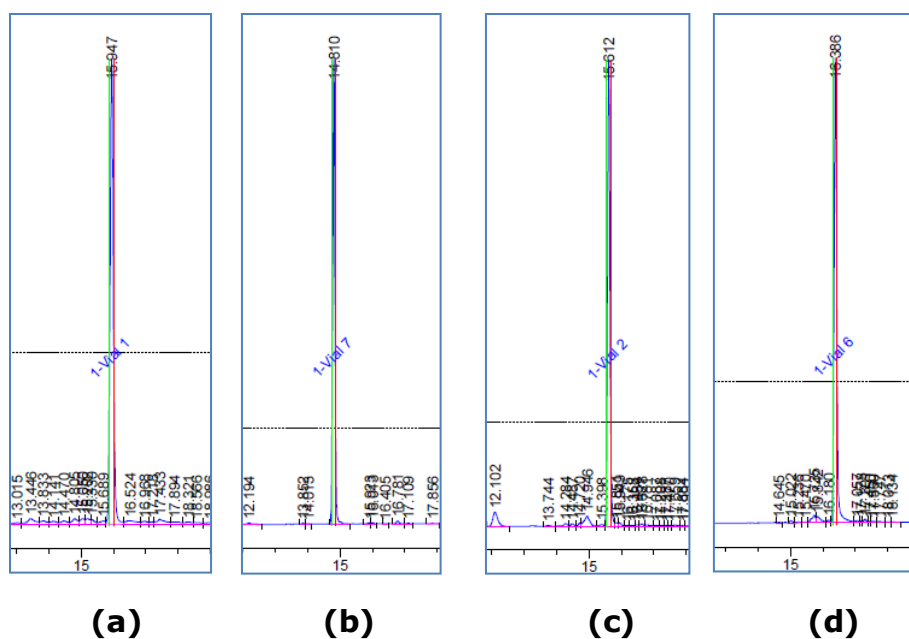


Figure 20 HPLC traces of the analogues, (a) 22; (b) 24; (c) 29; (d) 35.

2.3 *In silico* evaluation

In silico studies of the series of analogues was performed on the crystal structure of reduced drUGM (PDB code: 3HDQ)³⁶ using GOLD^{69, 70}. As mentioned earlier, UGM is catalytically active when it is in the reduced form. Also, reduced UGM has a threefold greater affinity for substrate than oxidized UGM (K_m values of 66 μM versus 220 μM), hence, the reduced form of UGM was chosen.³⁶ The crystal structure of drUGM_{red} was used for the docking experiments initially.

The crystal structure of the drUGM was obtained from the Protein Data Bank (PDB code: 3HDQ).³⁶ The analogues were sketched using Chemdraw and saved in SMILES file in order to be converted into 3D form in SYBYL 8.0 (Tripos International, 1699 South Hanley Rd., St. Louis, Missouri, 63144, USA). Both structures of the inhibitors and protein molecule were prepared using SYBYL 8.0. During the process of creating a 3D structure, the molecule might have unfavourable bond

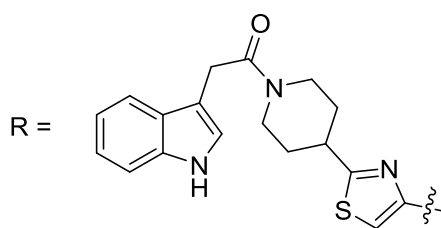
lengths, bond angles or torsion angles. Thus, the energy minimization step is important to generate molecules in their most stable conformation.

The active site was defined with reference to the binding of UDP-Galp. The coordination set to define the centre of the active site was $x = 24.1245$, $y = -106.2594$, and $z = 73.4552$. Then, the binding site radius was set to 10.0 \AA , so that the binding site will be defined as all atoms that lie within the radius of the specified point. Default parameters were used for docking studies and 5 poses were requested for each analogue.

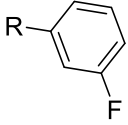
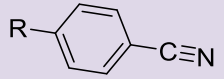
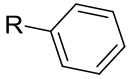
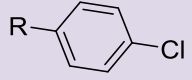
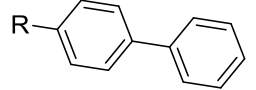
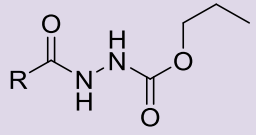
During the docking process, GOLD scored docking solutions according to the fitness function set at the start. In this case, Goldscore is the fitness function employed as it is the default fitness function provided in GOLD. This fitness function predicts the ligand binding positions by taking into account factors such as hydrogen bonding energy, van der Waals energy, metal interaction and ligand torsion strain. The scores obtained from the result of docking illustrate how good the poses were. Therefore, the higher the score, the better the docking results. The poses with the highest score were chosen in order to evaluate their binding position in the active site. The Goldscore obtained (Table 4) from the docking of 14 analogues were within the range of 79-86. By comparing to the Goldscore obtained for known inhibitor **17**, which is 77.5, these analogues are predicted to bind well into the active site of drUGM.

The images of the docking results were generated using PyMOL (The PyMOL Molecular Graphics System, Version 1.5.0.4 Schrödinger, LLC) in order to visualise the binding position.

Table 5 Docking result of the analogues.



Ranking	Inhibitors	Structure	Goldscores
1	24		85.2
2	29		85.0
3	22		84.4
4	31		84.1
5	27		83.9
6	25		83.7
7	35		83.2
8	26		82.0
9	28		81.7

10	33		81.4
11	30		81.4
12	23		80.3
13	34		80.1
14	32		79.5
15	17		77.5

Previously, Partha *et al.* has summarised the UGM active site into 3 regions: the uridine binding region; the diphosphate binding region; and the sugar binding region.³⁶ The uridine binding region consists of Phe176, Thr180, Trp184, Val199, and Tyr179. The diphosphate binding region was surrounded by Arg198, Arg305, and Tyr209. As for the sugar binding region, it was located close to isoalloxazine ring of FAD where it was surrounded by Pro84 and His109.

The binding of UDP-Galp and previously reported inhibitor 17 to the drUGM binding site are shown in Figure 21 to demonstrate the similarities and differences to the binding of the analogues (**22-35**).

Obviously, these analogues have similar structural features to those seen for **17**, except for the substituent of the thiazole ring.

However, the binding modes of the majority of these analogues are entirely different to **17**. The binding of the analogues, except **27** and **32**, are 180° relative to **17**, where the indole moiety of the analogues is pointing towards FAD isoalloxazine ring. This is because in this position, the indole moiety has more hydrogen interactions with the FAD isoalloxazine ring and Pro84, which may contribute to better inhibition comparing to other binding modes.

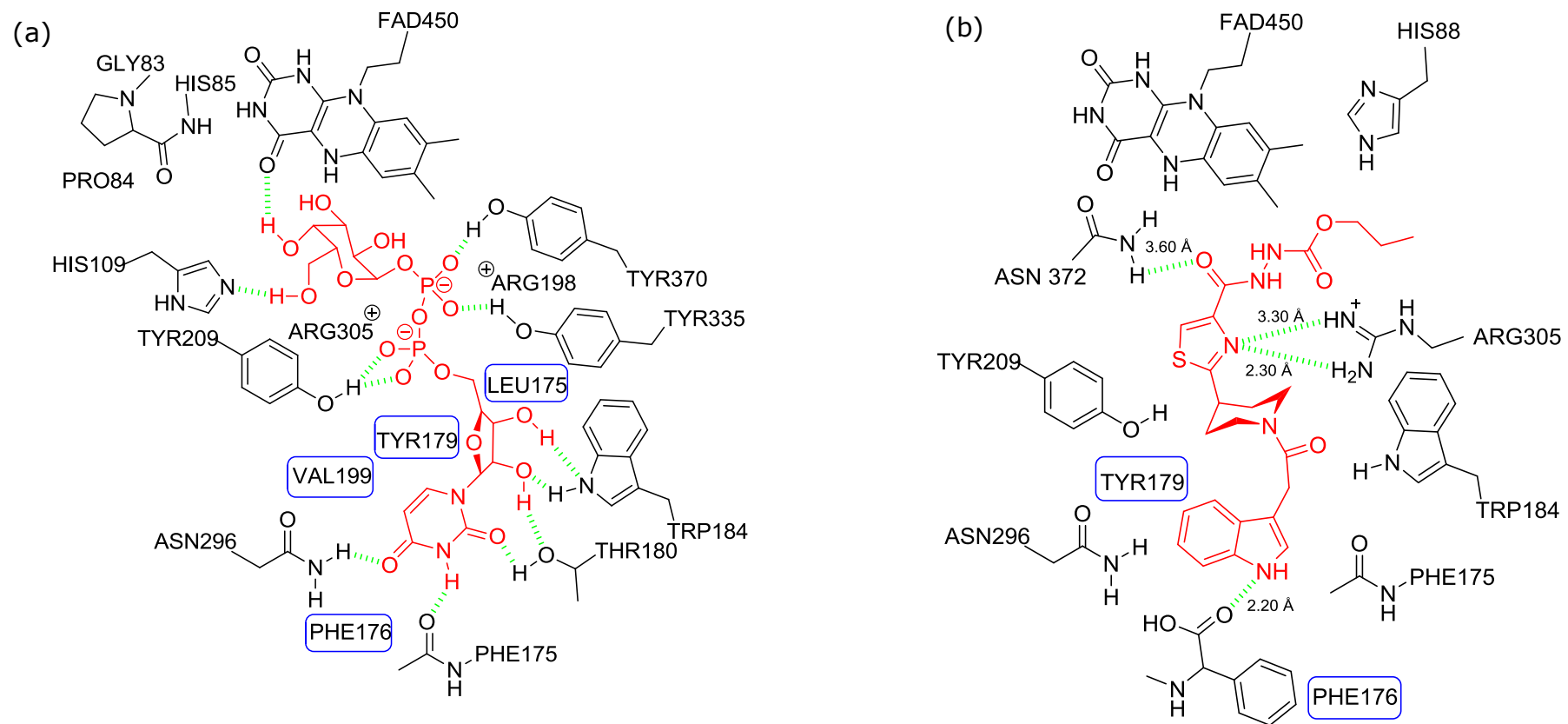


Figure 21 Chemdraw views of the binding of the substrate, (a) UDP-Galp and previously reported inhibitor, (b) 17 to the active site of drUGM.⁴² The hydrogen bond interactions to the amino acid residues are shown in green, and the π - π stacking/hydrophobic interaction are shown in blue boxes.

Based on the docking results obtained, it can be seen that all these analogues bind in the same binding mode as UDP-Galp (as mentioned earlier in section 1.3.1) in the active site of drUGM, which is a folded U-shaped conformation. The polar interactions between the inhibitors and the amino acid residues were generated as a dotted line, together with the bond distance. The strength of the hydrogen bonds is dependent on their bond distances. Jeffrey categorised hydrogen bonds with distances of 2.2-2.5 Å as strong, 2.5-3.2 Å as moderate, and 3.2-4.0 Å as weak.⁷¹ The bond strength might be affected by the charge transfer interaction between the electron-deficient substituted aromatic ring and the electron-rich indole ring at two end of all the analogues.

Analogue **24** appeared to have the highest score (Table 5) among the molecules. This is because it has more interactions to the amino acid residues compared to the others, including both hydrogen bonds and π - π stacking/hydrophobic interactions (Figure 22). It can be seen that most of the interactions occurred around the indole moiety, which is located in the sugar binding region. The indole NH has hydrogen bond interactions with OH of Pro84; carbonyl, and NH of FAD. The piperidine moiety is located in the phosphate binding region. The carbonyl group that connects the indole ring and the piperidine moiety has hydrogen bond interactions with the side chain of Arg305. The nitro substituted aromatic moiety is located in the uridine binding region. The nitro group is shown to form a hydrogen bond interaction with NH of Pro123. The only π - π stacking/ hydrophobic interaction can be found between the aromatic ring moiety and Phe176. Overall, analogue **24** has five hydrogen acceptors, one hydrogen donor and a π - π interaction.

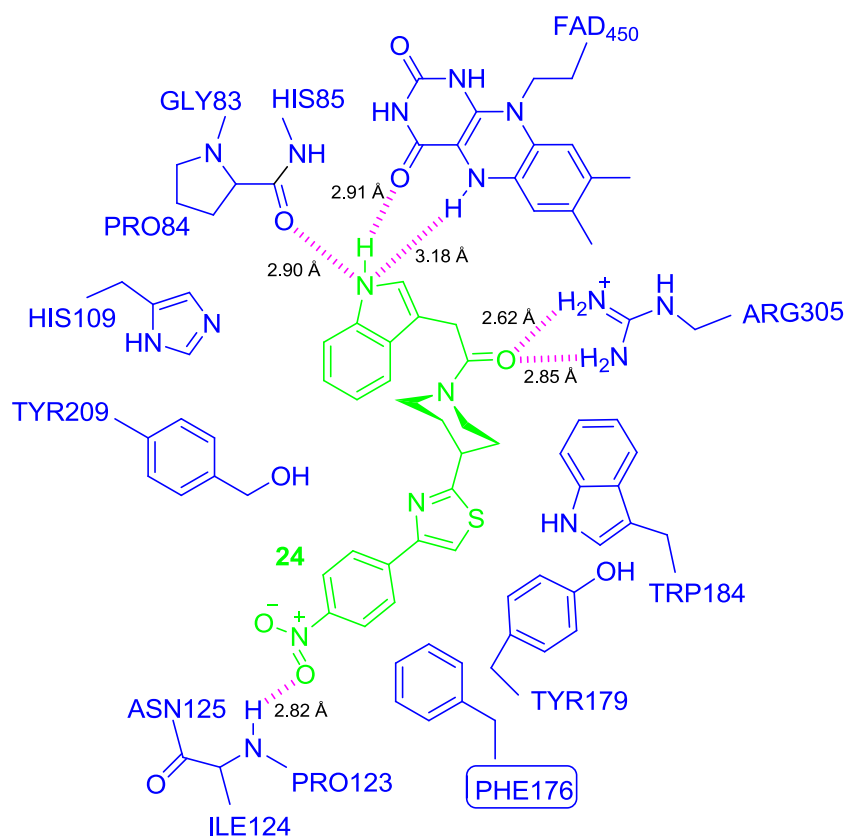
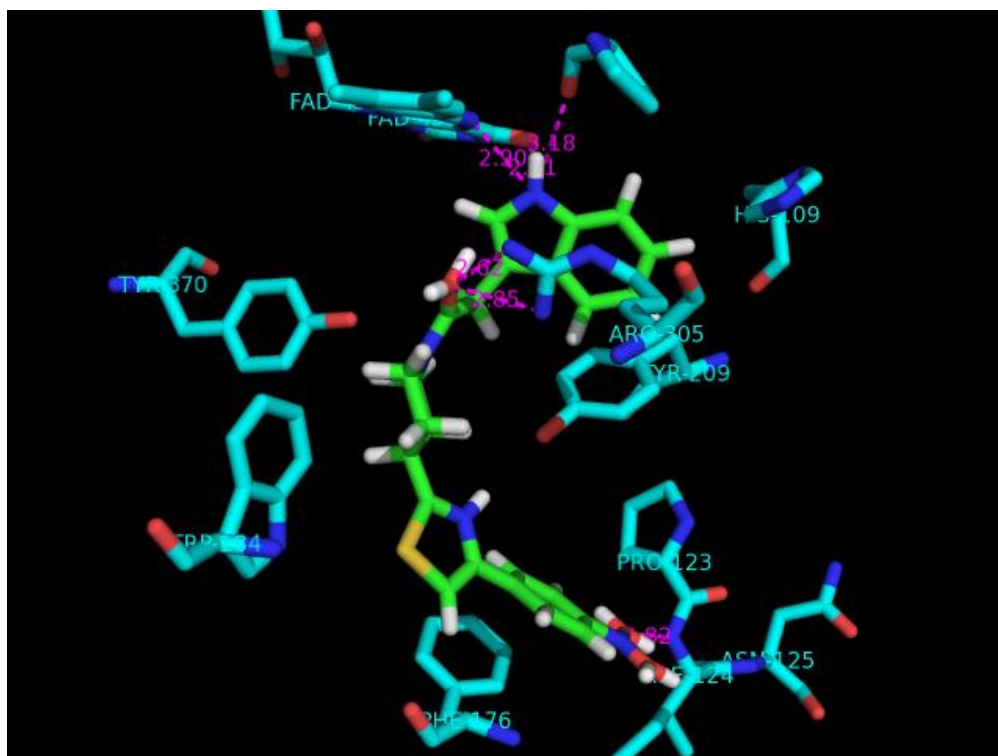


Figure 22 Stereo image and corresponding Chemdraw view of the binding of 24 to the active site of drUGM. The hydrogen bond interactions to the amino acid residues are shown in purple, together with bond distance, and the π - π stacking interaction is shown in box.

The rest of the analogues, except **27** and **32**, exhibit a similar binding mode to that of **24** in the active site. However, unlike **24**, the rest of the analogues do not show any hydrogen bond interaction between the aromatic substituents and the amino acid residues in the uridine binding region.

The binding modes of the selected analogues (**22**, **26**, and **29**) are shown in Figure 23, Figure 25, and Figure 24 respectively. **22** does not seem to have any hydrophobic interaction with the residues in the uridine binding region. This is because the aromatic moiety that is located in the uridine binding region is facing away from the aromatic side chain of Phe176 (Figure 23).

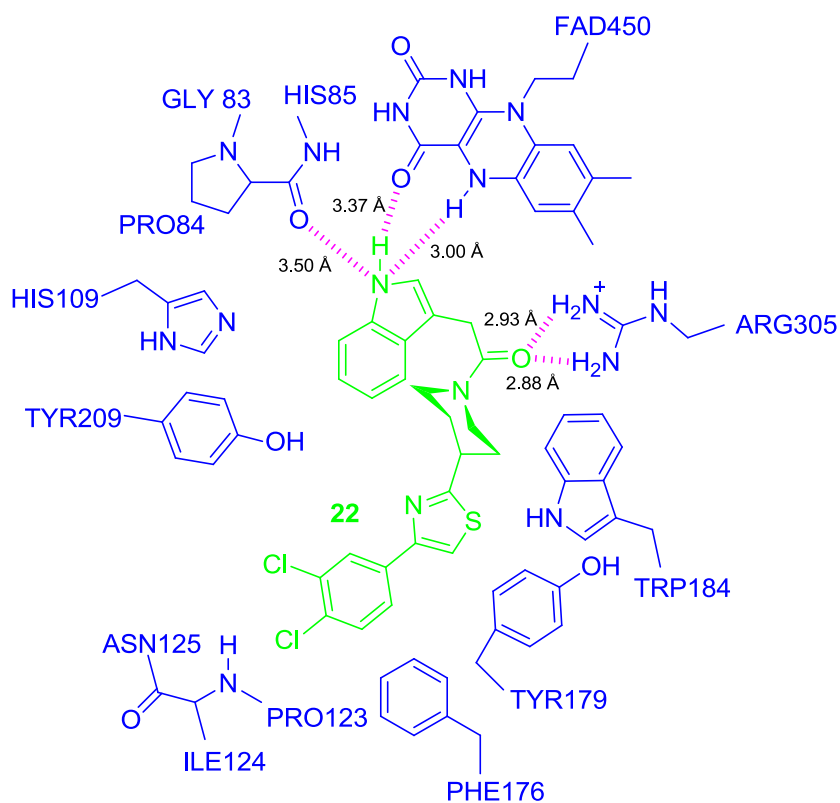
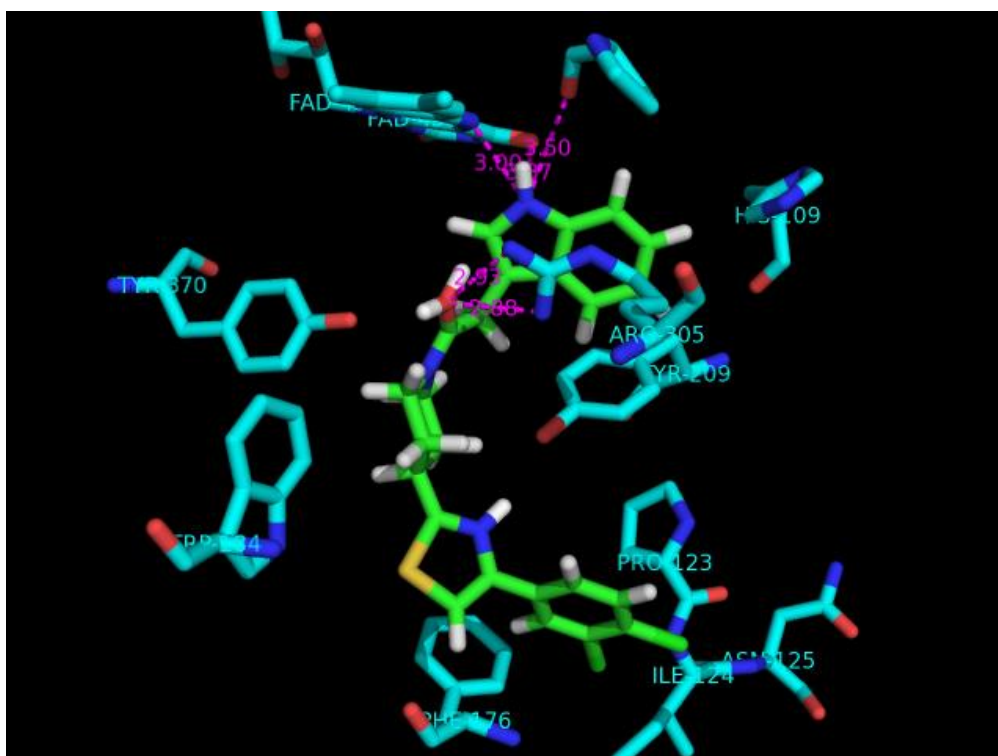


Figure 23 Stereo image and corresponding Chemdraw view of the binding of 22 to the active site of drUGM. The hydrogen bond interactions to the amino acid residues are shown in purple, together with bond distance.

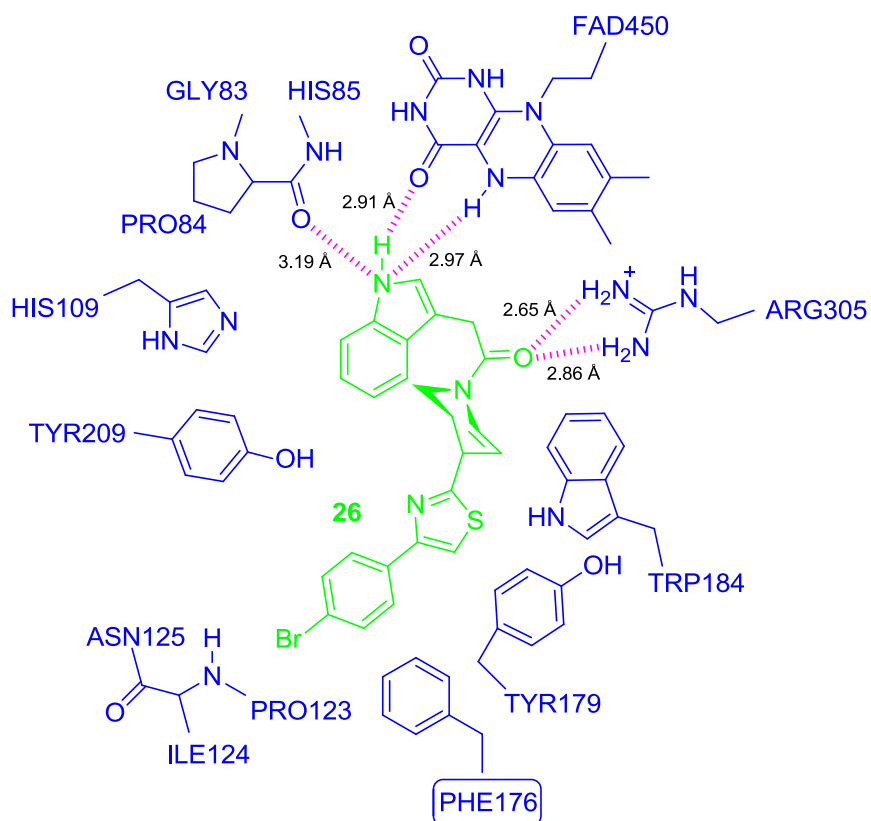
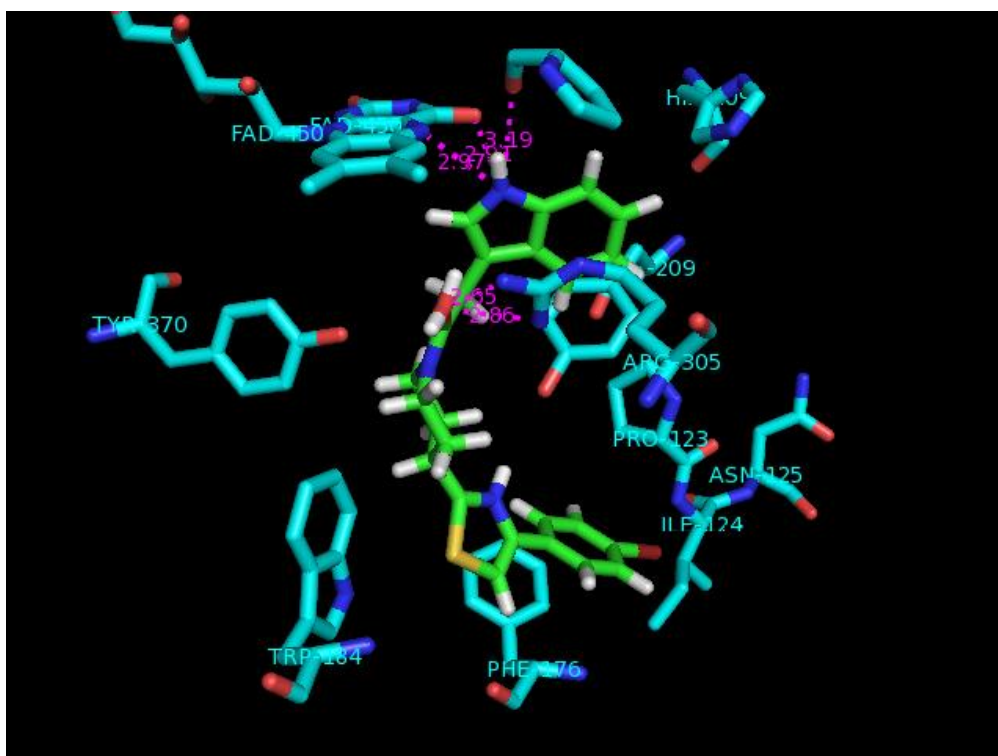


Figure 24 Stereo image and corresponding Chemdraw view of the binding of 26 to the active site of drUGM. The hydrogen bond interactions to the amino acid residues are shown in purple, together with bond distance, and the π - π stacking interaction is shown in box.

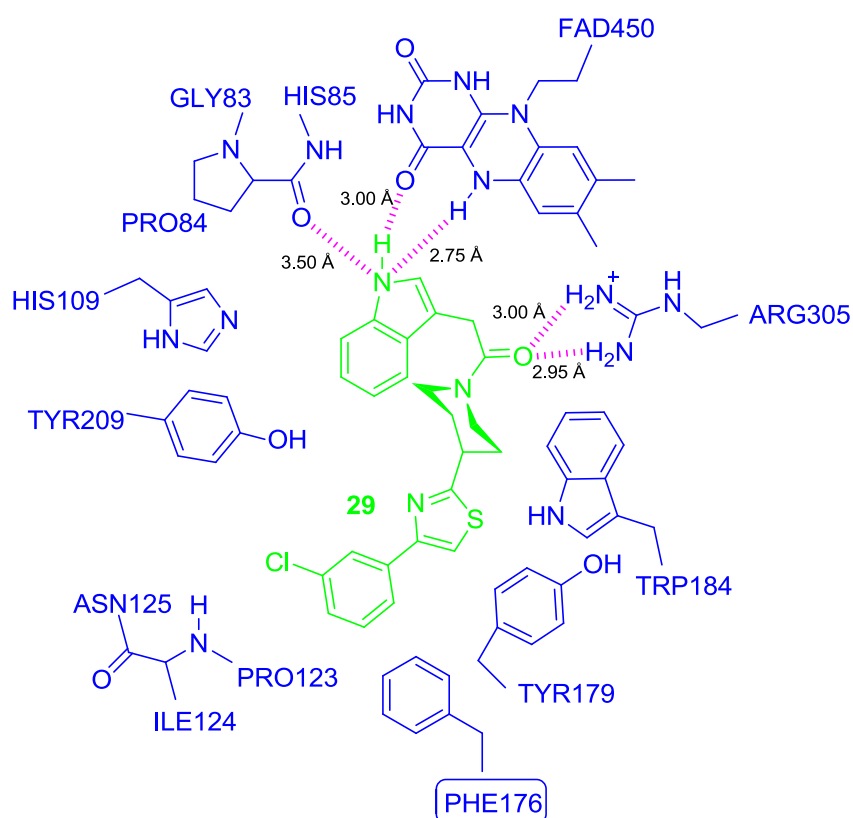
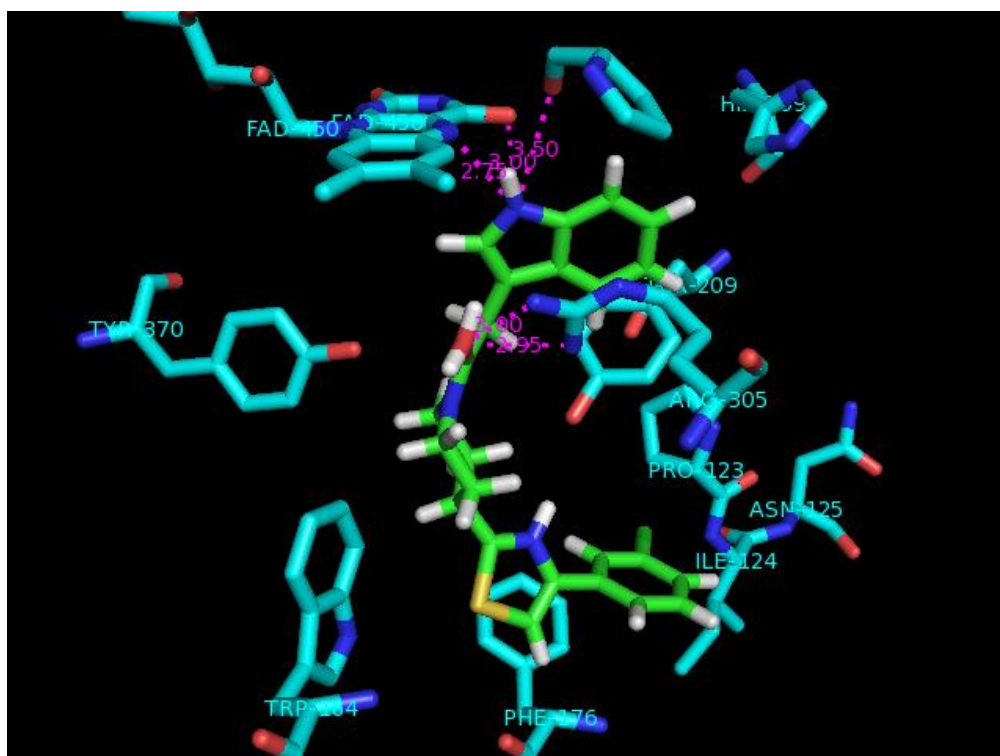


Figure 25 Stereo image and corresponding Chemdraw view of the binding of 29 to the active site of drUGM. The hydrogen bond interactions to the amino acid residues are shown in purple, together with bond distance.

The ligand binding was believed to be very flexible, and this could be explained by referring to the binding of **27** and **32** (Figure 26 and Figure 27). Their binding is 180° relative to the rest of the analogues. This is because in this position, the indole moieties of both analogues have π - π stacking/hydrophobic interaction with the aromatic ring of Phe176 and hydrogen bond interaction with carboxylic acid of Phe176, which may contribute to better binding affinity. Besides, with this binding position, the aromatic ring substituent of **32** exhibits π - π stacking/hydrophobic interaction with the pyrrole ring of Pro84, which may increase the inhibition of the inhibitor.

By comparing 27 and 32 to the previously synthesized inhibitor, 17 ((b)), their binding are similar. Their indole moieties are located in the uridine binding region, which is surrounded by Thr180, Phe175, and Phe176.

However, the interactions of **27** and **32** to the binding residues are a bit similar compared to **17**, except for the hydrophobic interaction of the indole rings to Tyr179 and hydrogen interaction of the carbonyl adjacent to the thiazole ring to Asn372. The indole NH of **27** forms a hydrogen bond to the carboxylic acid of Phe176. As for **32**, the indole NH forms two hydrogen bonds to both Phe176 and Phe175.

The thiazole N of **27** and **32** only forms a hydrogen bond to one of the NH, rather than both NH's of Arg305. This is because the distance between the thiazole N and the two NH's are 3.79 Å and 3.85 Å respectively. Nevertheless, a very weak hydrogen bond might be formed with the NH further away.

The overall result shows that all these analogues are predicted to bind well in the active site. Moreover, most of them exhibit moderate hydrogen bond strength with the amino acid residues. Thus, they have the potential to act as good inhibitors of UGM. Inhibition assays will be carried out to further prove the potency of these analogues.

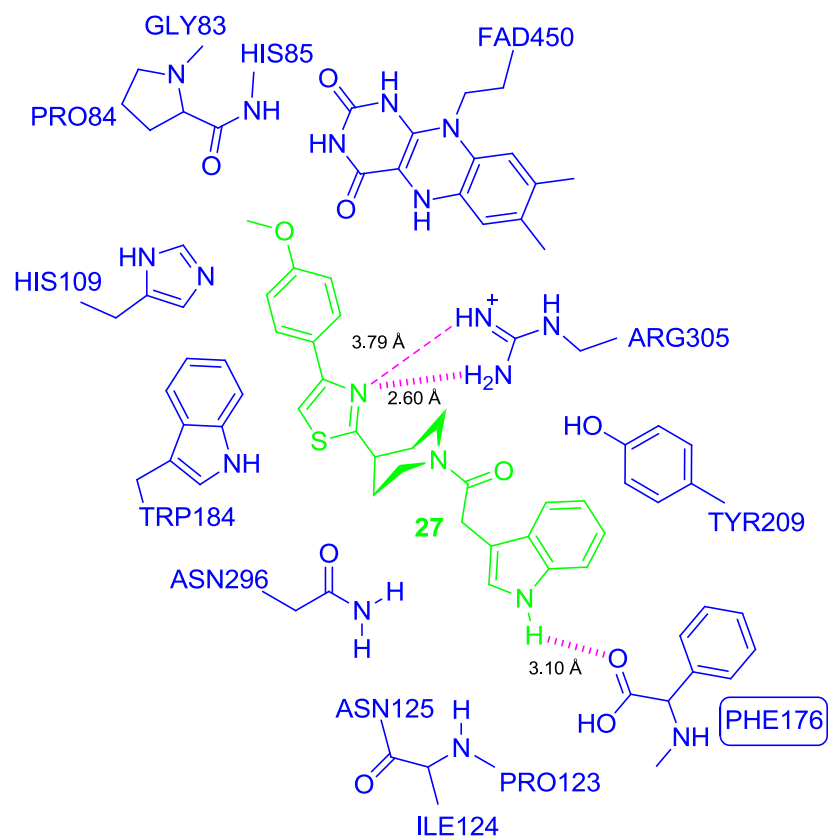
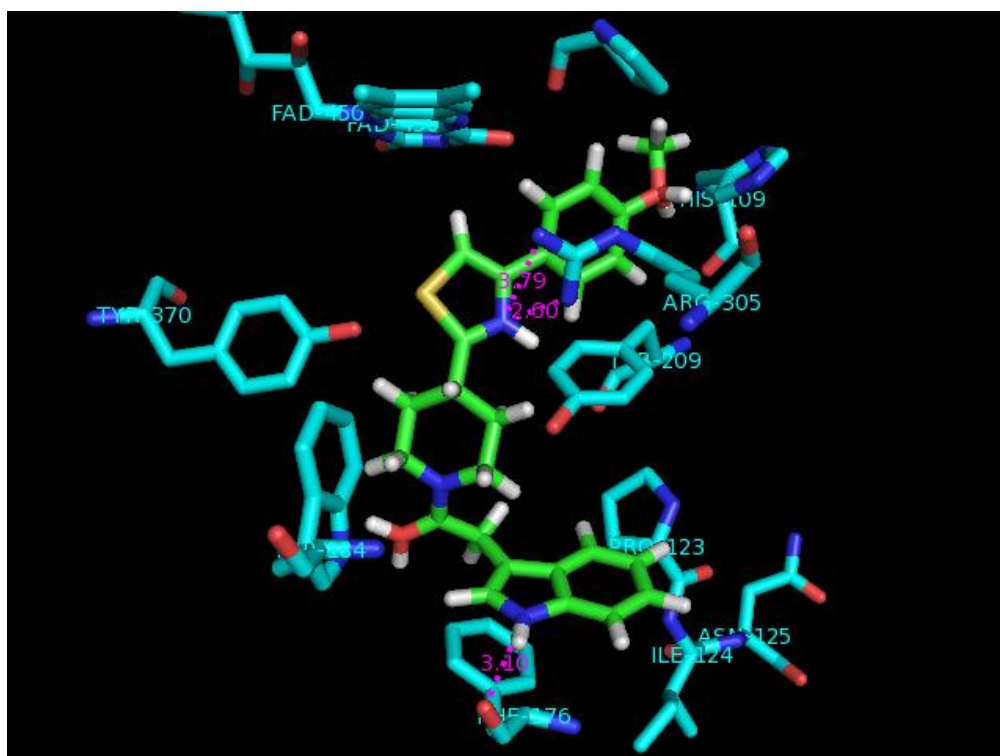


Figure 26 Stereo image and corresponding Chemdraw view of the binding of 27 into the active site of drUGM. The hydrogen bond interactions to the amino acid residues are shown in purple, together with bond distance, and the π - π stacking interaction is shown in box.

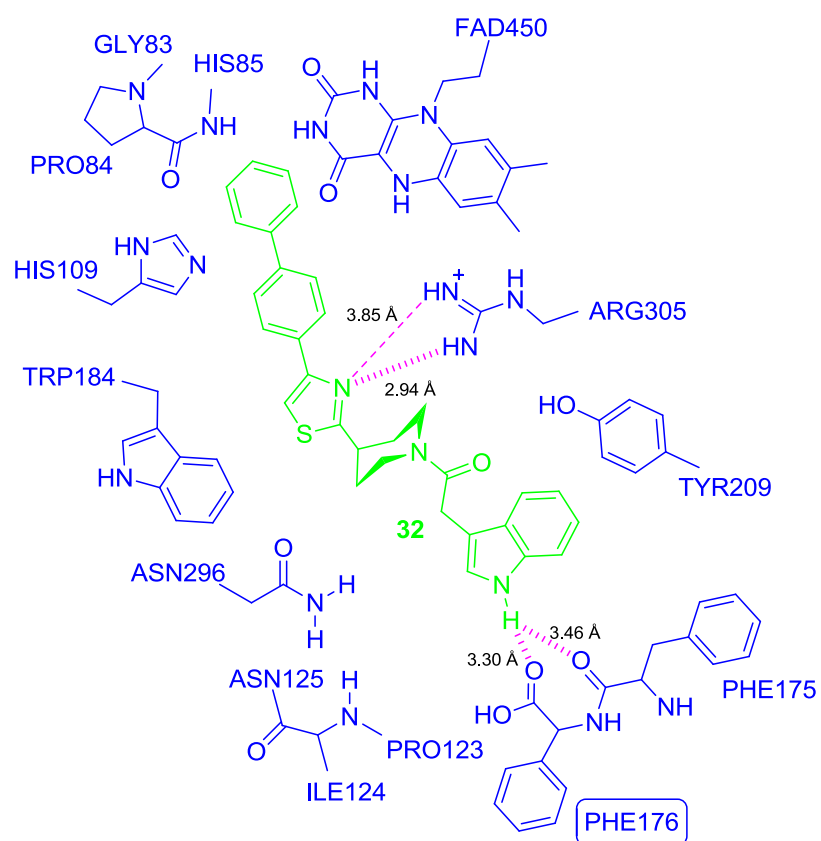
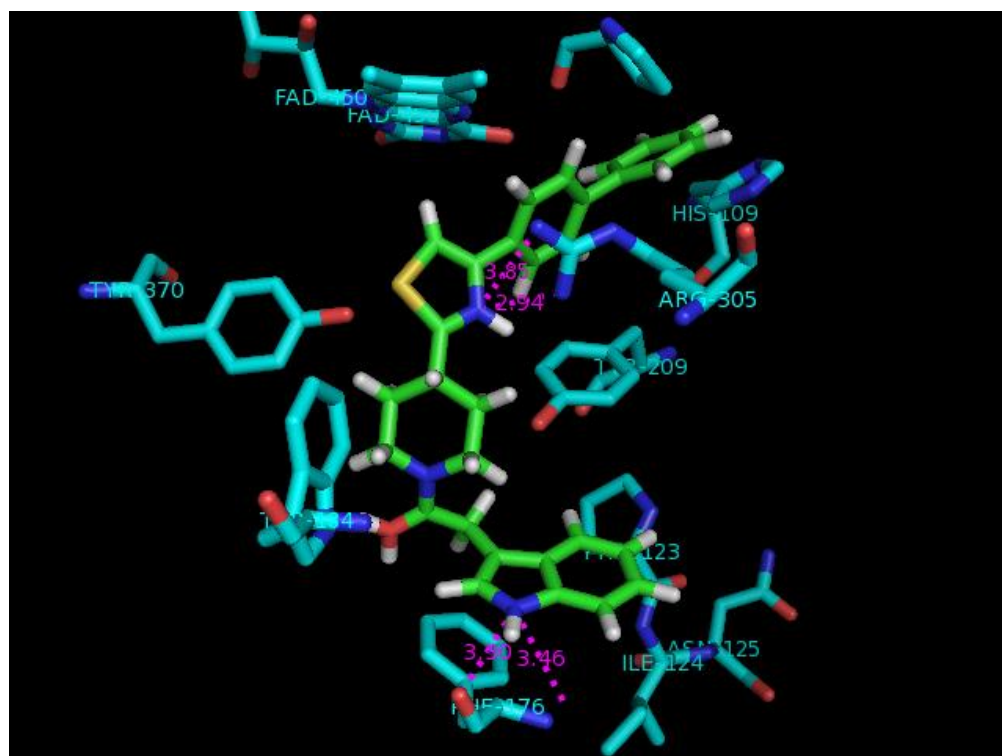


Figure 27 Stereo image and corresponding Chemdraw view of the binding of 32 into the active site of drUGM. The hydrogen bond interactions to the amino acid residues are shown in purple, together with bond distance, and the π - π stacking interaction is shown in box.

3 Conclusions and Future Work

In conclusion, 14 indole-thiazole based potential inhibitors of UGM, with overall yields of 23-78% have been synthesized and successfully purified. The purity of all these inhibitors has been determined using HPLC and the results summarized that their purities are within the range of 78-96%, some of which are acceptable to be used for biological testing (compounds with purity greater than 85%).

In silico studies of these compounds have been performed by docking them into the active site of the ligand-free drUGM crystal structure using the GOLD docking system. The Goldscore fitness function was employed to score the docking solutions, and the docking results obtained for these inhibitors are within the range of 79-86 *cf.* known inhibitor (**17**) 77.5. Subsequently, the interactions between the inhibitors and the UGM protein residues were evaluated. It can be concluded that these compounds show promising inhibitory activity towards drUGM.

Future work will involve biological testing of these potential inhibitors using the isolated enzyme and whole cell assays to test the potency of these analogues. A FP assay can be adapted for the high-throughput screening of these analogues. In FP, a fluorescent probe (Figure 28) is used to monitor the inhibitory activity of the analogues. This can be done by measuring the emission of a fluorescent compound excited with plane-polarized light. The variation of polarization depends upon whether the fluorescent probe is bound to UGM (high polarization, tumbling slowly) or displaced by competitive inhibitor and released into solution (low polarization, tumbling rapidly).⁶² This assay has high sensitivity.

Dissociation constant (K_d) values of the analogues are measured. The smaller the K_d values, the higher the binding affinity of the analogues to UGM.

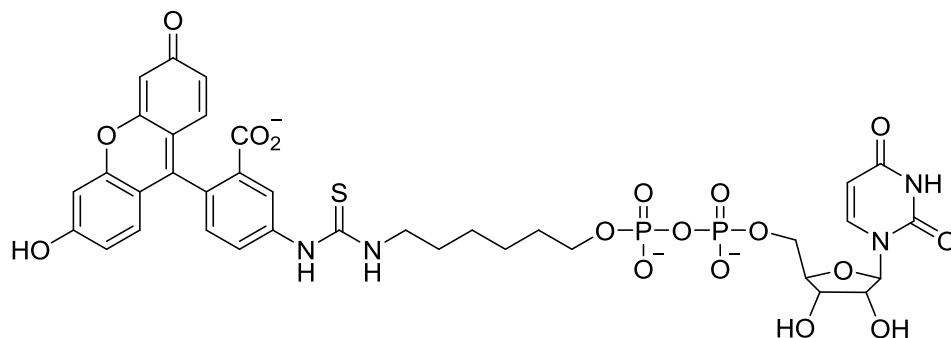


Figure 28 Fluorescent probe used in FP assay.⁶²

Furthermore, the inhibition of these analogues can also be tested by conducting the HPLC assay, which involves the assessment of the catalytic activity of UGM. This can be achieved by monitoring the production of UDP-Galp from UDP-Galf. The percentage inhibition of these analogues is obtained. The percentage inhibition can be calculated using Equation 1.

Equation 1 Calculation of the percentage inhibition.

$$\% \text{ conversion} = \frac{\text{area of UDP - Galp peak}}{(\text{area of UDP - Galp peak}) + (\text{area of UDP - Galf peak})}$$

In addition, further investigation of the inhibitory activity of these analogues will be achieved by performing docking experiments on UGM from different species, such as mtUGM, ecUGM, and kpUGM. Furthermore, some of the analogues with the purity lesser than 85% need to be further purified (using semi-preparative HPLC purification method) in order to be used for biological evaluation.

4 Experimental

4.1 General

All commercially available reagent grade solvents and reagents were purchased from Fischer Scientific[®], Sigma Aldrich[®], Alfa Aesar[®], and Maybridge chemicals.

All ¹H NMR spectra were recorded on Bruker[™] AV400, AV(III)400, or DPX 400 spectrometers at 400 MHz, or AV(III)500 at 500 MHz and at ambient temperature. The chemical shifts (δ) given are in parts per million (ppm) and *J* values in Hertz (Hz). Multiplets are designated by the following notations: singlet (s), doublet (d), triplet (t), quartet (q), and multiplet (m). All spectra were recorded relative to residual solvent peaks. Spectra were recorded in solutions of deuterated chloroform (CDCl₃, $\delta_{\text{solv}} = 7.26$) and deuterated methanol (CD₃OD, $\delta_{\text{solv}} = 3.31$).⁷²

All ¹³C NMR spectra were recorded on Bruker[™] AV400, AV(III)400, or DPX 400 spectrometers at 100 MHz at ambient temperature, and the spectra were recorded relative to residual solvent peaks. Spectra were recorded in solutions of deuterated chloroform (CDCl₃, $\delta_{\text{solv}} = 77.1$) and deuterated methanol (CD₃OD, $\delta_{\text{solv}} = 49.0$).⁷² All ¹⁹F NMR spectra were recorded on a Bruker[™] AV400 spectrometer at 376 MHz under ambient temperature, and relative to residual solvent peaks using CFCl₃ as a reference (CFCl₃, $\delta_{\text{solv}} = 0.00$). All the NMR spectra were processed and analysed using TopSpin 3.0. The characterisation of all the compounds was based on DEPT 135, HMBC, and HMQC spectra.

High resolution mass spectroscopy (HRMS) spectra were obtained on a Bruker[™] microTOF, an orthogonal Time of Flight instrument with

electrospray ionisation (ESI, both positive and negative ion) sources as indicated. The values of mass to charge ratio (m/z), are given to four decimal places. The mass of the counter ions are H^+ 1.0078, and Na^+ 22.9898.

Infrared spectroscopy was recorded on a Thermo Scientific NICOLET IR200 FT-IR infrared spectrometer, with samples prepared as KBr discs.

Thin layer chromatography was carried out on Merck Kieselgel 60 F254 plates. Visualisation was by UV light and staining with phosphomolybdic acid (PMA) with heating.

Flash column chromatography was performed using Merck Kieselgel silica gel 60 Å, 230-400 mesh, 40-63 μm ,.

A Stuart Scientific melting point apparatus (SMP3) was used to determine melting points, values are given in degrees Celsius ($^{\circ}C$) and are uncorrected.

An Agilent Technologies 1200 series HPLC with an Eclipse XDS-C18 5 μm column (4.6 x 150 mm) was used to run HPLC analyses at ambient temperature. All the HPLC grade solvents were purchased from Sigma Aldrich. Eluted HPLC peaks were detected by UV detector at 254 nm.

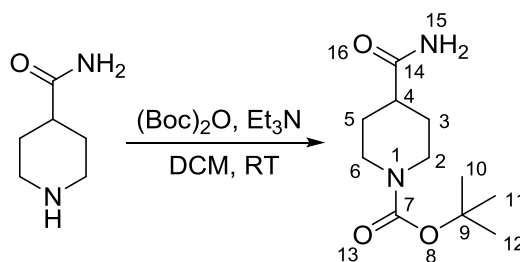
Computational experiments were performed using different programs. SYBYL 8.0 (Tripos International, 1699 South Hanley Rd., St. Louis, Missouri, 63144, USA) was used to sketch and convert the inhibitor molecules into 3D form, and prepare the target UGM protein. GOLD^{69, 70} was employed to perform the docking experiments. PyMOL (The PyMOL Molecular Graphics System, Version 1.5.0.4 Schrödinger, LLC) was used

to visualize the docking results, measure the interactions between the enzyme and substrates in 3D form, and generate the images of the docking results. The crystal structure of drUGM in complex with UDP-Galp was obtained from the RCSB Protein Data Bank (PDB code: 3HDQ), with the resolution of 2.36 Å.

4.2 Procedures and Data

4.2.1 Chemical synthesis

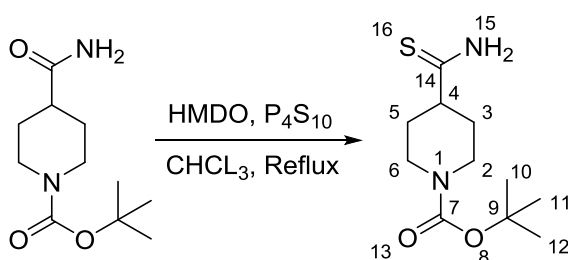
4.2.1.1 Synthesis of *tert*-Butyl 4-carbamoyl piperidine-1-carboxylate (19)⁷³



Isonipecotamide (5.15 g, 40.2 mmol) and triethylamine (11.2 ml, 39.4 mmol) were dissolved in dichloromethane (200 mL). *Di-tert*-butyl dicarbonate (9.63 g, 44.6 mmol) in dichloromethane (20 mL) was added dropwise over 10 minutes and the resulting suspension was stirred at room temperature for 4 h forming a clear solution. The colourless solution was then washed with hydrochloric acid (1 M, 2 x 100 mL) and brine (2 x 100 mL). The organic layer was dried over magnesium sulphate (MgSO₄), filtered and then concentrated *in vacuo* to yield a white solid (7.33 g, 32.1 mmol, 80%). Mp 156-158 °C (Lit. 154-156 °C).⁷⁴ IR ν_{\max} (KBr)/ cm⁻¹ 3363 (N-H amine), 3190 (N-H amide), 2976 (C-H alkanes), 1686 (C=O amide), 1433 (CH₂); ¹H NMR δ_{H} (400 MHz, CDCl₃) 1.46 (9H, s, 8-^tBu), 1.59-1.66 (2H, m, H_{3/5}), 1.85 (2H, dd, *J* 12.0

Hz and 4.0 Hz, H_{3/5}), 2.32 (1H, tt, *J* 12.0 Hz and 4.0 Hz, H₄), 2.77 (2H, t, *J* 12.3 Hz, H_{2,6}), 4.15 (2H, m, H_{2,6}), 5.64 (2H, s, H₁₅); ¹³C NMR δ_C (100 MHz, CDCl₃) 28.5 (C_{10/11/12}), 28.7 (C_{3/5}), 42.7 (C₄), 45.5 (C_{2/6}), 79.7 (C₉), 154.7 (C₇), 176.9 (C₁₄) ; HRMS (ESI) required for C₁₁H₂₁N₂O₃⁺ 229.1474 (MH⁺) observed MH⁺ 229.1486.

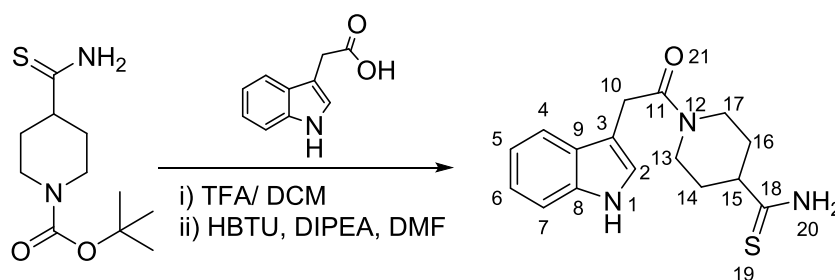
4.2.1.2 Synthesis of *tert*-butyl 4-carbamothioyl piperidine-1-carboxylate (20)⁶⁷



tert-Butyl 4-carbamoyl piperidine-1-carboxylate (7.33 g, 32.1 mmol) was dissolved in chloroform (150 mL). Hexylmethylsiloxane (6.26 mL, 53.3 mmol) and diphosphorus pentasulfide (1.87 g, 8.03 mmol) were added. The yellow resulting suspension was heated at reflux with stirring at 65 °C for 3 h. The solution was then cooled to 0 °C, aqueous potassium carbonate solution (5.3 M, 10.4 mL), acetone (15.7 mL) and water (8.35 mL) were added. The yellow solution was stirred at room temperature for 18 h before being extracted with ethyl acetate (1 x 100 mL). The organic layer was washed with potassium carbonate solution (5.3 M, 2 x 50 mL), water (2 x 50 mL) and brine (2 x 50 mL). The organic layer was then dried over MgSO₄, filtered and concentrated *in vacuo* to yield an oily yellow solid (5.86 g, 24.0 mmol, 75%). IR ν_{max} (KBr solid)/ cm⁻¹ 3346 (NH₂), 3177 (NH₂), 2976 (C-H), 1671 (C=O), 1416 (CH₃), 1169 (C=S); ¹H NMR δ_H (400 MHz, CDCl₃) 1.47 (9H, s, 8-^tBu), 1.67-1.78 (2H, m, H₅),

1.93 (2H, m, H₃), 2.72 (4H, m, H_{6/2}), 3.37 (1H, m, H₄), 4.25 (2H, s, H₁₅);
¹³C NMR δ_C (100 MHz, CDCl₃) 28.4 (C_{10/11/12}), 34.2 (C_{3/5}), 45.9 (C_{2/6}),
 51.2 (C₄), 79.8 (C₉), 159.5 (C₇), 214.2 (C₁₄); HRMS (ESI) required for
 C₁₁H₂₁N₂O₂S⁺ 245.1245 (MH⁺) observed MH⁺ 245.1337.

4.2.1.3 Synthesis of 12-(1*H*-indol-3-ylacetyl)piperidine-15-carbothioamide (**21**)^{75, 76}



tert-Butyl 4-carbamothioylpiperidine-1-carboxylate (5.86 g, 24.0 mmol) was dissolved in dichloromethane (100 mL) and trifluoroacetic acid (37.5 mL, 487 mmol) was added, the resulting suspension was stirred at room temperature for 3 h forming a solution. The yellow solution was co-evaporated with chloroform and dried over phosphorus pentoxide under vacuum. HBTU (12.0 g, 31.7 mmol) and 3-indoleacetic acid (5.05 g, 28.8 mmol) were added and dried under vacuum. DMF (30 mL) and DIPEA (15.3 mL, 88.0 mmol) were then added. The solution was stirred at room temperature for 23 h and then water (100 mL) was added and the solution was washed with ethyl acetate (2 x 100 mL), HCl (1 M, 2 x 70 mL), sodium hydrogen carbonate (aq. sat., 2 x 70 mL) and brine (2 x 70 mL). The organic layer was dried over MgSO₄, filtered and concentrated *in vacuo* to give oily brown solid. Purification by flash column chromatography using ethyl acetate R_f 0.22 to yield a brown oil (2.22 g, 7.37 mmol, 31%). Mp 105-107 °C. IR ν_{max} (KBr)/ cm⁻¹ 3298 (NH₂), 1617

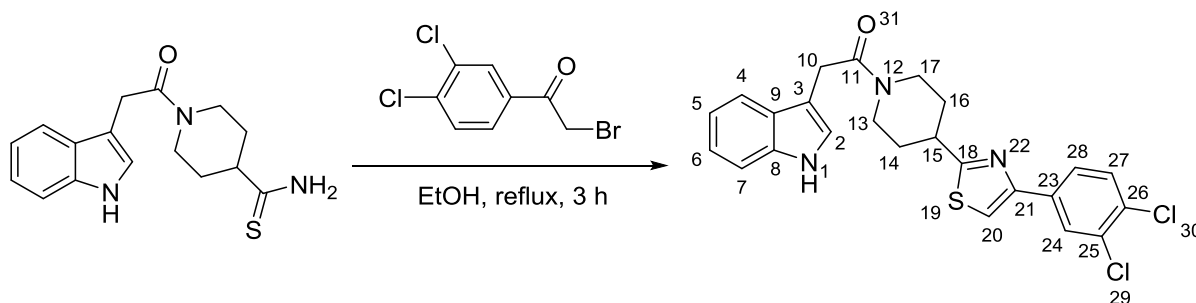
(C=O amide), 1456 (C=C aromatic), 774 (C-H aromatic); ^1H NMR δ_{H} (400 MHz, CD_3OD) 1.67-1.69 (4H, m, $\text{H}_{14/16}$), 2.59 (1H, td, J 12.0 Hz and 4.0 Hz, H_{17}), 2.69-2.73 (1H, m, H_{15}), 2.96-2.99 (1H, m, H_{13}), 3.84 (2H, s, H_{10}), 4.09 (1H, m, H_{13}), 4.63 (1H, d, J 12.0 Hz, H_{17}), 7.01-7.03 (1H, m, H_2), 7.09 (2H, m, $\text{H}_{5/6}$), 7.34 (1H, d, J 8.0 Hz, H_4), 7.57 (1H, d, J 8.0 Hz, H_7). ^{13}C NMR δ_{C} (100 MHz, CD_3OD) 32.4 (C_{14}), 32.7 (C_{16}), 33.3 (C_{10}), 42.9 (C_{13}), 47.3 (C_{17}), 51.1 (C_{15}), 109.3 (C_3), 112.5 (C_7), 119.5 (C_4), 120.1 (C_5), 122.8 (C_6), 124.2 (C_2), 128.5 (C_9), 138.1 (C_8), 172.9 (C_{11}), 213.9 (C_{18}); HRMS (ESI) required for $\text{C}_{16}\text{H}_{20}\text{N}_3\text{OS}^+$ 302.1249 (MH^+) observed MH^+ 302.1265.

4.2.1.4 General procedure of Hantzsch thiazole synthesis of indole analogues.⁷⁷

12-(1*H*-indol-3-ylacetyl)piperidine-15-carbothioamide (1.0 equiv.) and substituted 2-bromo-acetophenone (1.5 equiv.) were dissolved in ethanol (10 mL) and heated at reflux (90 °C) for 3-4 h. The ethanol was removed *in vacuo* to yield crude products. The crude products were purified by recrystallization or column chromatography.

The following compounds were prepared in this manner.

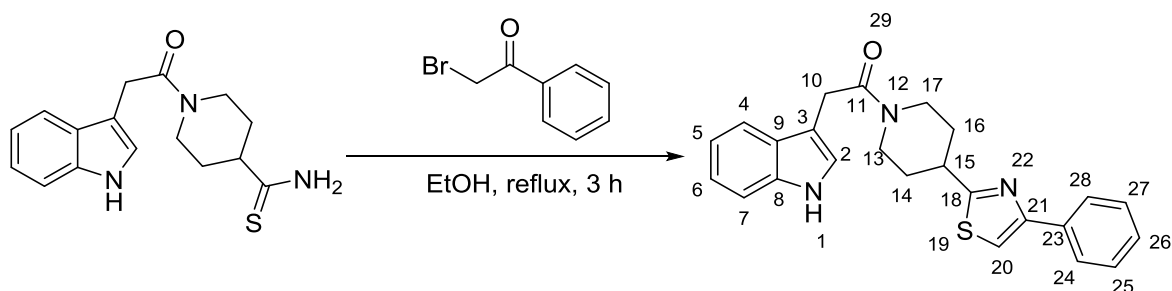
4.2.1.4.1 Synthesis of 11-{15-1-piperidin-12-yl}-10-(1*H*-indol-3-yl)-ethanone (22)



22 was prepared from 12-(1*H*-indol-3-yl)acetyl piperidine-15-carbothioamide (86 mg, 0.29 mmol) and 2-bromo-3,4-dichloroacetophenone (120 mg, 0.440 mmol). The crude product (purple foam) obtained was purified by flash column chromatography using dichloromethane: methanol (98: 2) R_f 0.38 as an oily brown solid (74 mg, 0.16 mmol, 55%). IR ν_{\max} (KBr)/ cm^{-1} 3279 (N-H), 1626 (C=O amide), 1441 (C=C aromatics), 742 (C-H aromatics); ^1H NMR δ_{H} (400 MHz, CDCl_3) 1.54-1.60 (1H, m, H_{17}), 1.72-1.80 (2H, m, H_{13}), 2.03 (1H, d, J 12.0 Hz, H_{17}), 2.15 (1H, d, J 12.0 Hz, H_{13}), 2.85 (1H, m, H_{16}), 3.19 (2H, m, $\text{H}_{15,14}$), 3.90 (2H, s, H_{10}), 4.05 (1H, d, J 12.0 Hz, H_{14}), 4.73 (1H, d, J 12.0 Hz, H_{16}), 7.07 (1H, d, J 4.0 Hz, H_2), 7.14 (1H, m, H_6), 7.21 (2H, m, H_5), 7.36 (2H, m, $\text{H}_{4,20}$), 7.46 (1H, d, J 8.0 Hz, H_7), 7.66 (2H, dd, J 4.0 Hz and 8.0 Hz, $\text{H}_{27,28}$), 7.98 (1H, d, J 2.0 Hz, C_{24}), 8.44 (1H, s, H_1); ^{13}C NMR δ_{C} (100 MHz, CDCl_3) 31.6 (C_{10}), 32.1 (C_{16}), 32.5 (C_{14}), 40.4 (C_{15}), 41.7 (C_{17}), 46.0 (C_{13}), 109.2 (C_3), 111.3 (C_{20}), 113.0 (C_7), 118.7 (C_4), 119.7 (C_5), 122.3 (C_6), 122.4 (C_2), 125.4 (C_{28}), 127.1 (C_9), 128.2 (C_{24}), 130.7 (C_{27}), 131.8 (C_{23}), 132.9 (C_{26}), 134.4 (C_{25}), 136.2 (C_8),

152.5 (C₂₁), 170.1 (C₁₁), 174.4 (C₁₈); HRMS (ESI) required for C₂₄H₂₂Cl₂N₃OS⁺ 470.0782 (MH⁺) observed MH⁺ 470.0801. HRMS (ESI) required for C₂₄H₂₂Cl₂N₃OS⁺ 472.0752 (MH⁺) observed MH⁺ 470.0771.

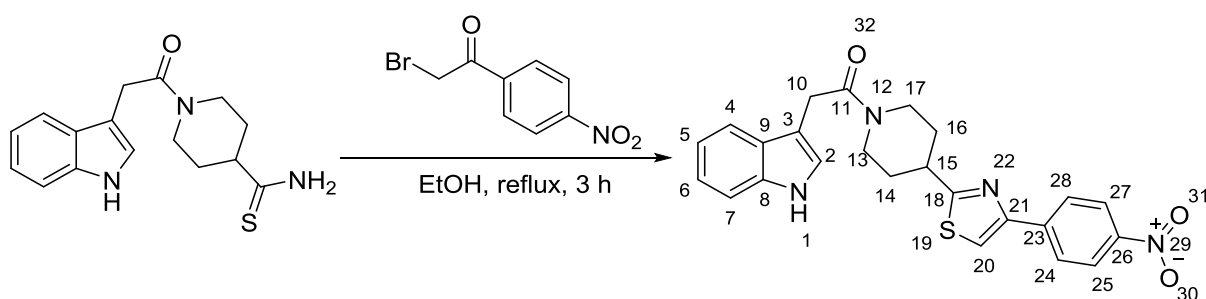
4.2.1.4.2 Synthesis of 10-(1*H*-indol-3-yl)-11-(15-(21-phenylthiazol-18-yl)piperidin-12-yl)ethanone (23)



23 was prepared from 12-(1*H*-indol-3-yl)acetyl piperidine-15-carbothioamide (100 mg, 0.330 mmol) and 2-bromoacetophenone (100 mg, 0.500 mmol). The crude product (a purple oil) obtained was purified by flash column chromatography using dichloromethane: methanol (3%) R_f 0.30 as a yellow oil. Further purification by flash column chromatography using dichloromethane: ethyl acetate (1: 1) R_f 0.42 to give brown foam (54 mg, 0.14 mmol, 41%). Mp 78-80 °C; IR ν_{max} (KBr)/cm⁻¹ 3427 (N-H), 1625 (C=O amide), 1445 (C=C aromatics), 741 (C-H aromatics); ¹H NMR δ_H (400 MHz, CDCl₃) 1.55-1.59 (1H, m, H₁₇), 1.73-1.78 (1H, m, H₁₃), 2.01 (1H, m, H₁₇), 2.15 (1H, m, H₁₃), 2.83 (1H, m, H₁₆), 3.12-3.18 (1H, m, H₁₄), 3.21-3.26 (1H, m, H₁₅), 3.88 (2H, s, H₁₀), 4.01 (1H, d, *J* 13.7 Hz, H₁₄), 4.73 (1H, d, *J* 13.4 Hz, H₁₆), 7.04 (1H, m, H₂), 7.13 (1H, m, H₆), 7.20 (1H, m, H₅), 7.30-7.34 (3H, m, H_{4,20,26}), 7.34 (1H, m, H₄), 7.41 (2H, m, H_{25/27}), 7.65 (1H, m, H₇), 7.87 (2H, m, H_{24/28}), 8.77 (1H, s, H₁); ¹³C NMR δ_C (100 MHz, CDCl₃) 31.6 (C₁₀), 32.2 (C₁₃),

32.7 (C₁₇), 40.5 (C₁₅), 41.7 (C₁₆), 46.0 (C₁₄), 108.9 (qC), 111.5 (C₄), 111.8 (C₂₀), 118.7 (C₇), 119.5 (C₆), 122.1 (C₅), 122.7 (C₂), 167.4 (C_{25/27}), 127.1 (qC), 128.1 (C₂₆), 128.8 (C_{25/27}), 134.4 (qC), 136.3 (qC), 155.0 (qC), 170.3 (qC), 173.9 (qC). HRMS (ESI) required for C₂₄H₂₄N₃OS⁺ 402.1562 (MH⁺) observed MH⁺ 402.1586.

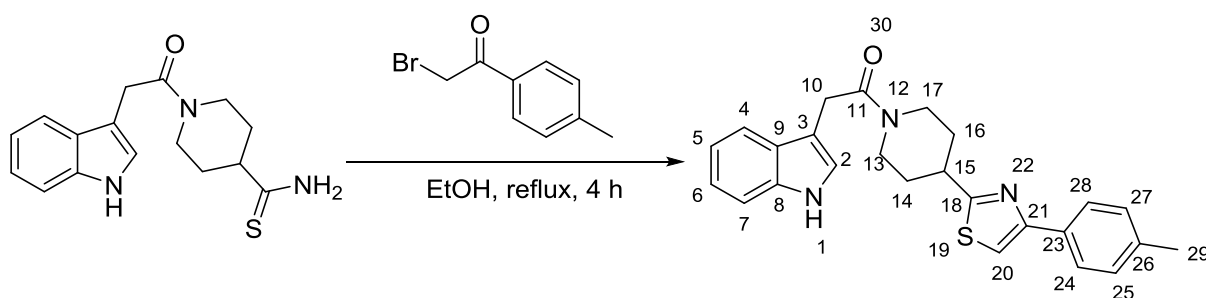
4.2.1.4.3 Synthesis of 10-(1*H*-indol-3-yl)-11-(15-(21-(26-nitrophenyl)thiazol-18-yl)piperidin-12-yl)ethanone (24)



24 Was prepared from 12-(1*H*-indol-3-yl)acetyl piperidine-15-carbothioamide (103 mg, 0.340 mmol) and 2-bromo-4'-nitroacetophenone (127 mg, 0.520 mmol). The crude product (a yellow residue) obtained was purified by flash column chromatography using dichloromethane: methanol (3% v/v) R_f 0.33 as a yellow oil. The yellow oil was purified further by recrystallization from methanol. The solid formed was filtered and washed with cold methanol to give yellow solid (36 mg, 0.26 mmol, 24%). IR ν_{\max} (KBr)/ cm⁻¹ 3434 (N-H amine), 3174 (N-H amide), 1603 (C=O amide), 1516 (NO₂), 1459 (C=C aromatics), 1343 (NO₂), 737 (C-H aromatics); ¹H NMR δ_{H} (400 MHz, CDCl₃) 1.54-1.60 (1H, m, H₁₇), 1.74-1.79 (1H, m, H₁₃), 2.04 (1H, d, *J* 12.0 Hz, H₁₇), 2.17 (1H, d, *J* 11.9 Hz, H₁₃), 2.86 (1H, m, H₁₆), 3.12-3.28

(2H, m, H_{14,15}), 3.90 (2H, s, H₁₀), 4.05 (1H, d, *J* 13.7 Hz, H₁₄), 4.73 (1H, d, *J* 13.6 Hz, H₁₆), 7.09 (1H, m, H₂), 7.14 (1H, m, H₆), 7.20 (1H, m, H₅), 7.35 (1H, d, *J* 8.0 Hz, H₄), 7.54 (1H, s, H₂₀), 7.65 (1H, d, *J* 7.9 Hz, H₇), 8.02 (2H, m, H_{24/28}), 8.25 (2H, m, H_{25/27}), 8.35 (1H, s, H₁); ¹³C NMR δ_C (100 MHz, CDCl₃) 31.7 (C₁₀), 32.2 (C₁₃), 32.6 (C₁₇), 40.6 (C₁₅), 41.8 (C₁₆), 46.1 (C₁₄), 109.4 (qC), 111.4 (C₄), 115.4 (C₂₀), 118.9 (C₇), 119.8 (C₆), 122.4 (C₅), 122.5 (C₂), 124.3 (C_{25/27}), 127.0 (C_{24/28}), 136.3 (qC), 140.4 (qC), 147.3 (qC), 152.7 (qC), 170.2 (qC), 174.9 (qC). HRMS (ESI) required for C₂₄H₂₃N₄O₃S⁺ 447.1413 (MH⁺) observed MH⁺ 447.1447.

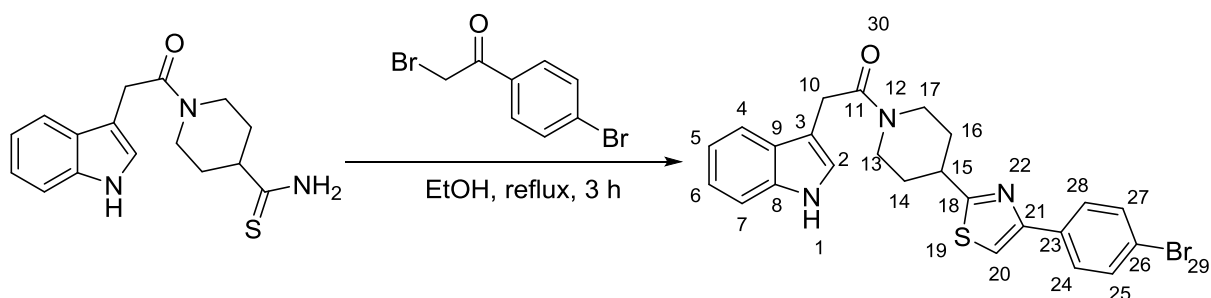
4.2.1.4.4 Synthesis of 10-(1*H*-indol-3-yl)-11-(15-(21-(*p*-tolyl)thiazol-18-yl)piperidin-12-yl)ethanone (25)



25 Was prepared from 12-(1*H*-indol-3-yl)acetyl)piperidine-15-carbothioamide (102 mg, 0.340 mmol) and 2-bromo-4'-methylacetophenone (109 mg, 0.550 mmol). The crude product obtained (a purple oil) obtained was purified by flash column chromatography using dichloromethane: methanol (3% v/v) R_f 0.21 as a yellow oil. The yellow oil was purified further by recrystallization from methanol. The solid formed was filtered and washed with cold methanol to give yellow solid (32 mg, 0.10 mmol, 23%). Mp 188-190 °C; IR ν_{max} (KBr)/ cm⁻¹ 3434 (N-H amine), 3278 (N-H amide), 1628 (C=O amide),

1443 (C=C aromatics), 742 (C-H aromatics); ^1H NMR δ_{H} (400 MHz, CDCl_3) 1.56-1.61 (1H, m, H_{17}), 1.76-1.81 (1H, m, H_{13}), 2.03 (1H, d, J 12.3 Hz, H_{17}), 2.17 (1H, d, J 12.0 Hz, H_{13}), 2.37 (3H, s, H_{29}), 2.85 (1H, m, H_{16}), 3.17 (1H, m, H_{14}), 3.25 (1H, tt, J 3.9 and 11.2 Hz, H_{15}), 3.89 (2H, s, H_{10}), 4.03 (1H, d, J 13.6 Hz, H_{14}), 4.73 (1H, d, J 13.4 Hz, H_{16}), 7.07 (1H, m, H_2), 7.14 (1H, m, H_6), 7.18 (1H, m, H_5), 7.20 (2H, m, $\text{H}_{25/27}$), 7.27 (1H, s, H_{20}), 7.35 (1H, d, J 8.0 Hz, H_4), 7.64 (1H, d, J 8.0 Hz, H_7), 7.75 (2H, d, J 8.2 Hz, $\text{H}_{24/28}$), 8.31 (1H, s, H_1); ^{13}C NMR δ_{C} (100 MHz, CDCl_3) 21.4 (C_{29}), 31.7 (C_{10}), 32.3 (C_{13}), 32.8 (C_{17}), 40.6 (C_{15}), 41.8 (C_{16}), 46.1 (C_{14}), 109.5 (qC), 111.1 (C_{20}), 111.4 (C_4), 118.9 (C_7), 119.8 (C_6), 122.4 (C_5), 122.5 (C_2), 126.4 ($\text{C}_{24/28}$), 127.2 (qC), 129.5 ($\text{C}_{25/27}$), 155.2 (qC), 170.3 (qC). HRMS (ESI) required for $\text{C}_{25}\text{H}_{26}\text{N}_3\text{OS}^+$ 416.1718 (MH^+) observed MH^+ 416.1747.

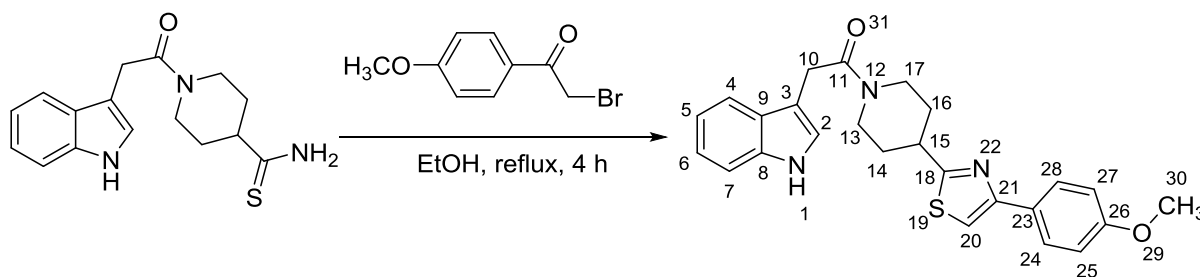
4.2.1.4.5 Synthesis of 11-(15-(21-(26-bromophenyl)thiazol-18-yl)piperidin-12-yl)-10-(1*H*-indol-3-yl)ethanone (26)



26 Was prepared from 12-(1*H*-indol-3-yl)acetyl)piperidine-15-carbothioamide (106 mg, 0.350 mmol) and 2-4'-dibromoacetophenone (146 mg, 0.530 mmol). The crude product (a purple oil) obtained was purified by flash column chromatography using dichloromethane: ethyl acetate (1: 1) R_f 0.49 as a yellow solid (57 mg, 0.12 mmol, 34%). Mp 191-193 °C; IR ν_{\max} (KBr)/ cm^{-1} 3431 (N-H amine), 3277 (N-H amide), 1627 (C=O amide), 1441 (C=C aromatics), 745 (C-H aromatics); ^1H NMR δ_{H} (400 MHz, CDCl_3) 1.52-1.59 (1H, m, H_{17}), 1.72-1.80 (1H, m, H_{13}), 2.05 (1H, m, H_{17}), 2.17 (1H, m, H_{13}), 2.85 (1H, m, H_{16}), 3.16 (1H, m, H_{14}), 3.26 (1H, m, H_{15}), 3.89 (2H, s, H_{10}), 4.03 (1H, d, J 13.6 Hz, H_{14}), 4.73 (1H, d, J 13.6 Hz, H_{16}), 7.04 (1H, m, H_2), 7.11 (1H, m, H_6), 7.21 (1H, m, H_5), 7.34 (1H, s, H_{20}), 7.36 (1H, m, H_4), 7.53 (2H, m, $\text{H}_{24/28}$), 7.65 (1H, m, H_7), 7.73 (2H, m, $\text{H}_{25/27}$), 8.16 (1H, s, H_1); ^{13}C NMR δ_{C} (100 MHz, CDCl_3) 31.7 (C_{10}), 32.3 (C_{13}), 32.8 (C_{17}), 41.0 (C_{15}), 41.8 (C_{16}), 46.1 (C_{14}), 109.6 (qC), 111.3 (C_4), 112.3 (C_{20}), 118.9 (C_7), 119.9 (C_6), 122.3 (C_5), 122.4 (C_2), 127.2 (qC) 128.1 ($\text{C}_{25/27}$), 132.0 ($\text{C}_{24/28}$), 133.2 (qC), 136.3 (qC), 153.7 (qC), 170.1 (qC), 174.4 (qC). HRMS (ESI) required for $\text{C}_{24}\text{H}_{23}\text{BrN}_3\text{OS}^+$ 480.0667 (MH^+) observed MH^+ 480.0695.

HRMS (ESI) required for $C_{24}H_{23}BrN_3OS^+$ 482.0651 (MH^+) observed MH^+ 482.0679.

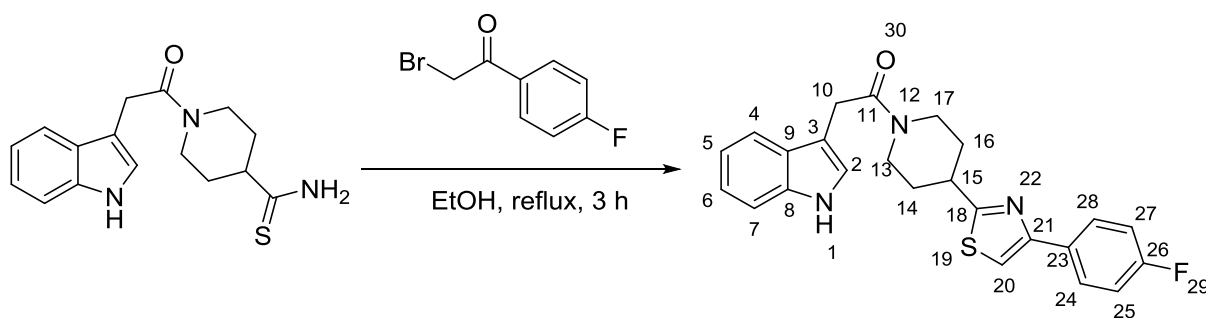
4.2.1.4.6 Synthesis of 10-(1*H*-indol-3-yl)-11-(15-(21-(26-methoxyphenyl)thiazol-18-yl)piperidin-12-yl)ethan-11-one (27)



27 Was prepared from 12-(1*H*-indol-3-yl)acetyl)piperidine-15-carbothioamide (0.840 g, 2.79 mmol) and 2-bromo-4'-methoxyacetophenone (0.960 g, 4.19 mmol). The crude product (a purple residue) obtained was purified by gradient flash column chromatography using dichloromethane: methanol (0-5% v/v) R_f 0.21 as an brown oil. The brown oil was purified further by recrystallization from methanol. The solid formed was filtered and washed with cold methanol to give yellow solid (0.33 g, 0.76 mmol, 27%). Mp 210-212 °C; IR ν_{max} (KBr)/ cm^{-1} 3268 (N-H), 2951 (C-H alkane), 1628 (C=O amide), 1438 (C=C aromatics), 1249 (COCH₃), 746 (C-H aromatics); ¹H NMR δ_H (400 MHz, CDCl₃) 1.51-1.57 (1H, m, H₁₇), 1.74-1.78 (1H, m, H₁₃), 2.04 (1H, m, H₁₇), 2.17 (1H, m, H₁₃), 2.85 (1H, m, H₁₆), 3.15 (1H, m, H₁₄), 3.26 (1H, m, H₁₅), 3.84 (3H, s, H₃₀), 3.89 (2H, s, H₁₀), 4.03 (1H, d, J 13.6 Hz, H₁₄), 4.73 (1H, d, J 13.4 Hz, H₁₆), 6.93 (2H, m, H_{25/27}), 7.08 (1H, m, H₂), 7.14 (1H, t, J 8.0 Hz, H₆), 7.20 (2H, m, H_{5,20}), 7.35 (1H, d, J 8.1 Hz, H₄),

7.65 (1H, d, *J* 7.8 Hz, H₇), 7.79 (2H, m, H_{24/28}), 8.28 (1H, s, H₁); ¹³C NMR δ_C (100 MHz, CDCl₃) 31.6 (C₁₀), 32.2 (C₁₃), 32.7 (C₁₇), 40.4 (C₁₅), 41.5 (C₁₆), 46.1 (C₁₄), 55.4 (C₃₀), 109.5 (qC), 110.1 (C₂₀), 111.4 (C₄), 114.2 (C_{25/27}), 118.9 (C₇), 119.8 (C₆), 122.4 (C₅), 122.5 (C₂), 127.2 (qC), 127.8 (C_{24/28}), 136.3 (qC), 170.2 (qC). HRMS (ESI) required for C₂₅H₂₆N₃O₂S⁺ 432.1667 (MH⁺) observed MH⁺ 432.1691.

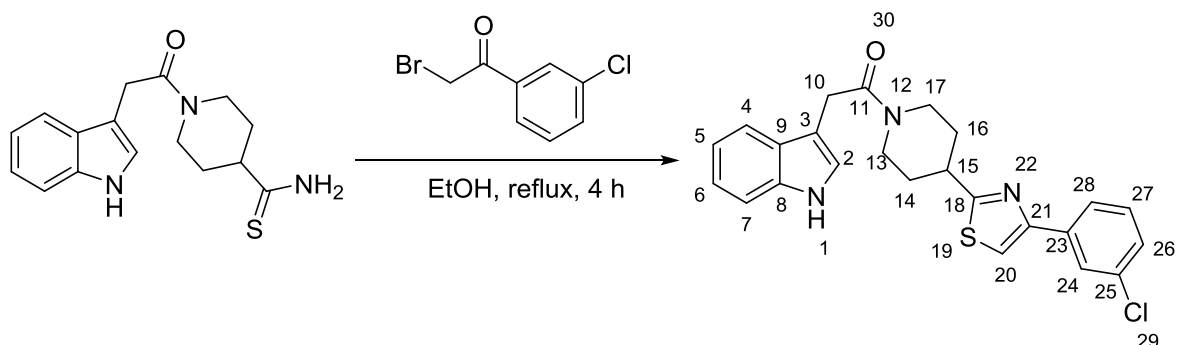
4.2.1.4.7 Synthesis of 11-(15-(21-(26-fluorophenyl)thiazol-18-yl)piperidin-12-yl)-10-(1*H*-indol-3-yl)ethanone (28)



28 Was prepared from 12-(1*H*-indol-3-yl)acetyl piperidine-15-carbothioamide (113 mg, 0.380 mmol) and 2-bromo-4'-fluoroacetophenone (122 mg, 0.570 mmol). The crude product (a purple oil) obtained was then dissolved in dichloromethane (100 mL) and washed with hydrochloric acid (1 M, 2 x 20 mL) and brine (2 x 20 mL). The organic layer was then dried over MgSO₄, filtered and concentrated *in vacuo* to yield yellow oil. The yellow oil was purified by flash column chromatography using dichloromethane: ethyl acetate (1: 1) R_f 0.49 as a yellow oil (81 mg, 0.19 mmol, 51%). Mp 83-85 °C; IR ν_{max} (KBr)/ cm⁻¹ 3430 (N-H), 1626 (C=O amide), 1456 (C=C aromatics), 744 (C-H aromatics); ¹H NMR δ_H (400 MHz, CDCl₃) 1.62-1.69 (1H, m, H₁₇), 1.81-

1.86 (1H, m, H₁₃), 2.07 (1H, m, H₁₇), 2.20 (1H, m, H₁₃), 2.91 (1H, m, H₁₆), 3.17 (1H, m, H₁₄), 3.26 (1H, m, H₁₅), 3.95 (2H, s, H₁₀), 4.08 (1H, d, *J* 13.4 Hz, H₁₄), 4.72 (1H, d, *J* 13.2 Hz, H₁₆), 7.03 (1H, m, H₂), 7.13-7.29 (4H, m, H_{24/28, 6,5}), 7.31 (1H, s, H₂₀), 7.39 (1H, m, H₄), 7.72 (1H, m, H₇), 7.90 (2H, m, H_{25/27}), 8.94 (1H, s, H₁); ¹³C NMR δ_C (100 MHz, CDCl₃) 31.4 (C₁₀), 32.1 (C₁₃), 32.6 (C₁₇), 40.4 (C₁₅), 41.7 (C₁₆), 46.0 (C₁₄), 108.8 (qC), 111.4 (C₄), 111.5 (C₂₀), 115.6 (d, *J*_{C-C-F} 21.1 Hz, C_{25/27}), 118.6 (C₇), 119.5 (C₆), 122.1 (C₅), 122.7 (C₂), 127.1 (qC), 128.1 (d, *J*_{C-C-F} 8.0 Hz, C_{24/28}), 130.8 (qC), 136.3 (qC), 153.9 (qC), 1612.7 (d, *J*_{C-F} 245.8 Hz, C₂₆), 170.3 (qC), 174.3 (qC). ¹⁹F NMR (376 MHz, CDCl₃) δ -113.6 (s, 1F, F₂₉). HRMS (ESI) required for C₂₄H₂₃FN₃OS⁺ 420.1468 (MH⁺) observed MH⁺ 420.1494.

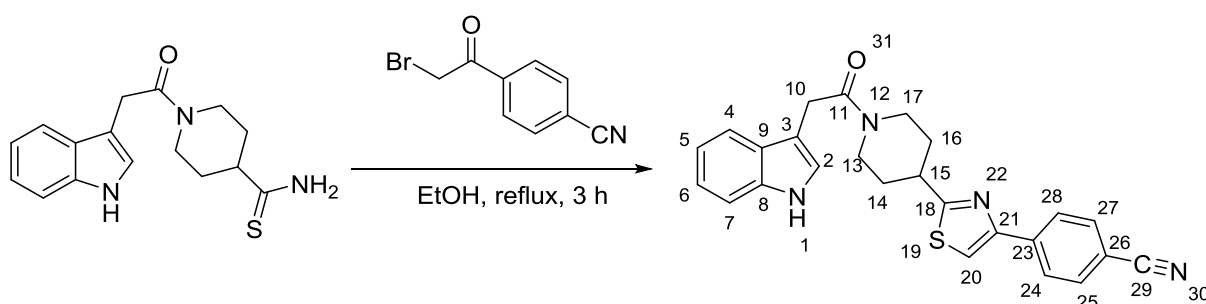
4.2.1.4.8 Synthesis of 11-(15-(21-(25-chlorophenyl)thiazol-18-yl)piperidin-12-yl)-10-(1H-indol-3-yl)ethanone (29)



29 Was prepared from 12-(1H-indol-3-ylacetyl)piperidine-15-carbothioamide (128 mg, 0.430 mmol) and 2-bromo-3'-chloroacetophenone (149 mg, 0.640 mmol). The crude product (a purple oil) obtained was then dissolved in dichloromethane (100 mL) and washed with hydrochloric acid (1 M, 2 x 20 mL) and brine (2 x 20 mL). The organic layer was then dried over MgSO₄, filtered and concentrated *in vacuo* to yield brown oil. The brown oil was purified by flash column chromatography using dichloromethane: ethyl acetate (1: 1) R_f 0.53 as a yellow oil (100 mg, 0.230 mmol, 54%). ¹H NMR δ_H (500 MHz, CDCl₃) 1.52-1.59 (1H, m, H₁₇), 1.71-1.77 (1H, m, H₁₃), 2.03 (1H, m, H₁₇), 2.15 (1H, d, m, H₁₃), 2.85 (1H, m, H₁₆), 3.15 (1H, m, H₁₄), 3.24 (1H, tt, *J* 3.9 and 11.3 Hz, H₁₅), 3.89 (2H, s, H₁₀), 4.03 (1H, d, *J* 13.5 Hz, H₁₄), 4.73 (1H, d, *J* 13.2 Hz, H₁₆), 7.08 (1H, m, H₂), 7.14 (1H, m, H₆), 7.20 (1H, m, H₅), 7.28-7.38 (4H, m, H_{28,27,4,20}), 7.65 (1H, m, H₇), 7.73 (1H, m, H₂₆), 7.87 (1H, m, H₂₄), 8.36 (1H, s, H₁); ¹³C NMR δ_C (100 MHz, CDCl₃) 31.6 (C₁₀), 32.1 (C₁₃), 32.6 (C₁₇), 40.4 (C₁₅), 41.7 (C₁₆), 46.0 (C₁₄), 108.9 (qC), 111.4 (C₄), 112.9 (C₂₀), 118.6 (C₇), 119.5 (C₆), 122.1 (C₅), 122.6

(C₂), 124.4 (C26), 126.5 (C24), 127.0 (qC), 128.0 (C28), 130.0 (C27), 134.7 (qC), 136.2 (qC), 136.3 (qC), 153.4 (qC), 170.2 (qC), 174.3 (qC). HRMS (ESI) required for C₂₄H₂₃ClN₃OS⁺ 436.1172 (MH⁺) observed MH⁺ 436.1199. HRMS (ESI) required for C₂₄H₂₂ClN₃OS⁺ 438.1142 (MH⁺) observed MH⁺ 438.1169.

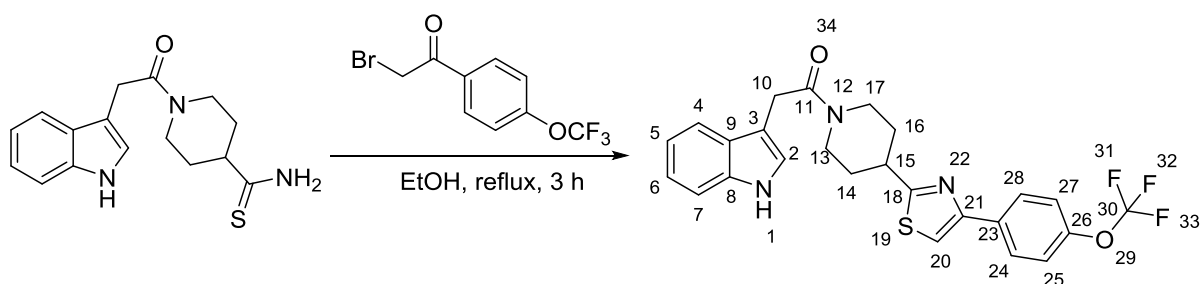
4.2.1.4.9 Synthesis of 26-(21-(15-(10-(1H-indol-3-yl)acetyl)piperidin-12-yl)thiazol-18-yl)benzonitrile (30)



30 Was prepared from 12-(1H-indol-3-yl)acetyl)piperidine-15-carbothioamide (133 mg, 0.440 mmol) and 2-bromo-4'-cyanoacetophenone (149 mg, 0.660 mmol). The crude product (a purple oil) obtained was then dissolved in dichloromethane (100 mL) and washed with hydrochloric acid (1 M, 2 x 20 mL) and brine (2 x 20 mL). The organic layer was then dried over MgSO₄, filtered and concentrated *in vacuo* to yield brown oil. The brown oil was purified by flash column chromatography using dichloromethane:ethyl acetate (1: 1) R_f 0.43 as a yellow solid (100 mg, 0.240 mmol, 53%). Mp 181-183 °C; IR ν_{max} (KBr)/cm⁻¹ 3419 (N-H amine), 3177 (N-H amide), 2224 (C≡N), 1605 (C=O amide), 1446 (C=C aromatics), 740 (C-H aromatics); ¹H NMR δ_H (500 MHz, CDCl₃) 1.55-1.61 (1H, m, H₁₇), 1.72-1.78 (1H, m, H₁₃), 2.03 (1H,

d, J 11.9 Hz, H₁₇), 2.16 (1H, d, J 11.9, H₁₃), 2.85 (1H, m, H₁₆), 3.17 (1H, m, H₁₄), 3.23 (1H, m, H₁₅), 3.90 (2H, s, H₁₀), 4.05 (1H, d, J 14.0 Hz, H₁₄), 4.73 (1H, d, J 13.6 Hz, H₁₆), 7.11 (1H, m, H₂), 7.14 (1H, m, H₆), 7.21 (1H, m, H₅), 7.27 (1H, m, H₄), 7.65 (1H, m, H₇), 7.69 (2H, m, H_{24/28}), 7.96 (2H, m, H_{25/27}), 8.19 (1H, s, H₁); ¹³C NMR δ_C (100 MHz, CDCl₃) 31.5 (C₁₀), 32.3 (C₁₃), 32.7 (C₁₇), 40.6 (C₁₅), 41.8 (C₁₆), 46.1 (C₁₄), 109.6 (qC), 111.4 (C₄), 114.7 (C₂₀), 118.9 (C₇), 119.9 (C₆), 112.3 (C₂), 112.4 (C₅), 126.9 (C_{25/27}), 127.2 (qC), 132.8 (C_{24/28}), 136.3 (qC), 138.6 (qC), 153.1 (qC), 170.1 (qC). HRMS (ESI) required for C₂₅H₂₃N₄OS⁺ 427.1514 (MH⁺) observed MH⁺ 427.1537.

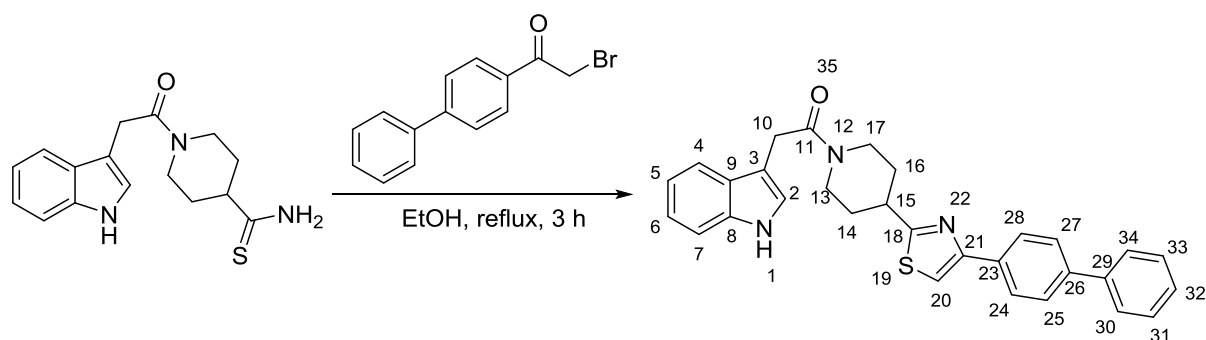
4.2.1.4.10 Synthesis of 10-(1*H*-indol-3-yl)-11-(15-(21-(26-(trifluoromethoxy)phenyl)thiazol-18-yl)piperidin-12-yl)ethanone (31)



31 Was prepared from 12-(1*H*-indol-3-yl)acetamide (130 mg, 0.430 mmol) and 2-bromo-1-[4-(trifluoromethoxy)phenyl]ethan-1-one (183 mg, 0.650 mmol). The crude product (a purple oil) obtained was then dissolved in dichloromethane (100 mL) and washed with hydrochloric acid (1 M, 2 x 20 mL) and brine (2 x 20 mL). The organic layer was then dried over MgSO₄, filtered and concentrated *in vacuo* to yield brown oil. The brown

oil was purified by flash column chromatography using dichloromethane: ethyl acetate (1: 1) R_f 0.57 as a yellow oil (108 mg, 0.220 mmol, 51%). Mp 176-178 °C; IR ν_{\max} (KBr)/ cm^{-1} 3272 (N-H), 1626 (C=O amide), 1445 (C=C aromatics), 1256 (COCF₃), 1224 (C-F), 744 (C-H aromatics); ¹H NMR δ_{H} (400 MHz, CDCl₃) 1.54-1.59 (1H, m, H₁₇), 1.74-1.81 (1H, m, H₁₃), 2.03 (1H, d, J 12.0 Hz, H₁₇), 2.17 (1H, d, J 12.0 Hz, H₁₃), 2.85 (1H, m, H₁₆), 3.16 (1H, m, H₁₄), 3.23 (1H, tt, J 3.9 and 11.2 Hz, H₁₅), 3.89 (2H, s, H₁₀), 4.03 (1H, d, J 13.7 Hz, H₁₄), 4.73 (1H, d, J 13.4 Hz, H₁₆), 7.05 (1H, m, H₂), 7.14 (1H, m, H₆), 7.20 (1H, m, H₅), 7.24 (2H, m, H_{24/28}), 7.33 (1H, s, H₂₀), 7.36 (1H, m, H₄), 7.64 (1H, m, H₇), 7.88 (2H, m, H_{25/27}), 8.29 (1H, s, H₁); ¹³C NMR δ_{C} (100 MHz, CDCl₃) 31.7 (C₁₀), 32.2 (C₁₃), 32.7 (C₁₇), 40.5 (C₁₅), 41.0 (C₁₆), 46.1 (C₁₄), 109.5 (qC), 111.4 (C₄), 112.4 (C₂₀), 118.9 (C₇), 119.8 (C₆), 121.3 (C_{25/27}), 122.4 (C₅), 122.5 (C₂), 127.2 (q, $J_{\text{C-F}}$ 277.1 Hz, C₃₀), 127.9 (C_{24/28}), 133.2 (qC), 136.3 (qC), 170.2 (qC), 174.5 (qC). ¹⁹F NMR (376 MHz, CDCl₃) δ -57.8 (s, 3F, F_{31/32/33}). HRMS (ESI) required for C₂₅H₂₃F₃N₃O₂S⁺ 486.1385 (MH⁺) observed MH⁺ 486.1409.

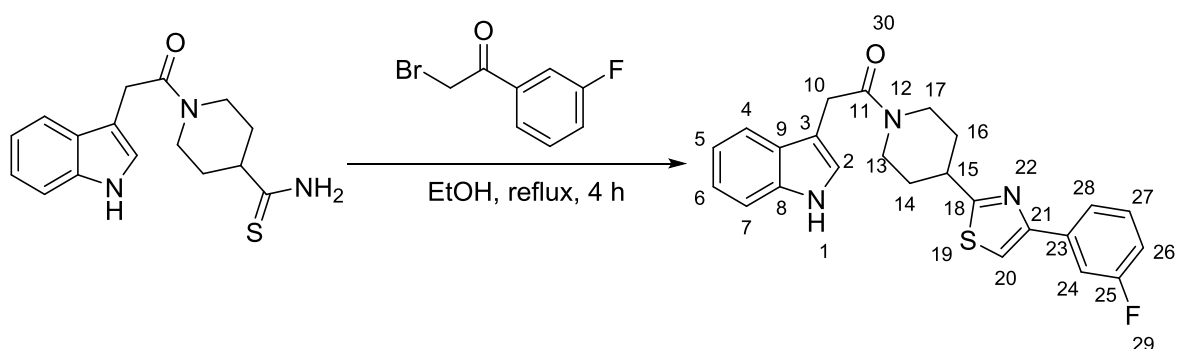
4.2.1.4.11 Synthesis of 11-(15-(21-([23,29'-biphenyl]-26-yl)thiazol-18-yl)piperidin-12-yl)-10-(1H-indol-3-yl)ethanone (32)



32 Was prepared from 12-(1H-indol-3-yl)acetyl piperidine-15-carbothioamide (123 mg, 0.410 mmol) and 2-bromo-4'-phenylacetophenone (169 mg, 0.620 mmol). The crude product (a purple oil) obtained was then dissolved in dichloromethane (100 mL) and washed with hydrochloric acid (1 M, 2 x 20 mL) and brine (2 x 20 mL). The organic layer was then dried over MgSO₄, filtered and concentrated *in vacuo* to yield brown oil. The brown oil was purified by flash column chromatography using dichloromethane: ethyl acetate (1: 1) R_f 0.56 as a yellow solid (92 mg, 0.19 mmol, 47%). Mp 171-172 °C; IR ν_{\max} (KBr)/cm⁻¹ 3421 (N-H amine), 3204 (N-H amide), 3107 (C-H aromatics), 1621 (C=O amide), 1447 (C=C aromatics), 749 (C-H aromatics); ¹H NMR δ_{H} (500 MHz, CDCl₃) 1.56-1.62 (1H, m, H₁₇), 1.75-1.81 (1H, m, H₁₃), 2.06 (1H, m, H₁₇), 2.19 (1H, d, *J* 12.0, H₁₃), 2.87 (1H, m, H₁₆), 3.16 (1H, m, H₁₄), 3.26 (1H, tt, *J* 3.9 and 12.3 Hz H₁₅), 3.90 (2H, s, H₁₀), 4.05 (1H, d, *J* 13.7 Hz, H₁₄), 4.74 (1H, d, *J* 13.4 Hz, H₁₆), 7.08 (1H, m, H₂), 7.14 (1H,

m, H₆), 7.21 (1H, m, H₅), 7.33-7.39 (3H, m, H_{4,20,32}), 7.46 (2H, m, H_{31/33}), 7.61-7.68 (5H, m, H_{7,24/28,30/34}), 7.94 (2H, m, H_{25/27}), 8.36 (1H, s, H₁); ¹³C NMR δ_C (100 MHz, CDCl₃) 31.7 (C₁₀), 32.2 (C₁₃), 32.8 (C₁₇), 40.6 (C₁₅), 41.8 (C₁₆), 46.1 (C₁₄), 109.4 (qC), 111.4 (C₄), 111.9 (C₂₀), 118.9 (C₇), 119.8 (C₆), 122.4 (C₅), 122.5 (C₂), 126.9 (C_{25/27}), 127.1 (C_{30/34}), 127.5 (C₃₂), 128.9 (C_{31/33}), 133.4 (qC), 140.7 (qC), 140.9 (qC), 154.6 (qC), 170.2 (qC), 174.2 (qC). ¹⁹F NMR (376 MHz, CDCl₃) δ -62.5 (s, 3F, F_{30/31/32}). HRMS (ESI) required for C₃₀H₂₈N₃OS⁺ 478.1875 (MH⁺) observed MH⁺ 478.1896.

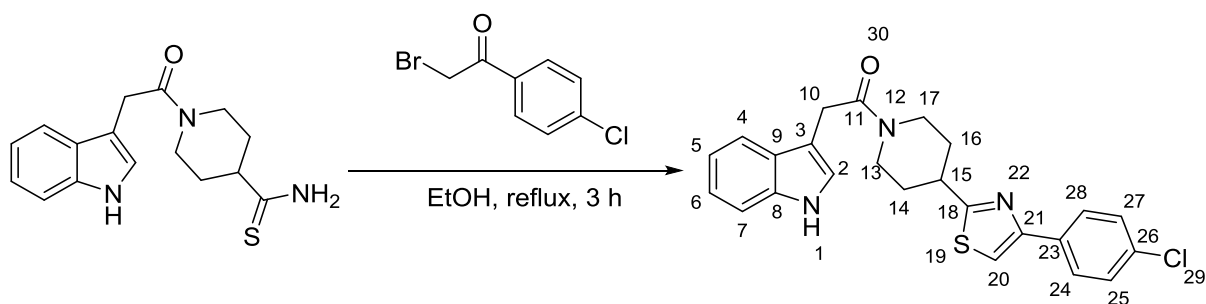
4.2.1.4.12 Synthesis of 11-(15-(21-(25-fluorophenyl)thiazol-18-yl)piperidin-12-yl)-10-(1H-indol-3-yl)ethanone (33)



33 Was prepared from 12-(1H-indol-3-yl)acetyl)piperidine-15-carbothioamide (136 mg, 0.410 mmol) and 2-bromo-1-(3-fluorophenyl)ethan-1-one (147 mg, 0.0680 mmol). The crude product (a purple oil) obtained was then dissolved in dichloromethane (100 mL) and washed with hydrochloric acid (1 M, 2 x 20 mL) and brine (2 x 20 mL). The organic layer was then dried over MgSO₄, filtered and concentrated *in vacuo* to yield brown oil. The brown oil was purified by flash column chromatography using dichloromethane: ethyl acetate (1: 1) R_f0.51 as a

yellow oil (97 mg, 0.23 mmol, 56%). ^1H NMR δ_{H} (500 MHz, CDCl_3) 1.52-1.58 (1H, m, H_{17}), 1.71-1.77 (1H, m, H_{13}), 2.03 (1H, d, J 12.3 Hz, H_{17}), 2.15 (1H, d, J 12.3 Hz, H_{13}), 2.85 (1H, m, H_{16}), 3.15 (1H, m, H_{14}), 3.24 (1H, tt, J 4.0 and 12.1 Hz, H_{15}), 3.89 (2H, s, H_{10}), 4.03 (1H, d, J 12.4 Hz, H_{14}), 4.73 (1H, d, J 12.3 Hz, H_{16}), 7.01 (1H, m, H_{27}), 7.07 (1H, m, H_2), 7.14 (1H, m, H_6), 7.20 (1H, m, H_5), 7.33-7.39 (3H, m, $\text{H}_{28, 4, 20}$), 7.58 (1H, m, H_{26}), 7.62 (1H, m, H_{24}), 7.65 (1H, m, H_7), 8.35 (1H, s, H_1); ^{13}C NMR δ_{C} (100 MHz, CDCl_3) 31.7 (C_{10}), 32.2 (C_{13}), 32.7 (C_{17}), 40.6 (C_{15}), 41.0 (C_{16}), 46.0 (C_{14}), 111.4 (C_4), 112.8 (C_{20}), 113.5 (d, $J_{\text{C-C-F}}$ 22.5 Hz, C_{24}), 114.9 (d, $J_{\text{C-C-F}}$ 21.1 Hz, C_{26}), 118.7 (C_7), 119.6 (C_6), 121.9 (d, $J_{\text{C-C-F}}$ 3.0 Hz, C_{27}), 122.2 (C_5), 122.6 (C_2), 127.1 (qC), 130.4 (C_{28}), 136.3 (qC), 136.7 (qC), 153.7 (qC), 163.2 (d, $J_{\text{C-F}}$ 243.7 Hz, C_{25}), 170.3 (qC), 174.3 (qC). ^{19}F NMR (376 MHz, CDCl_3) δ -112.9 (s, F_{29}). HRMS (ESI) required for $\text{C}_{24}\text{H}_{23}\text{FN}_3\text{OS}^+$ 420.1468 (MH^+) observed MH^+ 420.1489.

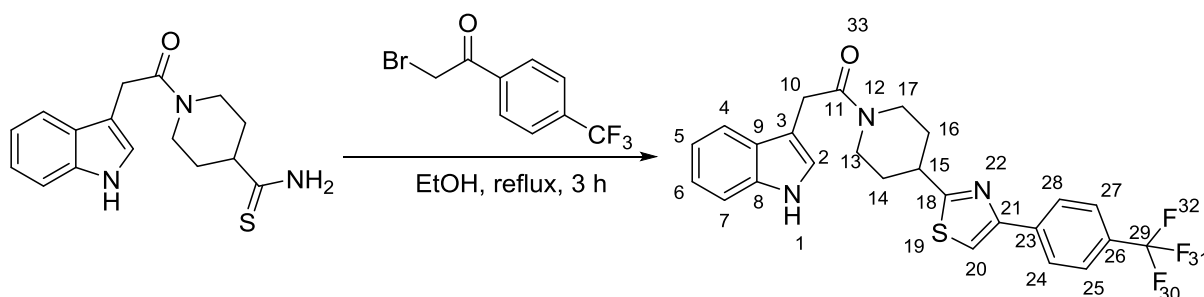
4.2.1.4.13 Synthesis of 11-(15-(21-(26-chlorophenyl)thiazol-18-yl)piperidin-12-yl)-10-(1*H*-indol-3-yl)ethanone (34)



34 Was prepared from 12-(1*H*-indol-3-yl)acetyl piperidine-15-carbothioamide (125 mg, 0.420 mmol) and 2-bromo-4'-cyanoacetophenone (145 mg, 0.620 mmol). The crude product (a purple oil) obtained was then dissolved in dichloromethane (100 mL) and washed with hydrochloric acid (1 M, 2 x 20 mL) and brine (2 x 20 mL). The organic layer was then dried over MgSO₄, filtered and concentrated *in vacuo* to yield brown oil. The brown oil was purified by flash column chromatography using dichloromethane: ethyl acetate (1: 1) R_f 0.61 as a yellow solid (89 mg, 0.21 mmol, 49%). Mp 192-194 °C; IR ν_{\max} (KBr)/cm⁻¹ 3278 (N-H), 1627 (C=O amide), 1442 (C=C aromatics), 745 (C-H aromatics); ¹H NMR δ_{H} (400 MHz, CDCl₃) 1.52-1.58 (1H, m, H₁₇), 1.74-1.79 (1H, m, H₁₃), 2.03 (1H, m, H₁₇), 2.15 (1H, m, H₁₃), 2.85 (1H, m, H₁₆), 3.15 (1H, m, H₁₄), 3.23 (1H, m, H₁₅), 3.89 (2H, s, H₁₀), 4.03 (1H, d, *J* 13.5 Hz, H₁₄), 4.72 (1H, d, *J* 13.4 Hz, H₁₆), 7.04 (1H, m, H₂), 7.14 (1H, m, H₆), 7.20 (1H, m, H₅), 7.32 (1H, s, H₂₀), 7.34 (1H, m, H₄), 7.37 (2H, m, H_{24/28}), 7.65 (1H, m, H₇), 7.78 (2H, m, H_{25/27}), 8.29 (1H, s, H₁); ¹³C NMR δ_{C} (100 MHz, CDCl₃) 31.7 (C₁₀), 32.2 (C₁₃), 32.7 (C₁₇), 40.6 (C₁₅), 41.0 (C₁₆), 46.0 (C₁₄), 109.4 (qC), 111.4 (C₄), 112.2 (C₂₀), 118.9 (C₇),

119.8 (C₆), 122.4 (C₅), 122.5 (C₂), 127.7 (C_{25/27}), 129.0 (C_{24/28}), 133.0 (qC), 134.0 (qC), 136.3 (qC), 153.8 (qC), 170.2 (qC), 174.3 (qC). HRMS (ESI) required for C₂₄H₂₃ClN₃OS⁺ 436.1172 (MH⁺) observed MH⁺ 436.1193. HRMS (ESI) required for C₂₄H₂₃ClN₃OS⁺ 438.1142 (MH⁺) observed MH⁺ 438.1163.

4.2.1.4.14 Synthesis of 10-(1*H*-indol-3-yl)-11-(15-(21-(26-(trifluoromethyl)phenyl)thiazol-18-yl)piperidin-12-yl)ethanone (35)



35 Was prepared from 12-(1*H*-indol-3-yl)acetyl piperidine-15-carbothioamide (133 mg, 0.440 mmol) and 2-bromo-4'-phenylacetophenone (178 mg, 0.660 mmol). The crude product (a purple oil) obtained was then dissolved in dichloromethane (100 mL) and washed with hydrochloric acid (1 M, 2 x 20 mL) and brine (2 x 20 mL). The organic layer was then dried over MgSO₄, filtered and concentrated *in vacuo* to yield brown oil. The brown oil was purified by flash column chromatography using dichloromethane: ethyl acetate (1: 1) R_f 0.56 as a yellow solid (120 mg, 0.260 mmol, 58%). Mp 167-169 °C; IR ν_{max} (KBr)/cm⁻¹ 3281 (N-H), 1627 (C=O amide), 1445 (C=C aromatics), 1327 (C-F), 745 (C-H aromatics); ¹H NMR δ_H (400 MHz, CDCl₃) 1.54-1.61 (1H, m, H₁₇), 1.74-1.79 (1H, m, H₁₃), 2.04 (1H, d, *J* 11.9 Hz, H₁₇), 2.17 (1H, d, *J*

12.3 Hz, H₁₃), 2.86 (1H, m, H₁₆), 3.16 (1H, m, H₁₄), 3.24 (1H, tt, *J* 3.8 and 11.3 Hz, H₁₅), 3.90 (2H, s, H₁₀), 4.03 (1H, d, *J* 13.6 Hz, H₁₄), 4.73 (1H, d, *J* 13.3 Hz, H₁₆), 7.03 (1H, s, H₂), 7.14 (1H, m, H₆), 7.20 (1H, m, H₅), 7.35 (1H, m, H₄), 7.24 (1H, m, H₂₀), 7.61 (1H, m, H₇), 7.65 (2H, d, *J* 8.0 Hz, H_{24/28}), 7.98 (2H, d, *J* 8.0 Hz, H_{25/27}), 8.40 (1H, s, H₁); ¹³C NMR δ_C (100 MHz, CDCl₃) 31.7 (C₁₀), 32.2 (C₁₃), 32.8 (C₁₇), 40.6 (C₁₅), 41.0 (C₁₆), 46.1 (C₁₄), 109.4 (qC), 111.4 (C₄), 113.7 (C₂₀), 118.8 (C₇), 119.8 (C₆), 122.4 (C₅), 122.5 (C₂), 125.8 (m, *J*_{C-C-C-F} 5.8 Hz, C_{25/27}), 126.6 (C_{24/28}), 127.2 (qC), 136.3 (qC), 137.7 (qC), 153.6 (qC), 170.2 (qC), 174.5 (qC). ¹⁹F NMR (376 MHz, CDCl₃) δ -62.5 (s, 3F, F_{30/31/32}). HRMS (ESI) required for C₂₅H₂₃FN₃OS⁺ 470.1436 (MH⁺) observed MH⁺ 470.1457.

4.2.2 HPLC purity analysis of the inhibitors

Chromatographic conditions:

An Eclipse XDS-C18 5 μm column (4.60 x 150 mm) was used at ambient temperature. The mobile phase was composed of acetonitrile (50% v/v) and methanol (50% v/v). Its flow rate was 1 mL/minute with a maximum pressure limit of 350 bar. The stop time was set at 20 minutes, injection volume of 20 μL, and signal detection at 254 nm. The experiments were conducted at ambient temperature.

Apparatus used:

Sonomatic Langford Ultrasonics was used to sonicate the sample solutions. 1 mL BD PlastipakTM syringe, Class A/B glasswares, and Fischer MH-124 balance were used to prepare all the sample solutions and

mobile phase. The analysis was carried out using Agilent Technologies 1200 Infinity series G1322A Degasser (Serial no.: JP73071492), G1311A Quat Pump (Serial no.: DE62971498), G1314B VDW (Serial no.: DE71365292), G164C Analyt FC (Serial no.: DE63056626), and G1328B Man. Inj. (Serial no.: DE60561146).

Sample preparation:

The sample solution (1 mg/mL) was prepared by dissolving 1 mg of each compound using 1 mL of mobile phase in a sample vial. Sample was sonicated to ensure that the compounds were completely dissolved in the mobile phase. The solution contained test analogues were then filtered using a 0.45 μm syringe filter fitted to a 1 mL syringe.

4.2.3 *In silico* studies

The crystal structure of *drUGM* in complex with UDP-Galp (PDB code: 3HDQ)³⁶ was used for docking studies using GOLD. The structures of the inhibitors were sketched and minimized using SYBYL 8.0. The protein molecule was energy minimized using SYBYL 8.0, UDP-Galp was removed, and hydrogen atoms were added. The active site was defined using UDP-Galp as the reference molecule. The coordination set to define the centre of active site was $x = 24.1245$, $y = -106.2594$, and $z = 73.4552$. The binding site radius was set to 10.0 Å. All default parameters were used for docking studies and 5 poses were requested for each molecule. Best fit was determined based upon the Goldscore fitness function. The highest score among the 5 poses of each molecule was chosen in order to observe the potential interactions to the protein residues and the binding conformation.

5 References

1. M.-T. Gutierrez-Lugo and C. A. Bewley, *J. Med. Chem.*, 2008, **51**, 2606-2612.
2. A. Konstantinos, *Aust. Prescr.*, 2010, **33**, 12-18.
3. *World Health Organization Global Tuberculosis Report 2012*, 2012.
4. G. Maartens and J. Wilkinson Robert, *Lancet*, 2007, **370**, 2030-2043.
5. V. Mclaughlin, *Tuberculosis [electronic resource] : infectious disease / Vernetta Mclaughlin*, Research World, Delhi, 2012.
6. S. D. Lawn, *Curr. Opin. Pulm. Med.*, 2013, **19**, 280-288.
7. M. P. Golden and H. R. Vikram, *Am. Fam. Physician*, 2005, **72**, 1761-1768.
8. W. J. H. McBride, *Sex. Health*, 2010, **7**, 218-218.
9. J. N. Kuria and S. M. Gathogo, *Onderstepoort J. Vet. Res.*, 2013, **80**, E1-4.
10. S. Niemann, S. Rusch-Gerdes, M. L. Joloba, C. C. Whalen, D. Guwatudde, J. J. Ellner, K. Eisenach, N. Fumokong, J. L. Johnson, T. Aisu, R. D. Mugerwa, A. Okwera and S. K. Schwander, *J. of Clin. Microbiol.*, 2002, **40**, 3398-3405.
11. G. Panteix, M. C. Gutierrez, M. L. Boschioli, M. Rouviere, A. Plaidy, D. Pressac, H. Porcheret, G. Chydenotis, M. Ponsada, K. Van

- Oortegem, S. Salloum, S. Cabuzel, A. L. Banuls, P. Van de Perre and S. Godreuil, *J. of Med. Microbiol.*, 2010, **59**, 984-989.
12. G. E. Pfyffer, R. Auckenthaler, J. D. A. van Embden and D. van Soolingen, *Emerging Infect. Dis.*, 1998, **4**, 631-634.
13. *Am. J. of respir. Crit. Care Med.*, 1997, **156**, S1-25.
14. E. C. Cole and C. E. Cook, *Am. J. Infect. Control*, 1998, **26**, 453-464.
15. M. Nicas, W. Nazaroff William and A. Hubbard, *J Occup. Environ. Hyg.*, 2005, **2**, 143-154.
16. *Introduction to the Core Curriculum on Tuberculosis: What the Clinician Should Know*, Centers for Disease Control and Prevention (CDC), Division of Tuberculosis Elimination, 2013.
17. N. Ahmed and E. Hasnain Seyed, *Tuberculosis (Edinb)*, 2011, **91**, 407-413.
18. P. Escalante, *Ann. of intern. med.*, 2009, **150**, ITC61-614; quiz ITV616.
19. R. Gandhi Neel, P. Nunn, K. Dheda, H. S. Schaaf, M. Zignol, D. van Soolingen, P. Jensen and J. Bayona, *Lancet*, 2010, **375**, 1830-1843.
20. I. M. Orme, *Mol. Med. Today*, 1999, **5**, 487-492.
21. H. McShane, *Philos. Trans. R. Soc. B-Bio. Sci.*, 2011, **366**, 2782-2789.

22. G. D. Wright and A. D. Sutherland, *Trends Mol. Med.*, 2007, **13**, 260-267.
23. K. J. R. C. George Ray, *Sherris Medical Microbiology, 4th Edition*, 4th (Fourth) Edition edition edn., McGraw-Hill Medical, 2004.
24. K. S. R. Patrick R. Murray, Michael A. Pfaller, *Med. Microbiol.*, 6th edn., Elsevier Mosby, 2009.
25. D. A. R. Sanders, A. G. Staines, S. A. McMahon, M. R. McNeil, C. Whitfield and J. H. Naismith, *Nat. Struct. Biol.*, 2001, **8**, 858-863.
26. S. Gagneux, in *Mycobacterium: Genomics and Molecular Biology*, ed. T. P. a. A. Brown, Caister Academic Press, Norfolk, UK, Editon edn., 2009.
27. J. L. Flynn and J. Chan, *Curr. Opin. Immunol.*, 2003, **15**, 450-455.
28. K. Wooldridge, *Bacterial Secreted Proteins: Secretory Mechanisms and Role in Pathogenesis*, 2009.
29. C. Bogdan, M. Rölinghoff and A. Diefenbach, *Curr. Opin. in Immunol.*, 2000, **12**, 64-76.
30. E. Bell, *Nat. Rev. Immunol.*, 2005, **5**, 746-747.
31. M. Ullrich, *Bacterial Polysaccharides: Current Innovations and Future Trends*, Caister Academic Press, Norfolk, UK, 2009.
32. E. C. Dykhuizen, J. F. May, A. Tongpenyai and L. L. Kiessling, *J. Am. Chem. Soc.*, 2008, **130**, 6706-6707.

33. M. Soltero-Higgin, E. E. Carlson, T. D. Gruber and L. L. Kiessling, *Nat. Struct. Mol. Biol.*, 2004, **11**, 539-543.
34. A. V. Efimov, *J. Mol. Biol.*, 1995, **245**, 402-415.
35. J. M. Chad, K. P. Sarathy, T. D. Gruber, E. Addala, L. L. Kiessling and D. A. R. Sanders, *Biochemistry*, 2007, **46**, 6723-6732.
36. S. Karunan Partha, K. E. van Straaten and D. A. R. Sanders, *J. Mol. Biol.*, 2009, **394**, 864-877.
37. J. B. Thoden and H. M. Holden, *Biochemistry*, 1998, **37**, 11469-11477.
38. C. Notredame, D. G. Higgins and J. Heringa, *J. Mol. Biol.*, 2000, **302**, 205-217.
39. K. Beis, V. Srikannathan, H. Liu, W. B. Fullerton Stephen, A. Bamford Vicki, A. R. Sanders David, C. Whitfield, R. McNeil Mike and H. Naismith James, *J. Mol. Biol.*, 2005, **348**, 971-982.
40. P. Gouet, E. Courcelle, D. I. Stuart and F. Metoz, *Bioinformatics*, 1999, **15**, 305-308.
41. K. E. van Straaten, F. H. Routier and D. A. R. Sanders, *J. Biol. Chem.*, 2012, **287**, 10780-10790.
42. S. Karunan Partha, A. Sadeghi-Khomami, S. Cren, R. I. Robinson, S. Woodward, K. Slowski, L. Berast, B. Zheng, N. R. Thomas and D. A. R. Sanders, *Mol. Inf.*, 2011, **30**, 873-883.

43. Q. Zhang and H.-w. Liu, *J. Am. Chem. Soc.*, 2000, **122**, 9065-9070.
44. J. N. Barlow, M. E. Girvin and J. S. Blanchard, *J. Am. Chem. Soc.*, 1999, **121**, 6968-6969.
45. R. Dhatwalia, H. Singh, M. Oppenheimer, B. Karr Dale, C. Nix Jay, P. Sobrado and J. Tanner John, *J. Biol. Chem.*, 2012, **287**, 9041-9051.
46. Q. Zhang and H.-w. Liu, *J. Am. Chem. Soc.*, 2001, **123**, 6756-6766.
47. S. W. B. Fullerton, S. Daff, D. A. R. Sanders, W. J. Ingledew, C. Whitfield, S. K. Chapman and J. H. Naismith, *Biochemistry*, 2003, **42**, 2104-2109.
48. G. Stevenson, B. Neal, D. Liu, M. Hobbs, N. H. Packer, M. Batley, J. W. Redmond, L. Lindquist and P. Reeves, *J. Bacteriol.*, 1994, **176**, 4144-4156.
49. Z. Huang, Q. Zhang and H.-w. Liu, *Bioorg. Chem.*, 2003, **31**, 494-502.
50. V. Massey, *Biochem. Soc. Trans.*, 2000, **28**, 283-296.
51. S. Ghisla and V. Massey, *Eur J Biochem*, 1989, **181**, 1-17.
52. A. Garcia Trejo, J. W. Haddock, G. J. F. Chittenden and J. Baddiley, *Biochem. J.*, 1971, **122**, 49-57.
53. P. Macheroux, J. Schmid, N. Amrhein and A. Schaller, *Planta*, 1999, **207**, 325-334.

54. M. T. Johnson and J. E. Gander, *Biochim. Biophys. Acta, Enzymol.*, 1978, **523**, 9-18.
55. W. S. Fobes and J. E. Gander, *Biochem. Biophys. Res. Commun.*, 1972, **49**, 76-83.
56. M. Soltero-Higgin, E. E. Carlson, J. H. Phillips and L. L. Kiessling, *J. Am. Chem. Soc.*, 2004, **126**, 10532-10533.
57. H. G. Sun, M. W. Ruzsyczky, W.-c. Chang, C. J. Thibodeaux and H.-w. Liu, *J. Biol. Chem.*, 2012, **287**, 4602-4608.
58. E. C. Dykhuizen and L. L. Kiessling, *Org. Lett.*, 2009, **11**, 193-196.
59. S. Borrelli, W. F. Zandberg, S. Mohan, M. Ko, F. Martinez-Gutierrez, S. K. Partha, D. A. R. Sanders, Y. Av-Gay and B. M. Pinto, *Int. J. Antimicrob. Agents*, 2010, **36**, 364-368.
60. A. Sadeghi-Khomami, J. Blake Alexander, C. Wilson and R. Thomas Neil, *Org. Lett.*, 2005, **7**, 4891-4894.
61. S. Scherman Michael, A. Winans Katharine, J. Stern Richard, V. Jones, R. Bertozzi Carolyn and R. McNeil Michael, *Antimicrob. Agents Chemother.*, 2003, **47**, 378-382.
62. E. E. Carlson, J. F. May and L. L. Kiessling, *Chem. Biol. (Cambridge, MA, U. S.)*, 2006, **13**, 825-837.
63. W. Huang and J. W. Gault, *J. Phys. Chem. B*, 2012, **116**, 14040-14050.

64. A. Sadeghi-Khomami, PH.D. Thesis, University of Nottingham, UK, 2004.
65. A. Gaulton, L. J. Bellis, A. P. Bento, J. Chambers, M. Davies, A. Hersey, Y. Light, S. McGlinchey, D. Michalovich, B. Al-Lazikani and J. P. Overington, *Nucleic Acids Res.*, 2012, **40**, D1100-D1107.
66. A. Wichlacz, Final Year Project, University of Nottingham, UK, 2013.
67. T. J. Curphey, *J. Org. Chem.*, 2002, **67**, 6461-6473.
68. A. Carpino Louis, H. Imazumi, A. El-Faham, J. Ferrer Fernando, C. Zhang, Y. Lee, M. Foxman Bruce, P. Henklein, C. Hanay, C. Mugge, H. Wenschuh, J. Klose, M. Beyermann and M. Bienert, *Angew. Chem., Int. Ed. Engl.*, 2002, **41**, 441-445.
69. G. Jones, P. Willett, R. C. Glen, A. R. Leach and R. Taylor, *J. Mol. Biol.*, 1997, **267**, 727-748.
70. M. L. Verdonk, J. C. Cole, M. J. Hartshorn, C. W. Murray and R. D. Taylor, *Proteins Struct., Funct., Genet.*, 2003, **52**, 609-623.
71. G. A. Jeffrey, ***An Introduction to Hydrogen Bonding***, Oxford University Press, New York, 1997.
72. H. E. Gottlieb, V. Kotlyar and A. Nudelman, *J. Org. Chem.*, 1997, **62**, 7512-7515.
73. H. Zhang, J. Wang, W. Mao, J. Huang, X. Wu, Y. Shen and M. Sui, *J. of Controlled Release*, 2013, **166**, 147-158.

74. J. R. Davies, P. D. Kane and C. J. Moody, *Tetrahedron*, 2004, **60**, 3967-3977.
75. R. Gitto, L. De Luca, S. Ferro, R. Citraro, G. De Sarro, L. Costa, L. Ciranna and A. Chimirri, *Bioorg. Med. Chem.*, 2009, **17**, 1640-1647.
76. H.-Y. Lin and B. B. Snider, *J. Org. Chem.*, 2012, **77**, 4832-4836.
77. J. A. Lafontaine, R. F. Day, J. Dibrino, J. R. Hadcock, D. M. Hargrove, M. Linhares, K. A. Martin, T. S. Maurer, N. A. Nardone, D. A. Tess and P. DaSilva-Jardine, *Bioorg. Med. Chem. Lett.*, 2007, **17**, 5245-5250.